2001

Surface Modification and Characterization of PMMA Used in the Construction of Microelectromechanical Systems.

Alyssa Catharyn Henry
Louisiana State University and Agricultural & Mechanical College

INFORMATION TO USERS

This manuscript has been reproduced from the microfilm master. UMI films the text directly from the original or copy submitted. Thus, some thesis and dissertation copies are in typewriter face, while others may be from any type of computer printer.

The quality of this reproduction is dependent upon the quality of the copy submitted. Broken or indistinct print, colored or poor quality illustrations and photographs, print bleedthrough, substandard margins, and improper alignment can adversely affect reproduction.

In the unlikely event that the author did not send UMI a complete manuscript and there are missing pages, these will be noted. Also, if unauthorized copyright material had to be removed, a note will indicate the deletion.

Oversize materials (e.g., maps, drawings, charts) are reproduced by sectioning the original, beginning at the upper left-hand corner and continuing from left to right in equal sections with small overlaps.

Photographs included in the original manuscript have been reproduced xerographically in this copy. Higher quality 6" x 9" black and white photographic prints are available for any photographs or illustrations appearing in this copy for an additional charge. Contact UMI directly to order.

ProQuest Information and Learning
300 North Zeeb Road, Ann Arbor, MI 48106-1346 USA
800-521-0600

UMI®

SURFACE MODIFICATION AND CHARACTERIZATION OF PMMA USED IN THE CONSTRUCTION OF MICROELECTROMECHANICAL SYSTEMS

A Dissertation

Submitted to the Graduate Faculty of the
Louisiana State University and
Agricultural and Mechanical College
in partial fulfillment of the
requirements for the degree of
Doctor of Philosophy

in

The Department of Chemistry

by
Alyssa Catharyn Henry
B.S., Indiana University of Pennsylvania, 1994
B.A., Indiana University of Pennsylvania, 1994
August, 2001

Dedication

This dissertation is dedicated to:

My mom, Arlene Timberlake Henry

My dad, Thomas Henry

My grandparents, Floyd and Gloria Timberlake and Franklin and LaRue Henry

The aunt pile, Carole Timberlake Byrd, Wanda Timberlake Dorsey, Karen "Pepper" Timberlake Boniol, Cher Timberlake Bordenave

My godfather, Keith Timberlake

My uncles, Thomas Bordenave, Johnny Boniol, Steven Dorsey, Emory Byrd

My cousins, Nicole, Angela, Joseph, Stevie, Kristi, and Allix

Louis and Mandina

I could not have asked for a more loving and interesting family

Acknowledgments

As with every paper I have ever written and every talk I have ever presented, my first and foremost acknowledgment is to my advisor, Dr. Robin L. McCarley. His guidance and genuine thoughtfulness played a crucial role in the completion of this work. I will always remember my graduate studies under Dr. McCarley's supervision with fondness.

I am truly blessed with a wide array of friends and family who have been so supportive over the years. I would like to thank Marianne McKee for proofreading every paper and listening to every presentation I have ever written or given. Thank you for the countless lunches and the endless road trips. Thanks to Kari Green-Church and Lenore Polo Rodicio for many hours of graduate school advice and wisdom. I would also like to thank Suzy Lassiter for cracking me up for five years. Many thanks to Dr. Tracy Donovan McCarley for her friendship and generosity.

My hours in the laboratory would not have been nearly as enjoyable without my fellow group members. I would like to thank Charles O. Noble, IV for countless brainstorming sessions and for his insight into the world of duct tape. Charles, may you forever make herstory whenever you're "in it to win it." Thanks to K. Cory Schomburg for making me laugh. Cory, I hope your dreams for The Redneck Network materialize. I would like to thank Sonya Caston Pierre for her kindness and courtesy, and I'd like to thank Song Lin for his imitations and vaporizations. Thank you to Jed Aucoin for his Cajun stories—aaaiiiiieeeeee! Thanks to Pierre N. Floriano for nanocluster conversations and for teaching me how to appreciate fine cognac. Thank you to Dr.

Bikas Vaidya for fresh insight into my research. I would also like to wish good luck to Alison Smith, Amy Morara, and Mariah McMasters. I am extremely fortunate to have had the experiences I have had with my fellow group members, and I am very proud to be affiliated with all of them.

Special thanks to our collaborators, including Dr. Steven A. Soper, Yolanda Y. Davidson, C. Scott McWhorter, Yun Wang, Michelle Galloway, Dr. Kevin Kelly, Dr. Michael Murphy, and Dr. Chantal Khan Malek. I would also like to thank all of the professors in the Department of Chemistry for all of their knowledge and help; in addition, thanks to all of the staff members for everything they have done for me.

Table of Contents

List of Tables

List of Figures

List of Abbreviations

AFM	atomic force microscopy
amu	atomic mass unit
AT-PMMA	amine-terminated PMMA
ATR	attenuated total reflectance
ATR-IR	attenuated total reflectance infrared spectroscopy
Au-EDNPFs	electrolessly deposited Au nanoparticle films
BMA	butyl methacrylate
CE	capillary electrophoresis
CEC	capillary electrochromatography
CT-PMMA	carboxylic acid-terminated PMMA
CV	cyclic voltammetry
d	thickness of film
DCC	dicyclohexylcarbodiimide
DSC	differential scanning calorimetry
E	electrochemical potential
EDC	1-ethyl-3-(3-dimethylaminopropyl)carbodiimide
EOF	electroosmotic flow
F_N	force
FITC	fluorescein isothiocyanate
FT-IR	Fourier-transform infrared spectroscopy
GC-MS	gas chromatography-mass spectrometry
GPC	gel-permeation chromatography

HAR	high aspect ratio
HARM	high-aspect-ratio microstructure
HEPES	4-(2-hydroxyethyl)-1-piperazineethanesulfonic acid
HPLC	high performance liquid chromatography
IAA	indoleacrylic acid
i	electrochemical current
IR	infrared
k_i	absorption coefficient (in infrared spectroscopy)
k_N	spring constant
LIGA	lithography, electroplating, and molding
M_w	molecular mass
MALDI	matrix-assisted laser desorption/ionization
MEM	microelectromechanical
MEMS	microelectromechanical systems
MMA	methyl methacrylate
n_i	refractive index
$\tilde{n}_l$	complex refractive index
NVOC	nitroveratryloxycarbonyl
NVOC-Gly	nitroveratryloxycarbonyl-glycine
PAS	poly(alkenesulfone)
PB	poly(butene)
PC	poly(carbonate)
PDMS	poly(dimethylsiloxane)

PLG	poly(lactide-co-glycolide)
PMI	poly(methacrylimide)
PMMA	poly(methyl methacrylate)
POM	poly(oxymethylene)
PS	poly(styrene)
PTFE	poly(tetrafluoroethylene)
RAIR	reflection-absorption infrared
RAIRS	reflection-absorption infrared spectroscopy
RPLC	reversed-phase liquid chromatography
SAM	self-assembled monolayer
SER	surface-enhanced Raman
SERS	surface-enhanced Raman spectroscopy
SFM	scanning force microscopy
SPME	solid-phase microextraction
SSCE	saturated sodium calomel electrode
ST-PMMA	sulfonic acid-terminated PMMA
T_g	glass transition temperature
TEA	triethylamine
THF	tetrahydrofuran
UV	ultraviolet
UV-vis	ultraviolet-visible absorption spectroscopy
XPS	X-ray photoelectron spectroscopy
β	phase change of light

γ_{LV}	free energy at liquid-vapor interface
γ_{SV}	free energy at solid-vapor interface
γ_{SL}	free energy at solid-liquid interface
λ	wavelength
ν	stretching mode (in infrared spectroscopy)
ν_a	asymmetric stretching mode (in infrared spectroscopy)
ν_s	symmetric stretching mode (in infrared spectroscopy)
δ	deformation mode (in infrared spectroscopy)
θ	angle of water contact

Abstract

Poly(methyl methacrylate), PMMA, is a standard photoresist and is also a popular material out of which microelectromechanical systems are made. Described within is the characterization of the bulk and surface properties of commercial PMMA sheets and their relevance to PMMA as a photoresist. The surface chemical modification and characterization of commercial PMMA sheets is discussed; these modifications and their chemical properties have direct pertinence to the use of PMMA as a substrate for the fabrication of microelectromechanical devices.

The molecular masses of pristine and irradiated PMMAs were determined by means of gel-permeation chromatography (GPC) and it was found that the molecular mass of irradiated PMMA is less than that of pristine PMMA. In addition, the glass transition temperatures (T_g) of pristine and annealed PMMA were determined and compared.

The surface topography of commercial PMMA sheets was assessed using scanning force microscopy (SFM) and related to the adhesive properties of sheet PMMA to metal surfaces. It was determined that thermally treated PMMA sheets displayed a higher surface area than those sheets not thermally treated, which is due to defects on the surface of the PMMA. The pits were determined, using gas chromatography-mass spectrometry (GC-MS) and solid-phase microextraction (SPME), to be due to the expulsion of MMA monomer from the matrix of the PMMA during annealing.

The surface chemical modification of PMMA sheets to yield primary amine-terminated PMMA surfaces is described. Characterizations of amine-terminated PMMA sheets conclude that the amines are covalently linked to the surface of PMMA and are accessible for further surface reactions; in addition, the amines are present at a surface density of 5 nmol cm^{-2}.

Amine-terminated PMMA sheets were used in reactions with isothiocyanates, isocyanates and carboxylic acids. Such functionalized PMMA surfaces can be used to manipulate the electroosmotic flow (EOF) of microcapillary electrophoresis devices and will be used as stationary phases in microcapillary electrophoresis. Amine-terminated PMMA surfaces have been used in the electroless deposition of several metals and for the fabrication of colloidal metal films. Finally, a photopatterning technique was developed that allows for the *selective deposition* of various organic moieties or metals with micrometer-level resolution.

Chapter 1

Introduction

1.1 Goals and Aims of Research

The overall goal of this research is to understand the bulk and surface properties of a common X-ray photoresist, poly(methyl methacrylate), PMMA, as well as to develop protocols for the surface derivatization of this material for its use as a substrate in the fabrication of microelectromechanical systems (MEMS).

As a photoresist, PMMA is one of the most common X-ray sensitive resists employed in the X-ray lithographic manufacture of microstructures and microdevices.[1-3] One of the many attractive characteristics of this photoresist is its availability, in sheet form, from a wide array of manufacturers in a variety of sizes and thicknesses. However, although several brands and thicknesses of PMMA sheets had been employed in the lithographic manufacture of microstructures and microdevices, the PMMA sheets had never been characterized, either before or after X-ray irradiation, prior to the work described here. Thus, one of the aims of this research is to probe the bulk properties, including molecular mass and thermal characteristics, of pristine and X-ray irradiated PMMA. Understanding the degradation of this material is important for the future use of commercial PMMA sheets as X-ray photoresists,[1, 3-5] due to the development step in the fabrication process.[1-2] It is important to understand the thermal characteristics of the commercial PMMA sheets in order to develop processes to improve the adhesion[2,4] of PMMA sheets to other PMMA sheets (thermal bonding), to improve the adhesion of

PMMA sheets to an electrically conducting substrate, or to gain an understanding of the relationship between PMMA sheet purity and thermal properties.

Another aim of this project is assessment of the surface properties of commercially available PMMA sheets and determination of how thermal treatment of PMMA sheets affect the adhesive strength of the PMMA sheet on an electrically-conductive substrate surface. The outcomes have direct pertinence to the overall robustness of microstructures or microstructured templates fabricated by means of X-ray lithographic processes.[1,4]

The surface chemical modification of PMMA sheets is another important aim of this research. Characterization of the bulk and surface properties of pristine, commercially available PMMA sheets, as well as characterization of the surface properties of X-ray irradiated PMMA sheets has direct consequences on PMMA *as a photoresist*. However, in addition to its excellent properties as a photoresist, PMMA is a popular polymer out of which microelectromechanical systems (MEMS), such as microanalytical separation devices, are made.[6-9] In order to develop microanalytical separation devices that perform in the same manner as conventional separation systems, surface modification of the separation device is necessary. That is, in order for a micro reversed-phase liquid chromatography (RPLC) system to separate the same analytes as its macrosized counterpart, the stationary phase of the microsystem must be similar to that of the conventional system. Thus, chemical modification of the PMMA surface is necessary in order to yield organic, surface-bound, stationary phase moeties. In addition, in micro capillary electrophoresis (CE) or micro capillary electrochromatography (CEC) devices, the electroosmotic flow, EOF, of buffers

through microchannels can be changed, in direction as well as in magnitude, simply by varying the ionizable functional groups on the surface of the microchannel.[10-11] Thus, chemically modifying the surface of the PMMA to yield ionizable functional groups could change the magnitude and direction of buffer ions through the PMMA microchannel.

Another aim of this research is the surface derivatization of PMMA surfaces with metal-coordinating species. By derivatizing the PMMA with certain metal-nucleating organic moieties, it is possible to deposit various metal films on the surface of the PMMA.[12] Metals deposition on PMMA surfaces will allow for the fabrication of microcircuitry on the devices, as well as a means for electrochemical or conductivity detection of analytes separated by means of microanalytical devices.[13-15]

Still another aim of this research is *selective* deposition organic moieties or metals on the surface of PMMA. This selective deposition will allow for the straightforward fabrication of patterned microcircuits and mixed organic moieties on microanalytical separation devices.[12] In addition, a PMMA-based microarrayed sensing substrate would be possible by selectively depositing organic moieties in discreet patterns on PMMA surfaces.

1.2 Research Synopsis

In order to achieve the goals and aims presented, the bulk properties of PMMA were assessed using a variety of different analytical techniques, including differential scanning calorimetry (DSC) and gel-permeation chromatography (GPC). It was found that the thermal properties of PMMA varied with vendor; the glass transition temperature, T_g, of Goodfellow PMMA was found to be 112 ± 1.7 °C, whereas the T_g of

AIN PMMA was determined to be 94.6 ± 2.5 °C.[16] The molecular mass of the PMMA sheets was determined, by gel-permeation chromatography, GPC, to be in the 1-3 Mamu range. After irradiation, the molecular mass of the PMMA was found to decrease by as much as 45-fold.[16]

Once a fundamental knowledge of the bulk properties of commercially available PMMA sheets was obtained, the surface properties of PMMA sheets were determined. It has been shown that thermally treating PMMA sheets increases the adhesive strength of the PMMA sheets to a metal-conducting substrate. It was postulated that thermally treating the PMMA sheets expelled unpolymerized methyl methacrylate (MMA) monomer from the matrix of the PMMA polymer. Scanning force microscopy (SFM) was employed in order to ascertain the surface topography of pristine and thermally treated PMMA sheets. It was found that the surface topography changed upon thermal treatment of the PMMA sheets; the surface area increased. In addition to the surface area increase, it was found, using gas chromatography-mass spectrometry (GC-MS) as well as solid-phase microextraction (SPME) coupled to GC-MS, that residual MMA monomer was present in the matrix of the PMMA polymer.[17]

The experiments involving characterization of the surface properties of commercially available PMMA sheets illustrated that thermally treating the PMMA sheets prior to gluing them to an electrically-conducting substrate increased the adhesive strength between the two surfaces. It was postulated that chemically modifying the PMMA sheets with a reactive functional group prior to gluing them with a polymerizable glue would further increase the adhesive strength between the PMMA sheet and the electrically-conducting substrate. The reactive functional group that was

chosen is the amine functionality. This particular reactive functional group was chosen due to the fact that reactions with amines are very popular and have been discussed at great lengths in the literature.[18]

N-lithiodiaminoethane and *N*-lithiodiaminopropane[19-20] were synthesized and reacted with pristine PMMA sheet surfaces to produce amine-terminated PMMA, referred to as NH_2-terminated PMMA or AT-PMMA.[21] The surface was characterized using sessile drop water contact angle goniometry, reflection-absorption infrared (RAIR) spectroscopy, X-ray photoelectron spectroscopy (XPS), scanning force microscopy (SFM), and confocal fluorescence microscopy. In addition, the surface-bound amines were quantificated using a modified ninhydrin method. It was found that the reaction of pristine PMMA with a lithiated diamine produces an amide linkage from the PMMA surface to a primary amine; these amines are accessible to reactions with a fluorescent dye containing a isothiocyanate group. The surface roughness of the amine-terminated PMMA sheets is roughly 3.5 times that of the pristine surface. Finally, it was found that amines populate the surface of NH_2-Terminated PMMA at a surface density of approximately 5 nmol cm^{-2}.[21]

The amines on the surface of AT-PMMA can be used in several reactions with various organic moieties;[18] in addition, because amines coordinate metals,[22] NH_2-terminated PMMA can be used as a substrate for metals deposition. AT-PMMA was reacted with *n*-octadecane-1-isocyanate with the presumption that long-chain alkane-terminated PMMA can be used in the fabrication of micro liquid chromatography (microLC) or micro capillary electrochromatography (microCEC) devices. The resulting $C_{18}H_{37}$-terminated PMMA was characterized using water contact angle

studies, RAIR spectroscopy, and SFM. It was found that the amines react with the isocyanates such that a urea linkage is produced; in addition, the alkane chains on the surface of the PMMA are very crystalline in nature and tilted somewhat from the surface normal.[21]

Amine-terminated PMMA was reacted with 1,9-nonanedioic acid, as well as 4-sulfobenzoic acid in order to create functional groups on the surface of PMMA that will alter the electroosmotic flow in a PMMA-based microanalytical separation device.[23] The carboxylic acid- and sulfonic acid-terminated PMMA (CT-PMMA and ST-PMMA, respectively) as well as carboxylic acid and sulfonic acid-terminated Au surfaces, were characterized using RAIR spectroscopy; the reaction involving surface-bound amines with carboxylic acids produces an amide bond which is readily evident in the infrared (IR) spectra. In addition, bands corresponding to carboxylates and sulfonates were present on the IR spectra. The electroosmotic flow profiles of CT- and ST-PMMA microdevices were assessed. It was found that the electroosmotic flow of several buffer systems was dependent on the organic moiety terminating the microdevice.[23]

AT-PMMA was used as a substrate for metals deposition.[12] Au and Ag colloids were synthesized and allowed to deposit on the surface of the AT-PMMA. The surface-bound metal colloids sustained a standard adhesion test and were characterized using ultraviolet/visible (UV/vis) spectroscopy. Metal colloids immobilized on PMMA surfaces could have direct relevance to surface-enhanced Raman (SER) spectroscopic detection schemes for microanalytical separation devices.[24-25] Thick metal films were fabricated with successive deposition of metal colloids on the PMMA surface and used as working electrodes. In addition to metal colloid deposition, an electroless deposition

method[26] for Au was employed to produce an Au seed layer for conventional electroless deposition on the surface of AT-PMMA. The surface-bound Au seed layer was characterized using UV/vis spectroscopy. The seed layer was subjected to a commercially available electroless Ag bath; reflective Ag films were evident on the surface of the PMMA and were utilized as Ag/AgCl reference electrodes in electrochemistry experiments.[12] The seed layer was also exposed to a conventional Cu electroless bath; reflective Cu films were evident on the surface of the PMMA. The deposition of metal films on the surface of PMMA has direct relevance to the fabrication of microcircuitry on the device surface, as well as for the fabrication of microelectrodes for electrochemical detection of analytes separated.[13-15]

In order to realize the goal of building microcircuitry on microanalytical separation devices, as well as to spatially direct the reaction of surface-bound amines with various organic moieties, a patterning method was developed.[12] In this method, a photolytic protecting group was synthesized. The protecting group was reacted with AT-PMMA; after this reaction, the photoprotected PMMA was masked and exposed to visible radiation for a given time. In the areas where the PMMA was exposed, the protecting group was cleaved, leaving behind surface-bound amines. The deprotected amines were used in subsequent metals deposition protocols.[12]

1.3 The LIGA Process

The development of the LIGA process, the German acronym for ***LIthographie*** (lithography), ***Galvanoformung*** (electroplating), and ***Abformtechnik*** (molding) has made possible a viable method for the effective and relatively inexpensive fabrication of high-aspect-ratio metal and polymer microstructures (HARMs);[1,3,27] the LIGA

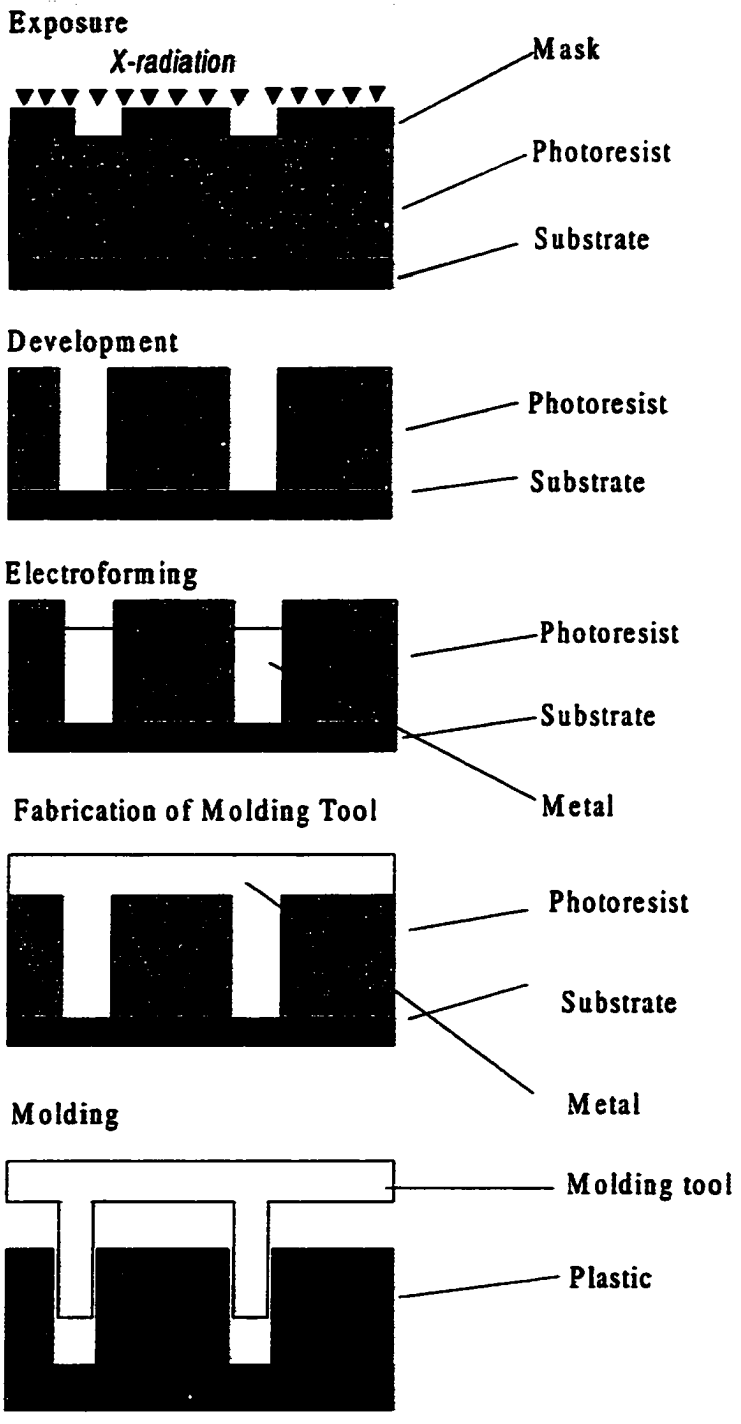

Figure 1.1 **Required steps of the LIGA process: Lithography, Development, Electroplating, Fabrication of Molding Tool, and Molding/Embossing.**

process is represented pictorially in Figure 1.1. Pioneered in the mid-1970s, Romankiw and coworkers[1,28] were the first to demonstrate the feasibility of LIGA. They exposed a 20- μm-thick resist and subsequently plated gold in the created voids of the resist. Ehrfeld et al. in 1982[1,3,27-29] were able to plate metals in the voids of a lithographically-patterned resist and subsequently remove the electroformed metal structure. This structure was used as a molding tool in injection molding applications.

The first major step in the LIGA process is deep X-ray lithography.[1,3,27-29] A 500-μm- to-a-few-mm-thick photoresist—poly(methyl methacrylate), PMMA, in most cases— is first bonded to an electrically conducting metal or metal oxide surface and subsequently irradiated with hard X-rays from a synchrotron source. A mask is used to direct a pattern of X-radiation onto the photoresist surface. As a result of the incident ionizing radiation, the PMMA undergoes chain scission reactions that result in a substantial decrease in the polymer molecular mass, as well as formation of a variety of gaseous small molecules (CO_2, CH_4, CH_3OH, etc.).[30-31] The reduction in molecular mass of the polymer in the exposed areas leads to its ready dissolution in certain developing solvents,[1,3,27-29] which in turn leads to a microstructured PMMA template supported on the conducting substrate, Figure 1.1. After the developing step, metals can then be deposited into the polymer template using standard electroplating methods. Removal of the polymer template results in a metal molding tool that can be used in the fabrication of polymeric microstructures. In addition, the PMMA template itself can be used as a mold for mass production of metal microstructures.

One of the primary advantages of the LIGA process is that high-aspect-ratio microstructures (HARMs) can be achieved. For example, construction of metal posts

that are 1 μm in diameter and several tenths of a millimeter in length have been fabricated.[32] These polymeric and metal microstuctures can be used as microsensors and microactuators, and in the construction of micropumps. Also, it is envisioned that the LIGA process will one day lead to microanalytical instrumentation that is both simple to use and relatively inexpensive.

1.3.1 PMMA as a Photoresist

The perfect deep X-ray resist employed in the LIGA process for the fabrication of HARM molds and microstructures should posses several qualities; most notably, high sensitivity to X-rays, insolubility in developing solvents, compatibility with the electroplating process, and proper adhesion of the resist to the conductive metal substrate.[1,28,33] In the case of X-ray sensitivity, PMMA is known to exhibit low lithographic sensitivity in the range of λ = 50-80 nm.[1,33] However, this problem is solved by exposing the PMMA to the X-ray radiation for longer periods of time.

Insolublity in developing solvents is a crucial quality in the choice of a X-ray resist. Due to its high molecular weight in its pristine form, PMMA that has not been exposed to X-radiation is insoluble in most developing solvents. However, the portions of the PMMA that have been exposed to the X-rays undergo chain scission reactions[30-31] (Figure 1.2), resulting in a decreased-molecular weight polymer that is soluble in developing solvents.

The electroforming step plays a vital role in the fabrication of a metal molding tool. In this step, metals are electroplated between into the voids, as well as over the microstructured plastic mold. The temperature of most electroplating baths is on average ~60 °C;[1,27] thus, the glass transition temperature, T_g, of the resist must be

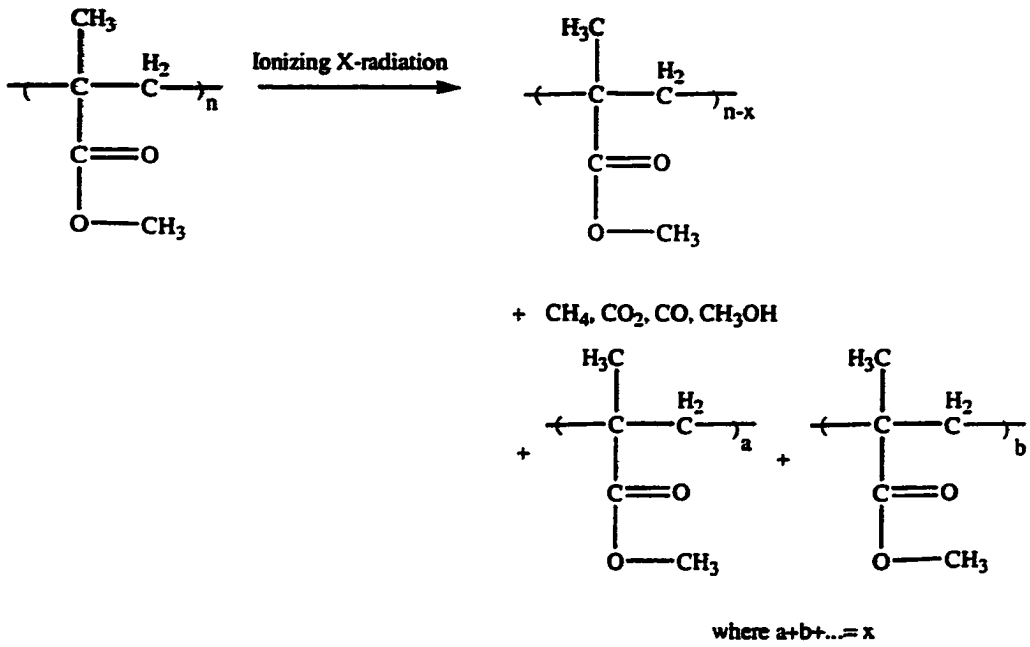

Figure 1.2 Chain scission reactions upon X-ray irradiation of PMMA.

greater than this temperature. In the case of commercial PMMA sheets, the T_g of PMMA was found to be 90-115 °C,[16] much greater than the temperature of commercial electroplating baths.

Finally, good adhesion of the photoresist to the conductive metal substrate is imperative for the prevention of ill-formed microstructured polymer molds and, subsequently, metal molding tools. Commercially available sheet PMMA has shown to exhibit poor adhesion to metal-conducting substrates. However, thermally treating (annealing) the PMMA sheets results in increased adhesion of the PMMA sheet to the substrate.[16]

1.3.2 Other X-ray Sensitive Photoresists

Although still in its infancy, research in the area of other X-ray sensitive photoresists is in progress. Some of the auxiliary X-ray resists being explored are poly(lactide-co-glycolide) (PLG), poly(methacrylimide) (PMI), poly(oxymethylene)

(POM), and poly(alkenesulfone) (PAS).[1] In addition, copolymers of PMMA have also been tested.[34]

PLG, PMI, POM, and PAS all exhibit better X-ray sensitivity than PMMA. Perhaps the most promising of these materials is PLG, as it exhibits similar resolution, sidewall smoothness, and adhesion to metal-conducting substrate to PMMA.[1] PLG is not yet commercially available.

1.4 Application of Thick PMMA Layers to the Conducting Metal Substrate

Thick PMMA layers can be applied to a conducting metal substrate in three different manners, including multilayer coating,[35] casting,[36-37] and sheet adhesion.[38-39] The most common of the three methods are casting and commercial sheet adhesion.

1.4.1 Multilayer Coating

Several different methods exist for applying PMMA to the metal-conducting substrate. One such method is the multiple layer spin-coating technique. In this technique, PMMA, dissolved in a solvent, is spin-coated onto the metal-conducting substrate and the solvent is allowed to evaporate. After evaporation, dissolved PMMA is spin-coated on the PMMA-coated substrate and the solvent is, again, allowed to evaporate. This process is repeated until multilayers of PMMA exist on the substrate. The multilayered PMMA is subject to cracks and fissures between the layers.[1,35] While annealing the PMMA-coated substrate results in less cracking, microstructures with heights of only 15 μm have been realized.[1]

1.4.2 Casting

Thick PMMA layers can be obtained by casting the PMMA on the substrate surface. In PMMA casting, a casting resin is mixed with a hardener and an initiator in

the absence of oxygen.[1, 36-37] The resin is then poured on the metal-conducting substrate and covered with a glass plate. Shims placed at the sides of the substrate define the PMMA thickness and shape. Due to the presence of the hardener, the MMA polymerizes in a few minutes, thus forming a thick PMMA block on the metal-conducting substrate. This PMMA can then be fly-cut to a desired thickness and polished smooth; the PMMA/substrate is then ready for the next step in the LIGA process.[1, 36-37]

1.4.3 Adhesion of Thick PMMA Sheets

The final method for obtaining thick PMMA layers on the metal-conducting substrate is by gluing commercially-available, thick PMMA sheets onto the surface of the substrate.[38-39] The PMMA is glued to the substrate surface by spin-coating neat methyl methacrylate (MMA) monomer on the substrate. The thick (0.5 — >3 mm) PMMA sheet is then pressed onto the MMA-coated substrate and held in place for several hours. The solvent-bonded PMMA/substrate assembly is then ready for the next step in the LIGA process.[39]

One common characteristic associated with merely adhering a thick PMMA sheet to the metal-conducting substrate lies in the adhesion between the two surfaces.[16] In some cases, it has been seen that the PMMA becomes debonded from the surface of the substrate.[16] Adhesion between the sheet PMMA and the substrate has been vastly improved by chemically treating (oxidizing) the surface of the substrate.[40] In this case, the surface area of the substrate is increased, thus resulting in better surface contact between the resist and the substrate. This in turn leads to a plastic microstructure mold that is firmly adhered to the substrate surface.

Surface modifiers, such as acrylate-terminated silanes, have been employed to promote the adhesion of cast PMMA layers on silicon (silanol) surfaces. Methacryloxypropyltrimethoxysilane was added to PMMA casting resins; the silane reacts with the silanols, thus producing a rigid link between the cast PMMA layer and the silicon surface.[37] However, in order to employ a *covalent* surface modifier for the improvement of adhesion between *sheet* PMMA and a derivatized silicon surface, the PMMA must possess reactive functional groups.

1.5 MEMS in Analytical Chemistry

Thus far, PMMA has been studied as a *photoresist*; that is, the major role that PMMA plays is one in which it is lithographically patterned to produce a microstructured mold for the fabrication of metal microstructures or molding tools. However, in recent years, PMMA has proved itself as a viable substrate for the manfacture of such MEMS as microanalytical separation devices.[6-9] These systems generally take the shape of microelectrophoretic devices that are used in the separation and detection of various samples, such as DNA fragments.[8-9] A typical microanalytical separation device consists of a microchannel, or series of microchannels, etched into a glass or polymer substrate. In addition to the channels, buffer reservoirs are present on the substrate. A top plate is thermally bonded on the top of the substrate, thus sealing the channels and buffer reservoirs present on the device.[6]

MEMS offer the researcher many advantages, including high sample throughput, high sample processing, minimized consumption of sample and reagent, and reduced cost.[6, 41-42] MEMS have traditionally been fabricated from glass or other

silicon-based materials;[41-43] however, polymeric materials, such as PMMA, are gaining more recognition as substrates out of which MEMS are fabricated.[6-9]

1.5.1 Glass-Based Microanalytical Separation Devices

Conventional microanalytical separation devices employ glass as the substrate.[1, 41-42] Channels are etched into the glass substrate by means of wet chemical etching using HF. In this process, the glass substrate is coated with a positive photoresist. An optical mask transfers the pattern to the resist-coated substrate. The portions of the resist that have been exposed to light are dissolved, leaving behind the exposed glass. This exposed glass is etched using a buffered HF solution. After etching, the unexposed photoresist is removed from the etched glass plate. The channels and buffer reservoirs in the glass substrate may be sealed by bonding a glass plate over the device.[1, 41-44]

While the fabrication of glass-based microanalytical devices is relatively simple, due to the isotropic nature of the etching process, trapezoidal channels with low aspect ratios result. Thus, band broadening effects are noted in glass-based microanalytical devices. In addition, bonding the top plate to the channel-etched glass substrate is accomplished by thermal annealing; the temperature required for this step is ~600 °C. However, two of the primary advantages to using glass as a substrate for the fabrication of MEMS lies in its optical transparency as well as in its compatibility with a host of organic solvents. Glass is optically transparent in the visible region of the electromagnetic spectrum and absorbs marginally in the infrared. In addition, glass will not dissolve in organic solvents such as acetonitrile; this fact will allow for its use in variety of separation schemes. Still another advantage to using glass as a substrate in

MEMS fabrication is its ease for chemical modification using organosilanes.[45-47] Thus, glass-based systems can be modified to yield surfaces with various chemical properties.

1.5.2 Silicon-Based Microanalytical Separation Devices

Microdevices fabricated from silicon are prepared similar to those manufactured in glass. The silicon wafer is first cleaned and polished; after the cleaning process, SiO_2 is deposited on the Si surface. A photoresist is then deposited on the SiO_2/Si surface. The photoresist/SiO_2/Si assembly is masked and subjected to irradiation; after irradiation, the portions of the resist exposed to radiation are dissolved in a developing solvent. The SiO_2 is then etched, leaving behind patterned Si. The resist is then removed such that the patterned Si is "protected" with SiO_2. The Si is etched using HF; after etching, the oxide is removed, resulting in an etched Si microdevice.[1]

Due to its prevalence in the semiconductor industry, Si has been widely used in the fabrication of early microdevices. However, like glass, the etching procedure often results in misshaped and low-aspect-ratio channels patterned in the Si substrate, leading to band broadening. In addition, silicon is very expensive compared to similar substrates such as glass.

1.5.3 Polymer-Based Microanalytical Separation Devices

An alternative to glass-based microdevices is that fabricated from polymers. One particular advantage to using polymer-based MEMS is the wide choice in microfabrication methods that can be selected to construct the device. Some of the common polymers that have been investigated for use as substrate in MEMS include PMMA, poly(carbonate (PC), poly(tetrafluoroethylene) (PTFE), poly(butene) (PB), poly(dimethylsiloxane) (PDMS), and poly(styrene) (PS).[6]

There are several properties that one must consider when choosing a polymeric substrate for use as a substrate in the fabrication of microanalytical separation devices. To begin, the material must be machinable.[6] In the case of polymers, some of the common methods for producing MEMS from polymeric materials include injection molding,[48] laser ablation,[49] imprinting,[7] and hot embossing.[50] Thus, the polymers must possess characteristics that make MEMS fabrication feasible. For example, in the case of laser ablation, the polymer must absorb radiation produced by the laser to allow for its ablation. Imprinting, injection molding, and hot embossing methods require materials possessing a low T_g. These methods employ a lithographically produced mold; the mold is a negative image of the device. Molds produced by means of the LIGA process are rapidly permeating the microanalytical separation device field due to their ability to produce HAR features.[1, 6] Devices produced using LIGA molds are characterized by deep, narrow microchannels; these microchannels are advantageous in that band broadening effects are diminished compared to a wide, shallow channel. Thus, LIGA-produced microanalytical separation devices are attractive for the fabrication of small-footprint separation devices that exhibit minimal analyte zone broadening.[6]

In addition to machinablilty, polymers that are used for the fabrication of microaalytical devices must be optically transparent due to the available detection schemes for these systems. For example, in a device employing fluorescence detection of analytes,[8-9] the substrate must possess a very low autofluorescence. Some other detection schemes that are currently under investigation include ultraviolet/visible (UV/vis) spectroscopy and Raman spectroscopy.

Still other characteristics that must be considered when choosing a material as a substrate for a microanalytical separation device are its thermal and electrical properties. The microanalytical devices presented here generally take the shape of microcapillary electrophoresis (microCE) or microcapillary electrochromatography (microCEC) devices. In these microCE and microCEC devices, a high electric field is applied to the device, thus producing a large quantity of heat. The polymeric material must tolerate the high electric fields and, to minimize Joule heating, have a high thermal conductivity.[6]

Separations employing conventional CE[51] and CEC[52] use various solvent systems such as water, methanol, acetonitrile, etc. Thus, the miniaturized versions of these separation techniques employ similar solvent systems. One of the characteristics of the polymeric material comprising the microdevice is compatibility with the analysis. For example, polymers that dissolve in methanol are clearly not feasible as substrates for separation devices that employ methanol as the solvent.

Microanalytical separation devices consist of series of channels etched, imprinted, or ablated in a substrate. Sealing the device, or enclosing the microchannels, consists of thermally bonding a top plate to the substrate.[6,42-43] Thus, another characteristic of polymers used in the fabrication of microanalytical separation devices is that they must possess a substantially low T_g in order to facilitate the thermal bonding process.

The final characteristic possessed by polymers used in the manufacture of microanalytical separation devices is the ability to chemically modify the surface of the substrate. Chemical modification of the microchannel is important due to the nature of

some separations. That is, some separations require a covalently bonded stationary phase;[52] thus, the polymer microchannel must be chemically modified to yield the stationary phase. In other separations, an increased or reversed electroosmotic flow (EOF) is necessary;[11, 53] the polymer microchannel must be chemically modified such that the EOF suits the separation at hand.

1.6 PMMA Used in the Fabrication of Microanalytical Separation Devices

PMMA is a viable substrate out of which microanalytical separation devices are fabricated due to several of its characteristics. To begin, PMMA can easily be machined using laser ablation, injection molding, imprinting, and hot embossing methods. In addition, molds produced using the LIGA process have been used to manufacture PMMA microanalytical separation devices. PMMA also possesses optical characteristics that allow for analyte detection by fluorescence[8-9] and visible spectroscopies. In addition, PMMA is able to tolerate high electric fields and also dissipates heat well, a trait that is necessary for its use in the microanalytical separation device industry. The T_g of commercially available PMMA sheets is ~100 °C;[16] thus, microdevices fabricated from PMMA can be sealed, using a PMMA top plate, by thermal bonding procedures. PMMA is soluble in many organic solvents; however, PMMA is insoluble in polar solvents such as water and alcohols, which comprise many solvent systems in conventional CE and CEC.[51-52] PMMA is also insoluble in nonpolar solvents such as hexanes and cyclohexane. Finally, as seen in Figure 1.3, the chemical structure of PMMA is such that its surface may be chemically modified through the pendant methyl ester group.

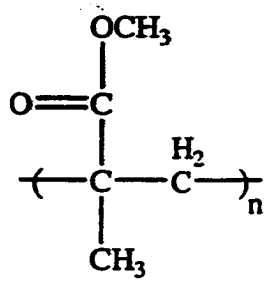

Figure 1.3 Chemical structure of PMMA.

1.7 Modification of Surfaces

The modification of surfaces to yield various functional groups has been accomplished using various chemistries on various surfaces. For example, in the case of polymers, ultraviolet (UV) radiation has been used to produce different organic moieties on polymer surfaces.[54-60] Glass surfaces have been chemically modified, using silane chemistry, to yield surfaces with various organic functional groups.[45-47] Finally, noble metals have been modified with self-assembled monolayers (SAMs) to yield organic moieties such as monomeric units for the polymerization of conducting polymers on noble metal surfaces.[61]

1.8 Chemical Modification of PMMA Surfaces

The *chemical* modification of polymers is still in its early stages. Reports have focused on the chemical modification of PMMA surfaces[19-21] and work is in progress concerning the chemical modification of PC.[62] However, in the case of PMMA, chemical modification protocols for its use in microanalytical separation devices have been marginally explored; however, the needs for such protocols are many. The chemical structure of PMMA, displayed in Figure 1.3, is amenable to reaction with strong nucleophiles, such as amine anions. However, it is sometimes necessary to terminate the PMMA surface in a more reactive functional group, thus producing a

scaffold for further chemical reactions on the PMMA surface. These further chemical reactions can yield PMMA surfaces terminated in organic moieties suitable for use as stationary phases. In addition, PMMA surfaces terminated in ionizable functional groups can be used to change the magnitude and direction of the EOF of buffer systems in PMMA microchannels. Finally, chemical modifications resulting in the termination of the PMMA surface in metal-coordinating species are important for the development of rigid metal films on the surface of the PMMA.

1.8.1 Chemical Modification of PMMA Surfaces to Yield Primary Amines

The objective for terminating PMMA surfaces in primary amines lies in the fact that the methyl ester-terminated pristine PMMA surface is relatively unsusceptible to further chemical reactions. Thus, a reactive functional group on the surface of the PMMA will provide for a robust scaffold onto which other organic moieties, such as enzymes or alkanes, may be covalently bound. Chemical modification techniques for glass substrates are well established using silane chemistry; however, the development of routine, simple, well-defined surface modification protocols for polymers is still in its infancy. Such modification techniques are essential to the development of MEMS technology in polymer-based substrates.

1.8.2 Chemical Modification of PMMA surfaces to Yield Long-Chain Alkanes

Besides microCE, microCEC is a possible separation technique that is used in analytical chemistry. Conventional CEC[52] employs primarily the same instrumental apparatus as CE;[51] however, in CEC, a stationary phase is also used.[52] Thus, in microCEC, a stationary phase must also be employed; in polymer microchannels, the stationary phase must be covalently bonded to the polymer microchannel. One

common stationary phase employed in conventional CEC is a long-chain alkane, $C_{18}H_{37}$.

In order to covalently link a long-chain alkane to a polymer surface, a chemical reaction between the surface and the target organic moiety must exist. Pristine PMMA does not possess any functional groups that will react with a long-chain alkane. However, in the case of AT-PMMA, the amines on the surface of the PMMA will react with isocyanates, isothiocyanates, and carboxylic acids; thus, AT-PMMA surfaces are essential for reactions yielding PMMA surfaces terminating in various organic moieties.

1.8.3 Chemical Modification of PMMA Surfaces to Yield Ionizable Functional Groups

In electrophoretic devices, the flow of buffer solutions carrying analytes is governed by the ionizable functional groups present on the surface of the microchannel.[63-64] Thus, in the case of a cationic, protonated functional group terminating the surface of a microchannel, at pH values less than its pK_a, the EOF is negative and runs from cathode to anode. At pH values higher than the pK_a, the surface is neutral. In the case of a microchannel terminated in an anionic functional group, at pH values lower than the pK_a, the surface is neutral. However, at pH values higher than the pK_a, the surface is negatively charged. The EOF is thus positive and runs from anode to cathode. Depending on the separation, it may be necessary to employ microchannels exhibiting various ionizable functional groups. Therefore, it is necessary to develop a procedure for the modification of PMMA surfaces to yield ionizable functional groups.

1.8.4 Deposition of Metal Colloids and Thick Metal Films on PMMA Surfaces

Primary amines are also known to have an affinity for certain metal ions and metal colloids.[22] Recent reports have focused on the deposition of thick metal films on amine-terminated glass or silicon surfaces.[24-25] These metal surfaces have been used in subsequent self-assembly of organothiols, as well as in electrochemical experiments. In addition, metal colloid monolayers and submonolayers have been immobilized on amine-terminated glass surfaces for the purpose of creating surface-enhanced Raman scattering (SERS) substrates.[65]

PMMA has not been utilized as a platform for the immobilization of metal nanoparticles or thick metal films deposited by wet chemical means (colloid multilayers). Such an accomplishment would be of great importance in the field of microanalytical devices. First, as the devices become smaller and the idea of the disposable microdevice draws near, it will be necessary to develop on-chip microcircuitry for control of the device. In addition, although fluorescence[8-9] and mass spectrometry[66-67] have proven to be very useful for the detection of analytes in microanalytical devices, other methods of detection will become important as "fieldable" devices become more prevalent. Electrochemical detection in microchannels is a viable method for the analysis of electroactive analytes or those that can be labeled with redox-active groups; this detection scheme requires microelectrodes immobilized on the wall of the microanalytical separation device. In addition, conductivity detectors require metallic contacts either in or outside of the microchannel. Surface-enhanced Raman scattering is another detection method that could prove useful

for microanalytical separation devices; this detection scheme would require immobilization of metal colloids on the surface of the channels in the microdevice.

1.8.5 Patterning of PMMA Surfaces

PMMA surfaces can be chemically modified to yield various organic moieties as well as metals films.[12, 21-23] However, in the case of microcircuitry immobilized on PMMA surfaces or arrays fabricated on PMMA surfaces, metal films or organic functionalities must be *patterned* on the surface of the PMMA. Due to the reactive nature of the amines on AT-PMMA,[18] the amines can be reacted with a photolabile protecting group.[12] This photolabile protecting group, once covalently bonded to the PMMA surface, protect the amines from reaction with organic moieties or metal film deposition. However, after deprotection, the amines are accessible for reaction or as coordinating species for metal film deposition.

The selective deposition method described within utilizes a photolabile amine-protecting organic functional group, 4,5-dimethoxy-2-nitrobenzyl carbonyl, otherwise known as nitroveratryloxycarbonyl, or NVOC.[68-70] This protecting group has been used for the selective deposition of redox species[71] and metal nanoparticles on glass surfaces,[72] and in array-based peptide/oligonucleotide synthesis.[68] NVOC is a viable compound for PMMA photoprotection due to its relatively high λ_{max}, 350 nm.[68-70] PMMA is not susceptible to photodegradation at this wavelength. Thus, NVOC is a viable photoprotecting group for AT-PMMA surfaces.

1.9 References

1) Madou, M. *Fundamentals of Microfabrication*, CRC Press: Boca Raton, FL, 1986.

2) Bowden, M.J.; Thompson, L.F. *Solid State Technology* **1979**, 72-82.

3) Becker, E.W.; Ehrfeld, W.; Hagman, P.; Munchmeyer, D. *Microelectron. Eng.* **1986**, *4*, 35-56.

4) Watts, R.K. *Solid State Technology*, **1979**, 68-71.

5) Mittal, K.L. *Solid State Technology* **1979**, 89-95.

6) Soper, S.A.; Qi, S.; Ford, S.M.; McCarley, R.L.; Kelly, K.; Murphy, M. *Anal. Chem.* **2000**, *73*, 643A-651A.

7) Martynova, L.; Locascio, L.E.; Gaitan, M.; Kramer, G.W.; Christensen, R.G.; MacCrehan, W.A. *Anal. Chem.* **1997**, *69*, 4783-4789.

8) Ford, S.M.; Davies, J.; Kar, B.; Qi, S.D.; McWhorter, C.S.; Soper, S.A.; Malek, C.K. *J. Biomech. Eng.* **1999**, *121*, 13-21.

9) Ford, S.M.; Kar, B.; McWhorter, C.S.; Davies, J.; Soper, S.A.; Klopf, M.; Calderon, G.; Saile, V. *J. Microcol. Sep.* **1998**, *10*, 413-422.

10) Barker, S.L.R.; Ross, D.; Tarlov, M.J.; Gaitan, M; Locascio, L.E. *Anal. Chem.* **2000**, *72*, 5925-5929.

11) Barker, S.L.R.; Tarlov, M.J.; Canavan, H.; Hickman, J.J.; Locascio, L.E. *Anal. Chem.* **2000**, *72*, 4899-4903.

12) Henry, A.C.; McCarley, R.L. *J. Phys. Chem. B*, submitted.

13) Martin, R.S.; Gawron, A.J.; Lunte, S.M. *Anal. Chem* **2000**, *72*, 3196-3202.

14) Gawron, A.J.; Martin, R.S.; Lunte, S.M. *Electrophoresis* **2001**, *22*, 242-248.

15) Rossier, J.S.; Roberts, M.A.; Ferrigno, R.; Girault, H.H. *Anal. Chem.* **1999**, *71*, 4294-4299.

16) Henry, A.C.; McCarley, R.L.; Das, S.; Khan Malek, C.; Poche, D.S. *Microsys. Technol.* **1998**, *4*, 104-109.

17) Henry, A.C.; McCarley, R.L.; Das, S.S.; Khan Malek, C.G. *J. Electrochem. Soc.* **1999**, *146*, 2631-2636.

18) March, J. *Advanced Organic Chemistry*, Wiley: New York, 1985.

19) Karandikar, B.; Puschett, J.; Matyjaszewski, K. *Polymer Prep.* **1989**, *30*, 250-251.

20) Ichijima, H.; Kobayashi, H.; Ikada, Y. *J. Cataract Refract. Surg.* **1992**, *18*, 395-401.

21) Henry, A.C.; Tutt, T.J.; Galloway, M.; Davidson, Y.Y.; McWhorter, C.S.; Soper, S.A.; McCarley, R.L. *Anal. Chem.* **2000**, *72*, 5331-5337.

22) Meissler, G.L.; Tarr D.A. *Inorganic Chemistry*, Prentice Hall: New Jersey, 1991.

23) Henry, A.C.; Galloway, M.; Soper, S.A.; McCarley, R.L. in preparation.

24) Grabar, K.C.; Freeman, R.G.; Hommer, M.B.; Natan, M.J. *Anal. Chem.* **1995**, *67*, 735-743.

25) Grabar, K.C.; Allison, K.A.; Baker, B.E.; Bright, R.M.; Brown, K.R.; Dolan, C.M.; Freeman, R.G.; Fox, A.P.; Musick, M.D.; Natan, MJ. *Langmuir* **1996**, *12*, 2353-2361.

26) Moberg, P.; McCarley, R.L. *J. Electrochem. Soc.* **1997**, *144*, 151-153.

27) Bacher, W.; Menz, W.; Mohr, J. *IEEE Trans. Ind. Elec.* **1995**, *42*, 431-441.

28) Spiller, E.; Feder, R.; Topalian, J.; Castellani, E.; Romankiw, L.; Heritage, M. *Solid State Tech.* **1976**, 62-68.

29) Becker, E.W.; Ehrfeld, W.; Munchmeyer, D.; Betz, H.; Heiberger, A.; Pongratz, P.; Glashauser, W.; Michel, H.J.; Siemens, V.R. *Naturwissenschaften* **1982**, *69*, 520-523.

30) Moore, J.A.; Choi, J.O. *Radiation Effects on Polymers*, R.L. Clough, S.W. Shaleby, Editors, p. 156, ACS Symposium Series 475, American Chemical Society: Washington, DC, 1991.

31) El-Kholi, A.; Bley, P.; Gottert, J.; Mohr, J. *Microelectron. Eng.* **1993**, *21*, 271-274.

32) Akkaraju, S.; Desta, Y.M.; Li, B.Q.; Murphy, M.C. *Microsys. Technol.* **1996**, *2*, 178-181.

33) Moreau, W.M. *Semiconductor Lithography*, Plenum Press: New York, 1988.

34) Bulgakova, S.A.; Lopatin, A.Y; Luchin, V.I.; Mazanova, L.M.; Molodnjakov, S.A.; Salaschenko, N.N. *Nucl. Meth. Phys. Res. A* **2000**, *448*, 487-492.

35) Yates, B.W.; Shinozaki, D.M. *J. Polym. Sci. B: Polymer Physics* **1993**, *31*, 1779-1784.

36) Sotobayashi, H.; Asmussen, F.; Thimm, K.; Schnabel, W.; Betz, H.; Einfeld, D. *Polym. Bull.* **1982**, *7*, 95-100.

37) Mohr, J.; Ehrfeld, W. Munchmeer, D. *J. Vac. Sci. Technol. B* **1988**, *6*, 2264-2267.

38) El-Kholi, A.; Mohr, J.; Nazmov, V. *Nucl. Inst. Met. Phys. Res. A* **2000**, *448*, 497-500.

39) Guckel, , H.; Skrobis, K.J.; Klein, J.; Christensen, T.R. *J. Vac. Sci.Technol. A* **1994**, *12*, 2559-2564.

40) Khan Malek, C.G.; Das, S.S. *J. Vac. Sci. Technol. B* **1998**, *16*, 3543.

41) Harrison, J.D.; Manz, A.; Fan, Z; Ludi, H.; Widmer, H.M. *Anal. Chem.* **1992**, *64*, 1926-1932.

42) Harrison, J.D.; Fluri, K.; Seiler, K.; Fan, Z.; Effenhauser, C.S.; Manz, A. *Science* **1993**, *261*, 895-897.

43) Seiler, K.; Harrison, D.J.; Manz, A. *Anal. Chem.* **1995**, *65*, 1481-1488.

44) Effenhauser, C.S.; Bruin, G.J.M.; Paulus, A. *Electrophoresis* **1997**, *18*, 2203-2213.

45) Culbertson, C.T.; Ramsey, R.S., Ramsey, J.M. *Anal. Chem.* **2000**, *72*, 2285-2291.

46) He, H.; Li, H.; Mohr, G, Kovacs, B.; Werner, T.; Wolbeis, O. *Anal. Chem.* **1993**, *65*, 123-127.

47) Proctor, K.G.; Ramirez, S.K.; McWilliams, K.L.; Huerta, J.L.; Kirkland, J.J. in *Chemically Modified Surfaces: Recent Developments*, pp. 45-60; Pesek, J.J.; Matyska, M.T.; Abuelafiya, R.R.; Eds., The Royal Society of Chemistry: Cambridge, 1996.

48) McCormick, R. M.; Nelson, R.J.; Alonso-Amigo, M.G.; Benvegnu, D.J.; Hooper, H.H. *Anal. Chem.* **1997**, *69*, 2626-2630.

49) Roberts, M.A.; Rossler, J.S.; Bercier, P.; Girault, H. *Anal. Chem.* **1997**, *69*, 2035-2042.

50) Becker, H.; Deitz, W. *Proc. SPIE* **1998**, *3515*, 177-182.

51) Gordon, M.J.; Huang, X.; Petoney, X.L.; Zare, N. *Science* **1988**, *242*, 224

52) Colon L.A.; Burgos G.; Maloney T.D.; Cintron J.M.; Rodriguez R.L. *Electrophoresis* **2000**, *21*, 3965-3993.

53) Liu, Y.; Fanguy, J.C.; Bledsoe, J.M.; Henry, C.S. *Anal. Chem.* **2000**, *72*, 5939-5944.

54) Zhang, J.-Y.; Esrom, H.; Kogelschatz, U.; Emig, G. *J. Adhesion Sci. Technol.* **1994**, *8*, 1181-1210.

55) Celina, M.; Kudoh, H.; Renk, T.J.; Gillen, K.T.; Clough, R.L. *Radiat. Phys. Chem.* **1998**, *51*, 191-194.

56) Fozza, A.C.; Roch, J.; Klemberg-Sapieha, J.E.; Kruse, A.; Hollander, A.; Wertheimer, M.R. *Nucl. Inst. Meth. Phys. Res.* **1997**, 205-210.

57) Ruckenstein, E.; Chen, J.-H. *J. Adhesion Sci. Technol.* **1992**, *6*, 611-623.

58) Loh, F.C.; Lau, C.B.; Tan, K.L.; Kang, E.T. *J. Appl. Polym. Sci.* **1995**, *56*, 1707-1713.

59) Qui, Y.X.; Klee, D.; Pluster, W.; Severich, B.; Hocker, H. *J. Appl. Polym. Sci.* **1996**, *61*, 2373-2382.

60) Kreutz, E.W.; Frerichs, H.; Stricker, J.; Wesner, D.A. *Nucl. Inst. Meth. Phys. Res. B* **1995**, *105*, 245-249.

61) Willicut, R.J.; McCarley, R.L. *Langmuir* **1994**, *11*, 296-301.

62) Vaidya, B.; McCarley, R.L., in preparation.

63) Jorgenson, J.W.; Lukacs, K.D *Anal. Chem.* **1981**, *53*, 1298-1302.

64) Wu, C.T.; Lopes, T.; Patel, B.; Lee, C.S. *Anal. Chem.* **1992**, *64*, 886-891.

65) Musick, M.D.; Pena, D.J.; Sotsko, S.L.; McEvoy, T.M.; Richardson, J.N.; Natan, M.J. *Langmuir* **1999**, *15*, 844-850.

66) Kornienko, O.; Reilly, P.T.A.; Whitten, W.B.; Ramsey, J.M. *Rapid Commun. Mass Spectrom.* **1999**, *13*, 50-53.

67) Kornienko, O.; Reilly, P.T.A; Whitten, W. E.; Ramsey, J.M. *Anal. Chem.* **2000**, *72*, 559-562.

68) Fodor, S.P.A.; Read, J.L.; Pirrung, M.C.; Stryer, L.; Lu, A.T.; Solas, D. *Science* **1991**, *251*, 767-769.

69) Cho, C.Y.; Moran, E.J.; Cherry, S.R.; Stephans, J.C.; Fodor, S.P.A.; Adams, A.; Sundaram, A.; Jacobs, J.W.; Schultz, P.G. *Science* **1993**, *261*, 1303-1305.

70) Patchornik, A.; Amit, B.; Woodward, R.B. *J. Am. Chem. Soc.* **1970**, *92*, 6333-6334.

71) Jennane, J.; Boutros, T.; Giasson, R. *Can. J. Chem.* **1996**, *74*, 2509-2517.

72) Vossmeyer, T.; DeIonno, E.; Heath, J.R. *Angew. Chem. Int. Ed. Engl.* **1997**, *36*, 1080-1083.

Chapter 2

Materials and Methods

2.1 Experimental

2.1.1 Chemicals

All solvents utilized were of chromatographic grade or better and were used without further purification. Methyl methacrylate (Aldrich, 99%), trans-3-indoleacrylic acid, butyl methacrylate (Aldrich, 99%), 1,2-diaminoethane (Aldrich, 99%), 1,3-diaminopropane (Aldrich, 99%), *n*-butyllithium (Aldrich, 2.0 M in cyclohexane), *n*-octane-1-isocyanate (Aldrich, 98%), ninhydrin (Aldrich, 99%), hydrindantin (Aldrich, 98%), fluorescein isothiocyanate (Aldrich, 90%), sodium borate, sodium acetate, tetrachloroaurate (Strem, 99%), silver nitrate (Aldrich, 99%), sodium citrate dihydrate (Aldrich, 99%), sodium borohydride (Aldrich, 99%), 2-aminoethane thiol (Sigma, 95%), 1,3-dicyclohexylcarbodiimide (Aldrich, 99%), 4,5-dimethoxy-2-nitrobenzyl chloroformate (Sigma, 97%), triethylamine, *N*-hydroxysuccinimide (Aldrich, 99%), glycine (Aldrich, 99%), sodium hydroxide, sodium bicarbonate, sodium sulfate, 1,9-nonanedioic acid (Aldrich, 98%), 4-(2-hydroxyethyl)-1-piperazineethanesulfonic acid (Aldrich, 98%), 4-sulfobenzoic acid (Aldrich, 95%), and 1-ethyl-3-(3-dimethylaminopropyl)carbodiimide (Sigma, 99%) were used as received. The electroless Ag bath was obtained from Peacock Laboratories and used per manufacturer's specifications. Distilled water was filtered using a Barnstead reverse-osmosis water system; the filtered water was further purified using a Nanopure system resulting in water with a resistivity of 18 MΩ•cm.

2.1.2 PMMA Sheets

Several different suppliers were used as sources of the PMMA sheets, including Goodfellow, AIN Plastics, and ATO-Haas. PMMA sheets referred to as pristine are as-received materials. Plastic-coated PMMA sheets were machined to a given size or cut, using side cutters, before cleaning. The cleaning process consisted of removing the plastic protective layer, immersing the PMMA in 2-propanol for at least 2 hours, rinsing the PMMA in 18 MΩ •cm water, and completely drying the PMMA under a stream of high-purity N_2.

2.1.3 Preparation of PMMA Surface Chemical Modifiers

2.1.3.1 Preparation of *N*-lithiodiaminoethane and *N*-lithiodiaminopropane

N-lithiodiaminoethane and *N*-lithiodiaminopropane[1-2] were synthesized by first placing 6 mmol of dry diamine in a round-bottom flask. The diamine was purged with nitrogen for 20 min before the introduction of 1 mmol of n-butyllithium. Upon introduction of the *n*-butyllithium, a dark purple product, in the case of *N*-lithiodiaminoethane, was observed. Similarly, a yellow-brown product was evident upon the addition of *n*-butyllithium to the purged 1,3-diaminopropane. Each product was stirred for 3 h before use and was kept in the purged, sealed vessel for no longer than 1 week.

2.1.3.2 Synthesis of Au Colloids

Au colloids were prepared using the procedure documented by Grabar et al.[3] as well as Frens.[4] Briefly, 50 mL of 1 mM $HAuCl_4$ in 18 MΩ •cm water was brought to a rolling boil in a 100 mL round-bottom flask equipped with a condenser. To the rapidly

boiling, yellow solution was added 5 mL of 38.8 mM sodium citrate. A deep raspberry solution was evident after addition of the sodium citrate. The solution was allowed to boil an additional 10 min before the heating mantle was removed. The solution was cooled to room temperature and stored in brown bottles for future use.

2.1.3.3 Synthesis of Ag Colloids

Ag colloids were prepared according to Lee and Meisel[5] as well as Grabar et al.[3] Briefly, 50 mL of 1 mM $AgNO_3$ in 18 MΩ •cm water was brought to a rolling boil in a conical flask. The colorless solution was allowed to boil for 2 min before 1 mL of 38.8 mM sodium citrate was added to the flask. The solution was removed from the heating plate and allowed to cool to room temperature before being placed in brown bottles for future use.

2.1.3.4 Synthesis of Nitroveratryloxycarbonyl-glycine (NVOC-Gly)

All synthetic procedures were performed in the dark employing Al foil-covered glassware and were similar to those describes by Lapatsanis et al.[6] 4,5-dimethoxy-2-nitrobenzyl chloroformate, also known as nitroveratryloxychloroformate, NVOC, was used without further purification. In a clean, dry, 100 mL round-bottom flask, 100 mmol NVOC and 100 mmol *N*-hydroxysuccinimide (NHS) were stirred in 40 mL purged, dry tetrahydrofuran (THF). Using an addition funnel, 100 mmol dry triethylamine (TEA) in 20 mL THF was added to the round-bottom flask. The flask was purged with N_2 during the reaction. The reaction was allowed to proceed at room temperature for 1 h; the triethylamine hydrochloride was filtered, and the filtered mixture was evaporated under reduced pressure. The residue was dissolved in ethyl acetate, washed with 15 mL 18 MΩ •cm H_2O (3X), 15 mL 5% sodium bicarbonate

solution (3X), and washed again with 15 mL 18 MΩ •cm H_2O (3X). The succinimide ester derivative was evaporated under reduced pressure; yellow crystals resulted.

In a 50 mL conical flask, 100 mmol of yellow crystals of the succinimide ester were dissolved in 20 mL dioxane. Glycine (100 mmol) was dissolved in 10 mL 1 M NaOH and 20 mL 1 M sodium bicarbonate in 18 MΩ •cm H_2O. The succinimide ester derivative in dioxane was added, in one portion, to the aqueous solution with rapid stirring. Stirring continued for 1 h. The dioxane was then evaporated under reduced pressure. The remaining solution was acidified to pH 2 with 1 M HCl. The solution was extracted with 20 mL ethyl acetate (6X). The ethyl acetate solution was washed with 15 mL water (3X) and dried over sodium sulfate. The ethyl acetate solution was evaporated under reduced pressure overnight. The glycine derivative of 4,5-dimethoxy-2-nitrobenzylcarbonyl, NVOC-Gly, was yellow in color and used without any further purification. The crystals were stored in an N_2-purged, sealed vessel for no longer than 2 weeks.

2.1.4 Preparation of Chemically Modified PMMA Surfaces

2.1.4.1 Preparation of NH_2-Terminated PMMA Surfaces

PMMA sheets were machined (on edges) to a given size and then soaked in isopropanol until needed. Before modification, the machined PMMA pieces were rinsed with copious amounts of 2-propanol followed by extensive rinsing with 18 MΩ •cm water. The PMMA pieces were then dried under a stream of nitrogen. Following a 20 min nitrogen purge in a sealed vessel, the PMMA pieces were exposed to *N*-lithiodiaminoethane or *N*-lithiodiaminopropane (transferred by cannula or syringe). After a given period of time, the reaction was quenched with 18 MΩ •cm water. After

removal from the purged reaction vessel, the PMMA was rinsed with copious amounts of 18 MΩ•cm water, followed by drying under a stream of nitrogen.

2.1.4.1.1 Quantification of Amines on the Surface of NH_2-Modified PMMA

For all studies presented here, PMMA sheets were machined using standard milling techniques to produce pieces with dimensions of 15 mm x 15 mm x 3 mm. The total number of diamine molecules present on a given NH_2-modified PMMA sheet was determined using a variation of the ninhydrin method in conjunction with the method described by Ichijima et al.[2] Briefly, individual pieces of NH_2-modified PMMA were placed in an autoclavable test tube, and then 2.5 mL of 1.5 M HCl was added. After being capped, the tubes were placed in an autoclave at 121°C for 30 min, removed and then 1.0 mL each of 3.75 M NaOH and ninhydrin reagent were added to each tube. The ninhydrin reagent consists of 0.4 g ninhydrin, 0.06 g hydrindantin, 15.0 mL ethyleneglycol monomethylether, and 5.0 mL of pH 5.2, 6 M acetate buffer. After addition of ninhydrin reagent to each of the test tubes, the tubes were placed back in the autoclave for 10 min at 121 °C. Upon removal of the tubes from the autoclave, the resulting solution was allowed to cool to room temperature. The absorbance at 570 nm for each solution was obtained. A standard curve was prepared using varying concentrations of ethylenediamine (correlation coefficient=0.989), and the amine concentrations on the surface of the PMMA were calculated using this standard curve. All results are reported as $x_{ave} \pm$ one standard deviation.

2.1.4.2 Preparation of $C_{18}H_{37}$-Terminated PMMA Surfaces

Freshly prepared NH_2-terminated PMMA pieces were placed in an air-tight vessel, and the vessel was purged with nitrogen for 20 min before introduction of neat

n-octadecane-1-isocyanate. After a 10 min exposure to the *n*-octadecane-1-isocyanate, the PMMA pieces were then quickly rinsed with copious amounts each of hexanes, toluene, and acetone and then dried under a stream of nitrogen.

2.1.4.3 Preparation of Sulfonic Acid-Terminated PMMA Surfaces

Sulfonic acid-terminated PMMA (ST-PMMA) was synthesized according to peptide synthesis procedures.[7] Freshly-prepared NH_2-terminated PMMA surfaces were placed in a solution of 0.001 M 4-sulfobenzoic acid, 0.100 M 1-ethyl-3-(3-dimethylaminopropyl)carbodiimide (EDC), and 1 M HEPES buffer (Fisher) at pH 9 in 18 MΩ•cm water. The PMMA sheets remained immersed in the solution for at least 3 h. The $SO_3^-K^+(C_6H_4)$-terminated PMMA sheets were rinsed with copious amounts of 18 MΩ•cm and dried in a stream of N_2 before use.

2.1.4.4 Preparation of Carboxylic Acid-Terminated PMMA Surfaces

Carboxylic acid-terminated PMMA (CT-PMMA) was synthesized similar to standard peptide coupling procedures.[7] Freshly-prepared NH_2-terminated PMMA sheets were placed in a solution of 0.005 M 1,9-nonanedioic acid and 0.095 M dicyclohexylcarbodiimide, DCC, in purged ethanol. The $HOOC(C_9H_{19})$-terminated PMMA sheets remained immersed in the solution for at least 3 h. The $HOOC(C_9H_{19})$-terminated PMMA sheets were rinsed with copious amounts of ethanol and dried in a stream of N_2.

2.1.4.5 Preparation of NVOC-Terminated PMMA

NVOC-terminated PMMA was synthesized similar to standard peptide coupling procedures.[7] In a glass tube, 0.095 M dicyclohexylcarbodiimide and 0.005 M NVOC-Gly was dissolved in purged ethanol. After dissolution, freshly-prepared NH_2-

terminated PMMA was placed into the glass tube. The tube was capped with a septum and purged with N_2 for 20 min. The tube was placed on a shaker and the reaction was allowed to proceed for 3 h. The NVOC-terminated PMMA piece was then removed and rinsed with copious amounts of ethanol.

2.1.4.6 Photolysis of NVOC-Terminated PMMA to Produce Deprotected NH_2-Terminated PMMA

An Ealing mercury arc lamp operated at 150 W was utilized for the deprotection of NVOC-terminated PMMA surfaces. A water-filled cylindrical filter was used to remove any infrared radiation, and a 320 nm-505 nm bandpass filter was used to filter any undesirable UV light. The NVOC-terminated PMMA was either irradiated without a mask or masked with a chrome/quartz mask or a printed transparency film. The NVOC-terminated PMMA was exposed to the visible radiation for 10-240 min. After exposure, the deprotected NH_2-terminated PMMA was rinsed with copious amounts of 18 MΩ •cm water and dried in a stream of nitrogen.

2.1.4.7 Electroless Deposition of Au on Amine-Modified PMMA Surfaces

Au was electrolessly deposited on PMMA pieces by first immersing clean, dry NH_2-modified PMMA pieces in 5.0 X 10^{-4} M $HAuCl_4$ for given amounts of time. The pieces were removed from the solution, rinsed with copious amounts of 18 MΩ •cm water and dried in a stream of nitrogen. The PMMA pieces were then placed in a solution of 0.1 M $NaBH_4$ (Aldrich) for 1 min in order to reduce the Au ions. After removal of the PMMA pieces from the $NaBH_4$ solution, the PMMA pieces were rinsed with copious amounts of 18 MΩ •cm water in order to remove any unbound species. The rinsed PMMA pieces were dried under a stream of nitrogen.

2.1.4.8 Electroless Deposition of Ag on Seeded PMMA Pieces

A conventional electroless Ag bath was employed to deposit Ag on Au-seeded PMMA surfaces. The bath was prepared according to manufacturer's specifications, which included first diluting each of the three components of the bath 1:32 in 18 MΩ •cm water and then mixing aliquots of the three diluted solutions together. Au-seeded PMMA pieces were placed in the three-component electroless Ag bath for no longer than 2 min. The pieces were removed from the electroless Ag bath, rinsed in 18 MΩ •cm water, and dried in a stream of nitrogen.

2.1.4.9 Deposition of Metal Colloids on NH_2-Modified PMMA Surfaces

Deposition of the metal colloids entailed immersing clean, dry NH_2-modified PMMA pieces in the gold colloid solution for given amounts of time. After deposition of the colloids on PMMA surfaces, the PMMA pieces were rinsed with copious amounts of 18 MΩ •cm water and dried in a stream of nitrogen. Thick colloidal films of metal colloids were prepared by immersing a metal colloid/PMMA surface in a 0.010 M solution of 2-aminoethanethiol in ethanol for 1 h. The metal colloid/PMMA sheet was rinsed with copious amounts of purged ethanol and 18 MΩ •cm water before being placed back into the Au colloid solution for 1 hour. These steps were repeated at least twelve times.[3, 9-10]

2.1.5 Analytical Techniques

2.1.5.1 Differential Scanning Calorimetry

Calorimetry measurements were obtained using a Seiko II Instruments SSC 5200 Differential Scanning Calorimeter coupled with a Seiko II Data Acquisition and

Analysis System. PMMA samples (~5 mg) were placed in aluminum pans designed for thermogravimetric analysis. An empty pan was used as the reference. The sample was heated from an initial temperature of 25 °C at a rate of 2 °C per minute to the final temperature of 155 °C under a nitrogen atmosphere. Glass transition temperatures (T_g) were measured at the onset temperature of the transition using the available Seiko II software.

2.1.5.2 Matrix-Assisted Laser Desorption/Ionization-Mass Spectrometry

Linear time-of-flight matrix-assisted laser desorption/ionization (MALDI) mass spectrometry (MS) of analytes was obtained using a PerSeptive Biosystems Voyager Model or a Bruker Proflex equipped with a nitrogen laser operating at λ=337 nm. The analytes were dissolved in HPLC grade acetone at a concentration of approximately 1 x 10^{-4} M. The matrix used, trans-3-indoleacrylic acid (IAA), was also dissolved in the same HPLC grade acetone to a concentration of 2 x 10^{-2} M. Matrix solution was mixed with the sample solution in a 5:1 ratio by volume. This proportion of matrix and sample was found to give the best results. Once the sample and matrix were mixed, a small volume (~10 μL) of the mixture was pipetted onto the sample plate of the mass spectrometer and allowed to dry in the laboratory ambient before introduction into the ionization chamber (pressure ~10^{-6} torr). Spectra were collected with the low mass gate on. Calibration was performed using insulin and angiotensin.

2.1.5.3 Gel-Permeation Chromatography (GPC)

Chromatographic data were obtained on a locally constructed instrument that employed a Waters 6000 Series chromatography pump delivering filtered tetrahydrofuran (THF) mobile phase to a 0.78 X 30 cm Polymer Laboratories cross-

linked polystyrene column (mixed bed particle size 10 μm). This column provides for linear separation of polymers with molecular masses in the range of 500-10 M amu. Dual detection was made possible through the use of a Chromatix KMX-6 low angle He-Ne laser (λ=632.8 nm) light scattering detector in series with a Varian RI-3 differential refractive index detector (DRI). Calibration of the system was performed before the start of each set of runs. After filtering the sample (approximately 5.00 mg PMMA sample/1.00 mL THF) with a 0.45 μm pore filter, the analyte was injected using a 20 μL injection loop. Data acquisition and analysis was performed with locally written software.

2.1.5.4 Gas Chromatography-Mass Spectrometry

A Hewlett Packard 5890 Series II Gas Chromatograph employing a 20 m, 0.18 mm inside diameter J&W column (0.25 μm thick, cross-linked 5%phenyl/95%methyl polysiloxane stationary phase) and He carrier gas were used in these studies. Detection was accomplished with a Hewlett Packard 5971 Mass Selective Detector. Approximately 0.1-0.3 g pieces of PMMA were cut from a given sheet using side cutter pliers, rinsed with IPA and 18 MΩ •cm water, followed by drying in a stream of nitrogen. The sample mass was then recorded before being dissolved in 5.00 mL of chloroform. Butyl methacrylate (BMA) was added as an internal standard (2 μL, 1.26 x 10^{-5} mol). Standard solutions of MMA were made by dissolving known amounts of MMA (1-70 μL) in 5.00 mL of chloroform and adding BMA (2 μL, 1.26 x 10^{-5} mol) as an internal standard. Standard solutions were injected and the integrated peak areas were plotted versus the known concentrations of added MMA. A standard calibration curve was constructed and the correlation coefficient was determined to be 0.9894.

Each concentration of standard and each PMMA sample were analyzed five times. The concentration of MMA in each PMMA sample was determined from this curve. Values are reported as $x_{ave} \pm$ one standard deviation.

2.1.5.5 Scanning Force Microscopy (SFM)

Pristine and chemically modified PMMA samples that were imaged with the SFM were rinsed with 2-propanol and then 18 MΩ •cm water, and dried with nitrogen before mounting on a magnetic sample puck with double-sided adhesive. PMMA pieces that were microtomed perpendicular to their faces were imaged without any further processing of the surface. A Digital Instruments Nanoscope III multimode scanning force microscope (Veeco, Inc., Santa Barbara, CA) operated in contact mode making use of the "D" scanner (13 μm x 13 μm) was used for all images presented here. After acquisition, images were corrected for piezoelectric bow by use of "flattening" software provided by the manufacturer.

2.1.5.6 Solid Phase Microextraction (SPME)

SPME[11] was employed to determine the identity of volatiles possibly produced upon heating the PMMA sheets. Various masses of Goodfellow 1.6 mm PMMA were placed in a 1.0 mL sampling vial, sealed with a septum, and held at 70°C for 2 hours. An SPME fiber (Supelco, Bellefonte, PA) coated with Carboxen/polydimethylsiloxane (75 μm in thickness) was in contact with the headspace during the heating period. The volatiles were absorbed into the coating of the fiber and subsequently desorbed in the 250°C injector port of the GC-MS. For the time period that the fiber was in the injector port of the GC-MS, the column was maintained at 40 °C. Due to the fact that MMA elutes from the column at ~3.2 min, a gradient temperature program was not employed.

The fiber was heated at 280 °C in the injector port of the GC-MS between runs in order to ensure total desorption of volatiles from the fiber coating.

2.1.5.7 Contact Angle Measurements

Sessile drop contact angle measurements utilizing 18 MΩ •cm water were performed with a VCA 2000 Contact Angle System (VCA, Billerica, MA). Approximately 6 μL of 18 MΩ •cm water was placed on the various PMMA surfaces using a syringe. Contact angle values were calculated using the software provided by the manufacturer. The left and right contact angles of the water drops were measured immediately after placement of the water droplet on the PMMA surfaces; it was found in all cases that there was no difference in the left and right contact angles. Each value reported here is the average of at least 5 separate drops of water on a given substrate; values were found not to vary significantly among a set of substrates from a given preparation.

2.1.5.8 Reflection-Absorption Infrared (RAIR) Spectroscopy

In order to examine the molecular nature of pristine and chemically modified PMMA, RAIRS studies were employed. In these experiments, glass microscope slides (Fisher, 3" x 1", 1 mm thick) were sonicated in 2-propanol for 30 min and then rinsed with copious amounts of 18 MΩ•cm water before exposure to 3:1 98% sulfuric acid:30% hydrogen peroxide solution. ***Caution! The cleaning solution is highly reactive and should be handled with extreme caution. This solution should be disposed of upon completion of glass slide cleaning to avoid explosions.*** After exposure to the cleaning solution, the slides were first rinsed with copious amounts of

18 MΩ•cm water and rinsed again with ethanol before being dried in a stream of nitrogen. The cleaned slides were placed in an Edwards 306A (Edwards, UK) cryogenically pumped vacuum chamber, and they were allowed to remain in the chamber until the pressure reached 1 x 10^{-7} torr. Chromium was evaporated onto the slides at a rate of 0.5 nm sec^{-1} to a final thickness of 5 nm. After the chromium deposition, gold was evaporated onto the slides at a rate of 1 nm sec^{-1} to a final thickness of 220 nm. The evaporation rates, as well as the final thicknesses of the Cr and Au layers, were determined by an *in vacuo* quartz crystal microbalance. After evaporation, the gold slides were immediately placed in absolute ethanol. The slides were removed from absolute ethanol prior to further experimentation.

PMMA was spin coated onto the gold slides by means of a Specialty Coating Systems Spin-Coater (Specialty Coating Systems, Indianapolis, IN). Commercial sheet PMMA (Goodfellow) was dissolved in dichloromethane to yield a solution with a final concentration of 0.5 mg PMMA mL^{-1} dichloromethane. This solution was dropped onto the spinning Au slide (2200 rpm), and the Au slide was allowed to spin for 70 sec. The PMMA-coated slide was then ready for chemical modification and/or analysis.

A Nicolet 740 FTIR Spectrometer (Nicolet, Madison, WI) with a liquid nitrogen-cooled, wide-band MCT detector was used in these studies. The instrument was outfitted with a versatile reflection accessory with a retro-mirror attachment (VRA-RMA) that was supplied by Harrick Scientific. Radiation impinged on the sample at an incident angle of 86° with respect to the substrate normal. A wire grid polarizer (Harrick Scientific) was used to provide *p*-polarized light. The analyzing chamber was sheathed in a glovebag, and the optical bench and sample compartment were purged

with house nitrogen that had been scrubbed with a homemade CO_2 and water scrubbing system. All reflection-absorption infrared spectra are the result of 1024 scans referenced against a bare Au background. Purge corrections to remove residual water vapor bands from the RAIR spectra and baseline corrections were performed with the Nicolet software.

2.1.5.9 X-ray Photoelectron Spectroscopy (XPS) Studies

Pristine PMMA and chemically modified PMMA surfaces were prepared as described above. The PMMA surfaces were analyzed with a Kratos AXIS Ultra X-ray Photoelectron Spectrometer (Kratos, UK). Measurements were obtained using a monochromatic Al-Kα X-ray source (240 W) and charge neutralization. The samples were analyzed with a 90° take-off angle. Deconvolution of spectral peaks was performed using the Kratos software.

2.1.5.10 Confocal Fluorescence Microscopy Studies

Freshly prepared NH_2-terminated PMMA surfaces, as well as pristine PMMA surfaces, were placed in a fluorescein isothiocyanate (FITC) conjugation solution (1 μM FITC, 1% IPA/99% H_2O, and 10 mM, pH 9.2 borate buffer) and held in the dark on a slow shake (shaker table) for 23 h. The PMMA pieces were removed from the conjugation solution, rinsed three times each with 18 MΩ •cm H_2O, 2-propanol, and 18 MΩ •cm H_2O, and then dried under a stream of nitrogen.

Two-dimensional confocal fluorescence microscopy images were collected through use of an Odyssey XL Confocal Laser Scanning Microscope (Noran Instruments) in conjunction with an Argon ion laser (Coherent Lasers, 488 nm excitation). The fluorescence emission was collected with a 100X microscope objective

then spectrally filtered using a 515 nm long pass filter and spatially filtered with a 10 μm slit before being detected with a charge-coupled device (CCD). One hundred Z-series images were collected at a rate of 0.10 μm per image and each image was a jump average of 32 frames.

2.1.5.11 Near-Infrared (NIR) Fluorescence Microscopy Studies

Freshly prepared NH_2-terminated PMMA surfaces, as well as pristine PMMA surfaces, were placed in a conjugation solution consisting of an infrared fluorescent dye, IRD-38 (1 μm), H_2O, and 10 mM, pH 9.2 borate buffer. The PMMA was immersed in the solution and placed on a shaker for 23 h. The PMMA pieces were removed from the conjugation solution, rinsed three times with 18 MΩ •cm H_2O, and then dried under a stream of nitrogen.

The scanning fluorescence microscope that was employed is a home-built system consisting of pulsed diode laser (PicoQuant GmbH, model 800, Berlin, Germany) operated at 780 nm and focused onto the surface by a 40X microscope objective. The data was collected using a charge-couple device; home-built software was used to view the data.

2.1.5.12 Electrochemical Studies of $K_3Fe(CN)_6$

All electrochemistry experiments were performed in normal three-electrode mode using a Princeton Applied Research Potentiostat/Galvanostat Model 273A and a Yokogawa 3025 X-Y Recorder. Conventional glass electrochemical cells with medium porosity ceramic frits were used. The electrolyte in these experiments was 1 M KCl (Aldrich) and the electroactive species was 5 mM $K_3(Fe(CN)_6)$. All voltammetry is displayed as standard *i* vs. *E* (current vs. potential) curves.

2.1.5.13 Ultraviolet-Visible Spectroscopy

Au colloids and electrolessly deposited Au layers on PMMA surfaces were characterized using an Aviv Model 14DS UV-VIS-IR Spectrophotometer with the averaging time set to 2 s. Grooved Teflon slips were placed in quartz cuvettes and PMMA pieces (45 mm long X 6 mm wide X 0.5 mm thick) were inserted into the grooves of the Teflon slips. In all cases, AT-PMMA was used as the background for these experiments.

2.2 Theory of Reflection-Absorption Infrared (RAIR) Spectroscopy

Two common methods for studying the molecular nature of surface species include attenuated total reflectance (ATR) infrared spectroscopy and reflection-absorption infrared (RAIR) spectroscopy. A conventional infrared instrument is used with both ATR-IR and RAIR spectroscopy; the only exception is that the sample compartment is modified such that the infrared radiation interacts with the sample on a reflective surface. In the case of ATR-IR, the sample is firmly pressed onto an internal reflection element. The internal reflection element is a high-refractive-index material such as zinc selenide, silicon, or germanium. The element is cut to a trapezoidal shape such that the angles of the trapezoid are 30°, 45°, or 60° with respect to the surface normal. Incident infrared radiation enters the ATR element and propagates through the element by total internal reflection. This total internal reflection is possible due to the refractive index of the highly dense ATR element versus the less dense sample. Total internal reflection occurs when the angle of reflection reaches a critical angle. In spite of total internal reflection, a small amount of radiation does penetrate into the sample due to diffraction at the edges of the incident beam. This radiation interacts

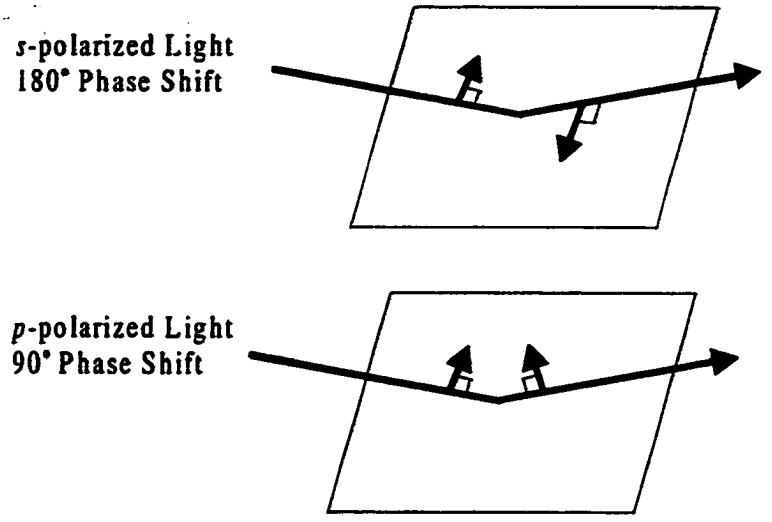

Figure 2.1 **Schematic of the electric field vectors associated with impingement and reflection from a reflective surface.**

with the sample before reentering the ATR element. The depth of penetration, d_p, of the radiation into the sample depends on the wavelength of radiation, the difference in the refractive indices of the ATR element and the sample, and the angle of the radiation at the ATR element/sample interface.[12]

Reflection-absorption infrared (RAIR) spectroscopy is still another technique developed for the characterization of thin films on surfaces. In RAIR spectroscopy, infrared radiation is directed at a highly reflective surface onto which has been adsorbed a monolayer or thin film.[13] The infrared radiation is directed at the surface at near grazing angles; thus, the incident and reflected radiation are able to constructively combine and form a standing wave positioned normal to the surface. This standing wave interacts with the adsorbed species present on the surface, resulting in intensity losses corresponding to matches of the frequency of the infrared radiation to the vibrational modes of the surface-bound species. It has been shown by Greenler[14] that

the incident radiation must impinge on the reflective surface at near-grazing angles; at angles higher than near grazing, the incident and reflected beams destructively interfere, resulting in no appreciable standing wave. The importance of this concept can be more properly explained by considering the polarization of the infrared radiation impinging on the reflective surface. Displayed in Figure 2.1 is a schematic of the electric field vectors associated with impingement and reflection of radiation from a reflective surface at grazing angles. In the case of *s*-polarized light, there is a 180° phase shift at all angles of incidence; thus, the incident and reflected vectors cancel each other, resulting in no interaction with adsorbed species on the surface. In contrast, the *p*-polarized light undergoes a 90° phase shift upon reflection from the surface. Thus, the incident and reflected electric vectors combine, forming a surface wave of non-zero amplitude that can interact with the adsorbed surface-bound species. This phase shift is highly dependent on the angle of incidence, as noted in studies performed by Greenler.

The optimum angle of incidence of a given material i can be ascertained by considering Equations 2.1 and 2.2.

Equation 2.1 $\tilde{n}_i = n_i - ik_i$

In this equation, $\tilde{n}_i$ refers to the frequency-dependent complex refractive indices of the material, n_i is the real refractive index, and k_i is the absorption coefficient. From this equation, it is understood that the frequency-dependent complex refractive indices are directly related to the real refractive index and the absorption coefficient. The optimum angle at which light of a given wavelength impinges on a reflective metal surface can be determined by the use of Equation 2.2.

Equation 2.2 $\beta = (2\pi\tilde{n}_i d \cos \Phi_i)/\lambda$

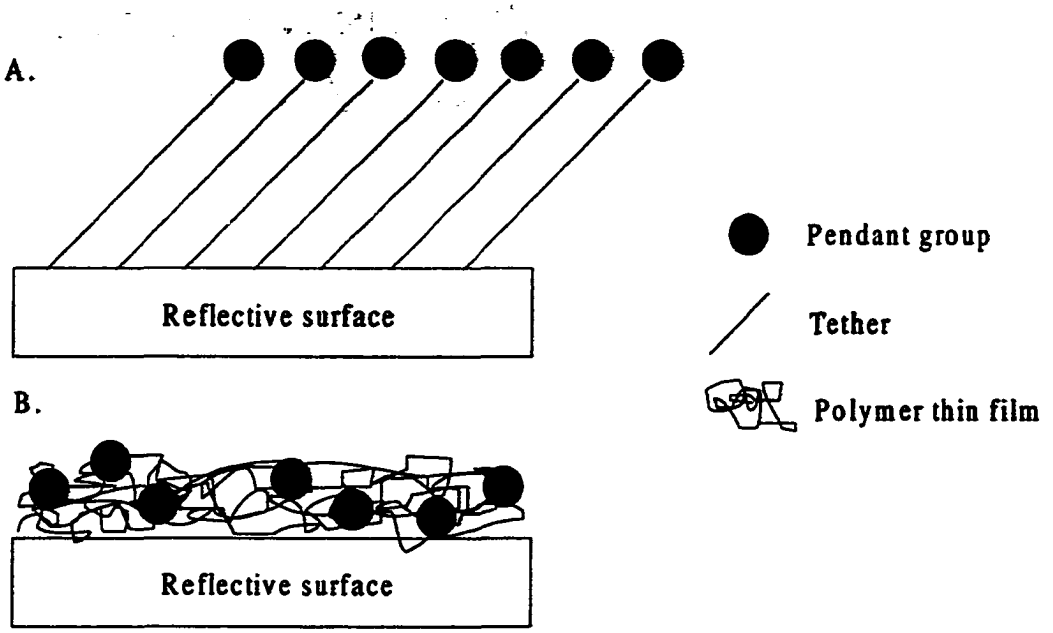

Figure 2.2 **Depiction of A. the highly ordered surface present in the case of self-assembled monolayers compared to B. the disordered nature of the pendant groups in polymer thin films.**

In this equation, β represents the change in phase of the light beam caused by one traversal of the film, d is the thickness of the film, and λ is the wavelength of radiation. Studies by Greenler[14] concluded that the optimum angle of incidence is 88° for Au; however, this angle is experimentally optimized depending on the film thickness and the reflective substrate used.

RAIR spectroscopy has traditionally been used as a tool for the characterization of self-assembled monolayers on reflective surfaces. In the studies presented here, RAIR spectroscopy is utilized for the characterization of spin-coated polymer films on reflective substrates. These films, pristine or chemically modified, are present not as close-packed, ordered entities bearing functional groups but rather as random, unordered polymer pendant groups tethered to a common backbone, Figure 2.2. Thus,

the modifiable pendant groups that are of interest can be present at all angles from the surface normal as compared to the relatively ordered nature of thiols self-assembled on a metal surface. An important aspect of this discussion is that *p*-polarized radiation will excite molecules only if they contain transition dipole moments with a component perpendicular to the surface normal. It is possible, using RAIR spectroscopy, to ascertain the direction of the transition dipoles; thus, in the case of self-assembled monolayer characterization, the orientation of the surface-bound adsorbed molecules can be deduced.[17]

2.3 Theory of Scanning Force Microscopy (SFM)

Scanning force microscopy (SFM), or atomic force microscopy (AFM), was first described by Binnig et al. in 1986 and is employed to image the two-dimensional architecture of non-conducting or conducting surfaces. SFM has been used to

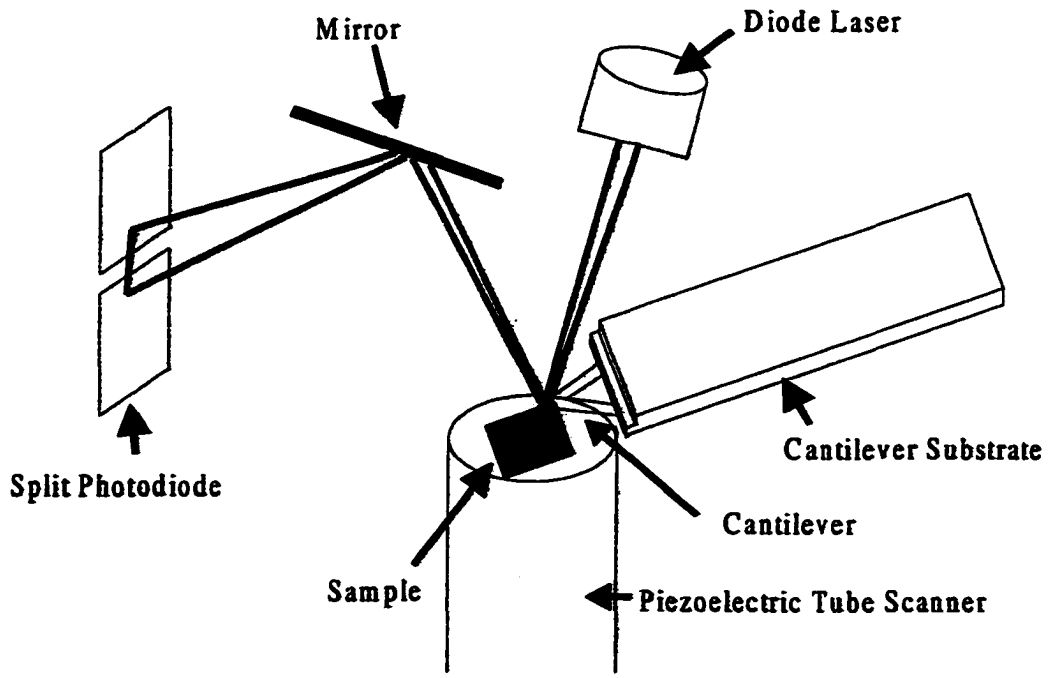

Figure 2.3 Primary components of the scanning force microscope.

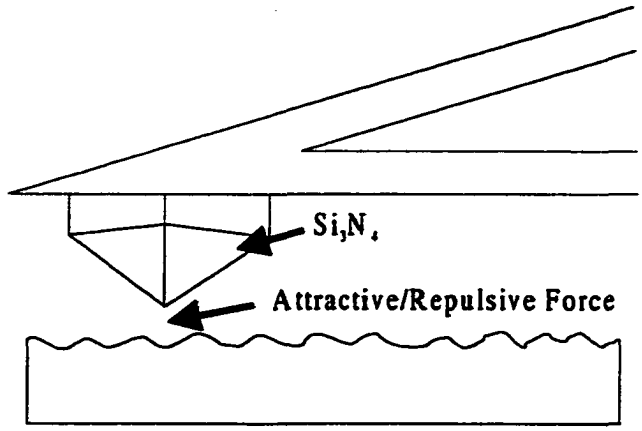

Figure 2.4 Pictorial depiction of the interaction of an SFM tip with a sample surface.

determine the surface topographical features of such biological molecules as DNA[19] and proteins[20] adsorbed on surfaces; in addition, SFM has been used to probe the intermolecular spacings of organized organic thin films.[21]

A scanning force microscope consists of four primary components, including a piezoelectric tube scanner, a cantilever-mounted tip, a position-sensitive photodiode detector, and an electrical feedback mechanism for the micropositioner. These components are displayed in Figure 2.3. The sample is mounted on the piezoelectric tube scanner that moves the sample in the X and Y directions below the cantilever-mounted, pyramidal, Si_3N_4 tip. A laser beam is positioned over the cantilever-mounted tip and reflected off of the cantilever to a mirror. The mirror reflects the laser beam to a position-sensitive photodiode. This detection system is used to follow the vertical displacement of the cantilever as the surface is scanned.

The cantilever onto which the tip is mounted acts as a spring with a force constant between 0.1-100 N/m; this spring deflects according to the force between the

tip and the surface.[22] The deflection is monitored as a function of the lateral displacement of the tip. This sensor, the cantilever-mounted tip, is perhaps the most important part of a scanning force microscope and is depicted in Figure 2.4. The force between the tip and the sample, F_N, is related to the spring constant of the cantilever, k_N, and the cantilever displacement, Δz, by the relationship presented in Equation 2.3.

Equation 2.3 $$F_N = k_N \Delta z$$

The forces in question are those present when the tip and the sample are brought into close contact and include Van der Waals forces and contact repulsion forces when the microscope is operated in contact mode. These forces are monitored by the vertical deflection detector, and as the sample is scanned, a topographic image is obtained.

2.4 Theory of Water Contact Angle Measurements

Water contact angle studies represents a fast, qualitative test of the wettability characteristics of surfaces. Several tables and data sets have been constructed reporting the angle of water contact on various surfaces of known molecular composition.[23] By comparing water contact angles on surfaces with unknown molecular composition with those water contact angles on surfaces of known molecular composition, a qualitative characterization of the unknown surface can be attained.[24]

A sessile drop water contact angle goniometry system consists of a stage and magnifying optical camera. The sample is placed on the stage; a drop of water of known volume is placed on the sample and allowed to remain on the surface in the same position for a given amount of time. The magnifying camera captures the image of the water drop and the angle of water contact is measured using a software package or by direct microscopic measurement.

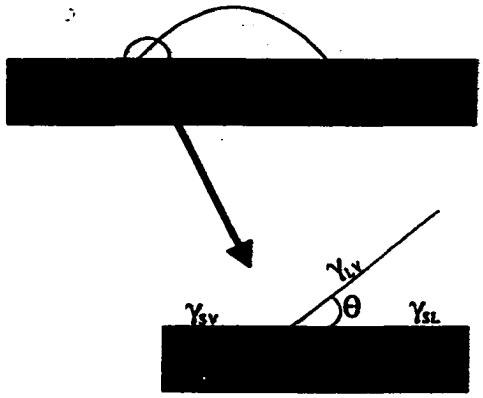

Figure 2.5 Contact angle geometry used in deriving Young's equation.

In the chapters that follow, water contact angle measurements are used strictly as a qualitative determination of surface energetics. That is, in water contact angle goniometry, the surface energies are qualitatively assigned depending on the measured water contact angle. When the measured angle of water contact is low, the surface energy is high; the surface is hydrophilic.[24] Conversely, when the measured angle of water contact is high, the surface energy is low; the surface is hydrophobic. This result is derived from Young's equation, Equation 2.4.

Equation 2.4 $$\gamma_{SV} - \gamma_{SL} = \gamma_{LV} \cos \theta$$

In Young's equation, γ_{SV} refers to the free energy at the solid-vapor interface, γ_{SL} refers to the free energy at the solid-liquid interface, γ_{LV} refers to the free energy at the liquid-vapor interface, and θ is the angle of water contact. The geometry used to derive Young's equation is represented in Figure 2.4.

While water contact angle studies have been used for the quantitative determination of interfacial tensions, only qualitative, comparitive studies have been performed in this work. In all cases, water contact angle goniometry was used only as a

quick and simple characterization tool for the comparison of surfaces before and after chemical modification.

2.5 References

1) 1) Karandikar, B.; Puschett, J.; Matyjaszewski, K. *Polymer Prep.* **1989**, *30*, 250-251.

2) Ichijima, H.; Kobayashi, H.; Ikada, Y. *J. Cataract Refract. Surg.* **1992**, *18*, 395-401.

3) Grabar, K.C.; Freeman, R.G.; Hommer, M.B.; Natan, M.J. *Anal. Chem.* **1995**, *67*, 735-743.

4) Frens, G. *Nature Phys. Sci.* **1973**, *241*, 20-22.

5) Lee, P.C.; Meisel, D. *J. Phys. Chem.* **1982**, *86*, 3391-3395.

6) Lapatsanis, L.; Milias, G.; Froussios, K.; Kolovos, M. *Synthesis* **1983**, 671-673.

7) Atherton, E. *Solid-Phase Peptide Synthesis: A Practical Approach*, IRL Press: New York, 1989.

8) Moberg, P.; McCarley, R.L. *J. Electrochem. Soc.* **1997**, *144*, 151-153.

9) Bright, R.M.; Musick, M.D.; Natan, M.J. *Langmuir* **1998**, *14*, 5965-5701.

10) Grabar, K.C.; Brown, K.R.; Keating, C.D.;Stranick, S.J.; Tang, S.; Natan, M.J. *Anal. Chem.* **1997**, *69*, 471-477.

11) Zhang, Z.; Yang, M.J.; Pawliszyn, J. *Anal. Chem.* **1994**, *66*, 844A-853A.

12) Harrick, N.J. *Internal Reflection Spectroscopy*, Interscience Publishers: New York, 1967.

13) Francis, S.A.; Ellison, A.H. *J. Opt. Sci.* **1959**, *49*, 131-138.

14) Greenler, R.G. *J. Chem. Phys.* **1966**, *44*, 310-315.

15) Nuzzo, R.G.; Allara, D.L. *J. Am. Chem. Soc.* **1990**, *112*, 558-569.

16) Porter, M.D.; Bright, T.B.; Allara, D.L.; Chidsey, C.E.D. *J. Am. Chem. Soc.* **1987**, *109*, 3559-3568.

17) Nuzzo, R.G.; Dubois, L.H.; Allara, D.L. *J. Am. Chem. Soc.* **1990**, *112*, 558-569.

18) Binnig, G.; Quate, C.F.; Gerber, C. *Phys. Rev. Lett.* **1986**, *56*, 930-933.

19) Hansma, H.G.; Vesenka, J.; Siegerist, C.; Kelderman, G.; Morrett, H. Sinsheimer, R.L.; Elings, V.; Bustamante, C.; Hansma, P.K. *Science* **1992**, *256*, 1180-1184.

20) Aucoin, J.P.; Hammer, R.P; McCarley, R.L.; McLaughlin, M.L.; Russo, P.S., in preparation.

21) Widrig, C.A.; Alves, C.A.; Porter, M.D. *J. Am. Chem. Soc.* **1991**, *113*, 2805-2810.

22) Takano, H.; Kenseth, J.R.; Wong, S.-S., O'Brien, J.C.; Porter, M.D. *Chem. Rev.* **1999**, *99*, 2845-2890.

23) Bain, C.D.; Evall, J.; Whitesides, G.M. *J. Am. Chem. Soc.* **1989**, *111*, 7155-7164.

24) Ulman, A. *An Introduction to Ultrathin Organic Films: From Langmuir-Blodgett to Self-Assembly*, Academic Press, Inc.: New York, 1991.

Chapter 3

Bulk Properties of Commercial PMMA Sheets

3.1 Introduction

Described here are initial studies of several commercially available PMMAs both before and after exposure to hard X-rays. In order to gain knowledge about the chemical changes that occur during resist preparation (gluing to substrate, etc.) and exposure, several analytical spectroscopic, chromatographic, and thermal methods have been applied. Thermal analysis methods were employed to gain knowledge about the effects of pre-exposure annealing of PMMA on radiation-induced swelling. In addition, gel-permeation chromatography (GPC) and matrix-assisted laser desorption/ionization-mass spectrometry (MALDI-MS) were used to obtain information concerning polymer/oligomer characteristics.

3.2 Radiation-Induced Swelling

One of our first observations from the exposure of thick PMMA sheets (d_{sheet}>50 μm) was that there was significant swelling in exposed areas. This observation has recently been noted by other authors in work associated with latent image formation.[1] Our work indicates that the degree of swelling upon X-ray exposure is a function of the source (vendor) and the thickness of the PMMA sheet. That is, for the same equivalent dose (4666 mA min), swelling was found to be a function of PMMA thickness and vendor, but there was no clear trend. The use of various-sized Al filters resulted in minimized swelling upon exposure of the PMMA sheet with X-rays. Without proper filtering, swelling increases with increasing PMMA thickness. As an example of

optimization of Al filtering conditions, two PMMA sheets, 300 μm in thickness, were exposed (bottom dose of 3 kJ/cm^3) using 3 μm and 6 μm thick Al filters. The amount of swelling for the thinner Al filter was found to be 295 μm and 0 μm (undetectable) for the thicker filter. By using the thicker filter, the radiation peak intensity was reduced and the peak energy shifted to a higher value. Such conditions for the thicker filter led to an increased time of exposure in order to obtain the same equivalent dose. Thus, from results of the thicker Al filter, we propose that the reduced rate of chain scission and the smaller rate of volatiles production that accompanies it result in decreased swelling in the PMMA sheets. Thicker sheets would then be more prone to swelling if the dose rate were the same as that used for a thinner sheet. These arguments all have as their basis the idea that the rates of production of volatiles in and their subsequent diffusion out of the *solid* PMMA must be near equal to prevent swelling of the PMMA. If volatiles are produced too quickly, bubbles form in the PMMA which eventually lead to cracking, the formation of micro-voids, and delamination of the plating base substrate.

3.3 Determination of PMMA Molecular Mass by Gel-Permeation Chromatography (GPC)

In order to determine whether or not the traditional mechanism of radiation-induced decomposition of PMMA was applicable to the thick PMMA sheets, we employed two techniques to obtain the average molecular weight of the PMMA before and after irradiation. Gel-permeation chromatography (GPC) indicated that the M_w of the various pristine PMMAs was in the 1-3 million amu range. Shown in Figure 3.1 are GPC chromatograms of a pristine Goodfellow PMMA sheet before and after irradiation.

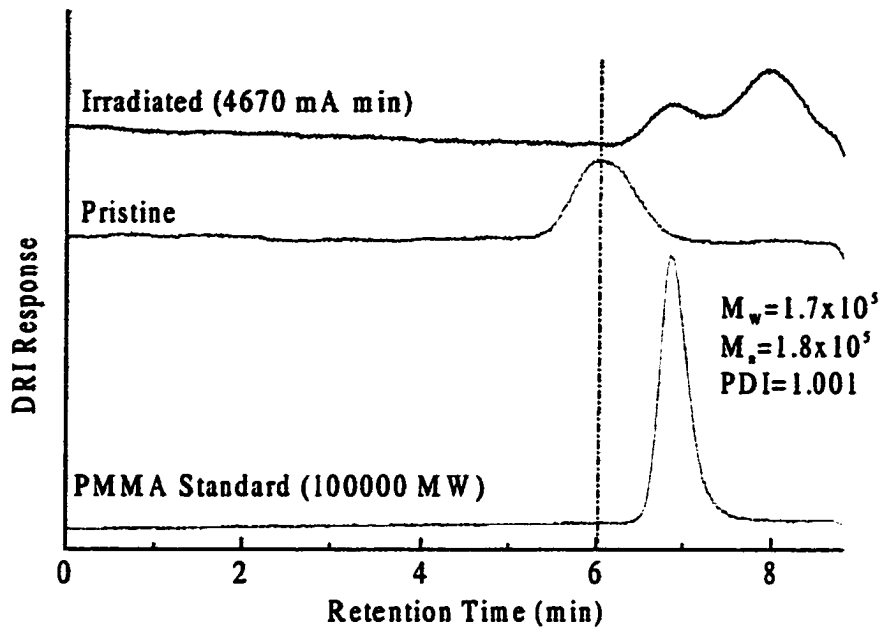

Figure 3.1 **Gel-permeation chromatograms of pristine and irradiated commercial PMMA as well as M_w = 100000 amu standard.**

Upon irradiation there is a reduction in the average molecular mass by early 45-fold. This result is typical of that seen for all other PMMAs used here, but the magnitude of the molar mass decrease appeared to be a function of total dose. It is clear that there is a substantial reduction in the polymer mass, as previously observed with powders,[2] multilayers,[3] cast films,[4] and blocks[5] of PMMA.

3.4 Determination of PMMA Molecular Mass by Matrix-assisted Laser Desorption/Ionization-Mass Spectrometry (MALDI-MS)

Due to the fact that there is no *absolute* molecular weight determination with GPC, we undertook a fundamental study of the mass spectrometric determination of PMMA molecular weights. Matrix-assisted laser desorption/ionization-mass spectrometry (MALDI-MS) has recently become a powerful tool in the analysis of synthetic polymers.[6-7] Information regarding the absolute average molecular weight of

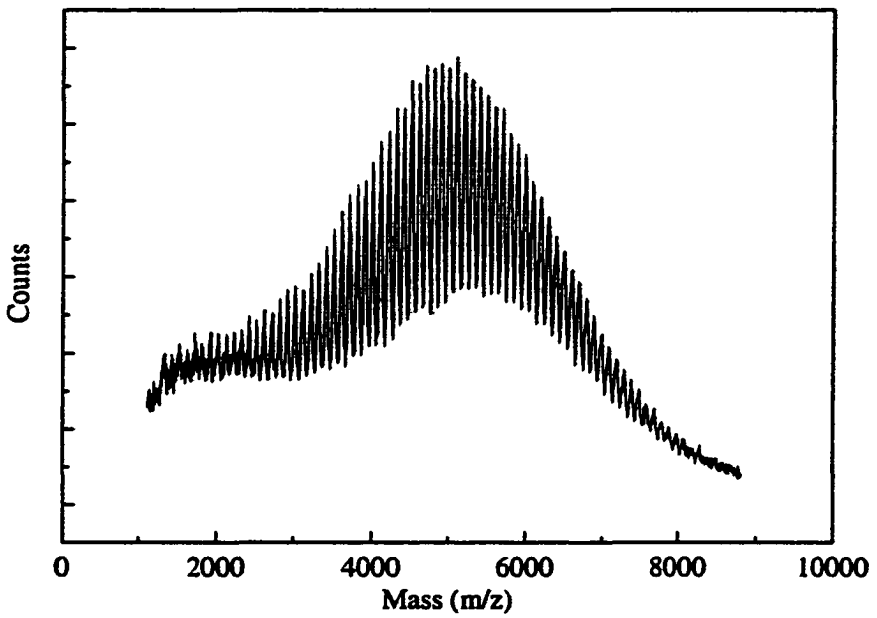

Figure 3.2 MALDI mass spectrum of PMMA standard (M_w = 5700 amu).

polymers can be obtained if the analyte can be transferred to the gas phase and ionized. This can be accomplished by the use of ultraviolet light absorbing matrices that act as a vehicle for gas-phase transfer and ionization. A study by Belu et al.[8] and another by Pasch and Gores,[8] as well as other works,[10-11] indicated that small molecular weight PMMAs could be analyzed by MALDI-MS when indoleacrylic acid or 2,5-dihydroxybenzoic acid were used as the matrix. Shown in Figures 3.2 and 3.3 are MALDI mass spectra of M_w = 5700 and M_w = 28350 PMMA standards (manufacturer-stated polydispersity index, PDI = 1.06 and 1.03, respectively) obtained in our laboratories using indoleacrylic acid as the matrix. The individual monomer repeat masses (ΔM = 100 amu) are resolved in the spectrum of the M_w = 5700 sample, but not in the M_w = 28350 spectrum. We find the molecular weights of the two standards, as found by manufacturer's GPC analyses, agree quite well with the values found by

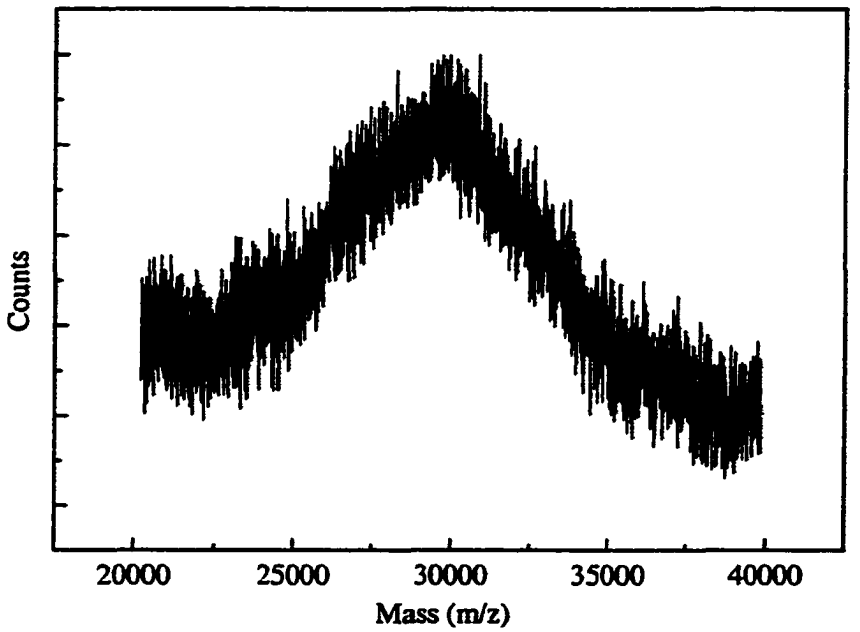

Figure 3.3 MALDI mass spectrum of PMMA standard (M_w = 28350 amu).

MALDI-MS. The ability to obtain high quality spectra for higher molecular weight polymers is strongly dependent on the ratio of the polymer sample to matrix. This ratio must be found by trial and error in most cases, although the matrix:sample ratio generally must increase as the mass of the polymer increases.[8] One characteristic of the MALDI event that is crucial to the formation of ions in the gas phase is the efficiency of transfer of the solid polymer to the gas phase.[6-7] This efficiency will tend to rapidly decrease with increasing analyte molecular weight, particularly in the case of synthetic polymers. In addition, increases in the polydispersity index for a given polymer M_w will result in poorer spectra. Attempts at obtaining MALDI mass spectra for PMMA standards with M_w > 30000 amu or the pristine PMMA sheet samples (M_w ~ 1.5 Mamu) were met with frustration. It is believed that this inability to obtain spectra is due to the aforementioned difficulties with high molecular weight polymers.

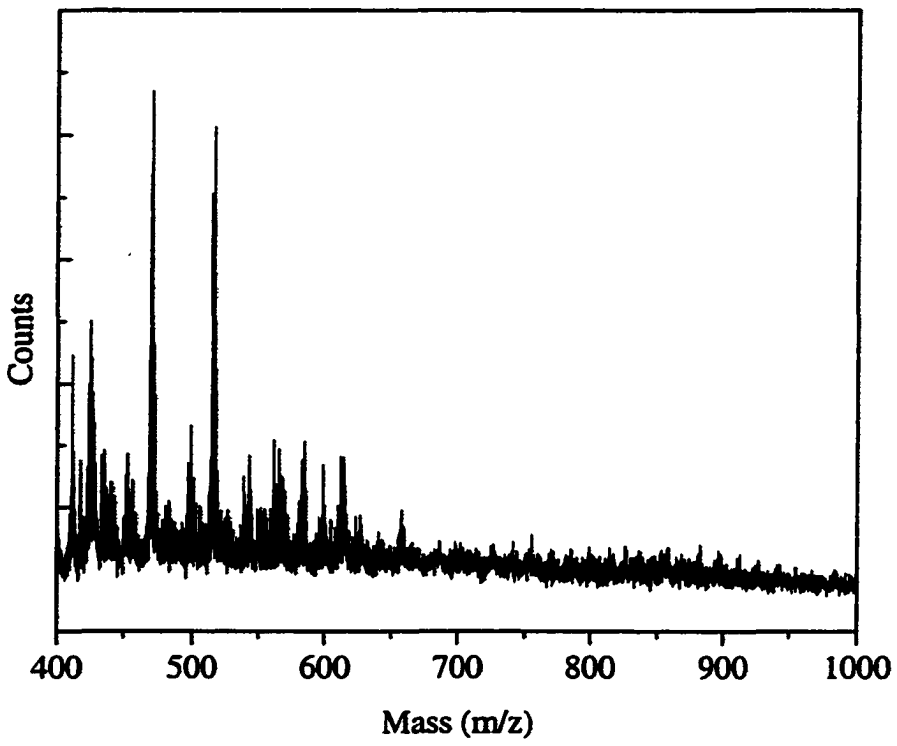

Figure 3.4 **MALDI mass spectrum of irradiated PMMA standard (M_w = 100000 amu).**

PMMA standards with molecular masses of M_w = 5700, M_w = 28350, and M_w=100000 were spin-coated on Si wafers and exposed to X-ray irradiation in an effort to determine, using MALDI-MS, the difference in molecular weight between pristine and X-ray irradiated PMMA. MALDI mass spectra of irradiated 5700 amu and 28350 amu PMMA standards were not obtained due to, presumably, full ablation of the polymer and irradiation products from the Si surface during irradiation. Displayed in Figure 3.4 is a MALDI mass spectrum of a 100000 amu PMMA film that was exposed to X-ray irradiation for 20 min at a dose of 2700 mA min. The peaks present on the

spectrum at m/z <400 amu (not shown) are due to the matrix, IAA. However, at m/z >400 amu, the peaks present are due to irradiated PMMA products. The chemical structures of these irradiated PMMA products are as yet unknown and will be the subject of a future study.

3.5 Determination of Volatile Materials formed Upon X-ray Irradiation of PMMA by Solid-Phase Microextraction

In order to determine the extent of gaseous products formed upon X-ray irradiation of PMMA, a chamber was constructed and positioned in the X-ray beam. A PMMA piece was positioned inside the chamber and in the path of the X-ray beam. A solid-phase microextraction[12] (SPME) fiber was placed, away from the X-ray beam, in the N_2-purged chamber. The PMMA was irradiated and the gaseous materials partitioned into the stationary phase present on the SPME fiber.[12-13] The gaseous materials were desorbed from the fiber in the injection port of the GC-MS and separated.

The composition of each of the species present in the chromatograms is under investigation and is the subject of future studies. However, on the chromatograms were several peaks corresponding to methyl methacrylate, MMA, and various oligomeric MMAs. It may be stated that a variety of materials are formed upon X-ray irradiation of commercial PMMA sheets, many of which are volatile in nature.

3.6 Effects of Pre-exposure Annealing on PMMA Swelling

In an effort to ascertain whether thermal annealing of the PMMA sheets (before gluing and irradiation) would decrease swelling during irradiation (due to heating of residual MMA or production of volatiles from chain-scission reactions), PMMA sheets

were annealed at various temperatures for one hour. While under a pure nitrogen atmosphere, the temperature of the PMMA sheets was ramped to the final annealing temperature at 3 °C/min and ramped back down to room temperature (~25 °C) at 1 °C/min so as to prevent thermal shock in the thick PMMA sheets. The amount of *initial* swelling is drastically reduced when annealing temperatures greater than 60 °C are used. The amount of swelling in the PMMA that occurs upon storage in the laboratory ambient seems to be time invariant for non-annealed samples and samples annealed to temperatures greater than 60 °C, but does increase for those samples that displayed minimal initial swelling (80 °C and 100 °C annealing).

The reduction in swelling by pre-exposure thermal annealing can be explained by considering the physical state of the PMMA sheets before and after heat treatment. Initially, the PMMA should be in an amorphous, glassy state typical of PMMA formed by radical polymerization. Upon slow thermal annealing, this polymer could have small regions of cracks and/or fissures found throughout the sheet, indicative of a glassy polymer that has been subjected to stresses, such as elevated temperatures. Indeed, if PMMA sheets are annealed at 100 °C for several days, the polymer becomes opaque, indicating the formation of cracks and fissures throughout the polymer sheet with dimensions large enough to scatter light. This phenomenon is known as crazing and has been reported for glassy PMMAs.[14] Thus, we propose that the slight amount of annealing that the PMMA samples experience in the current study cause crazing of the PMMA sheet. This crazing in turn results in the formation of nanochannels within the matrix of the sheet PMMA. These nanochannels would allow for rapid exit of any

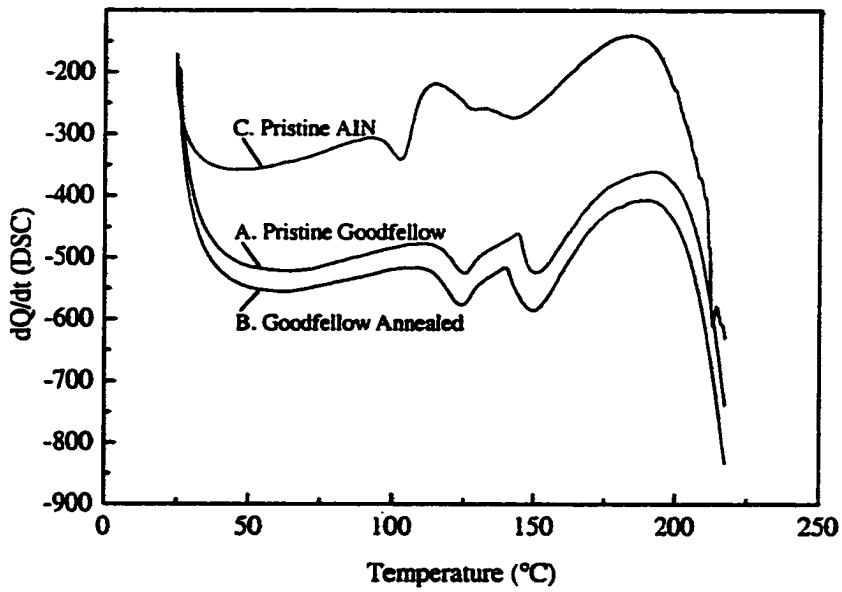

Figure 3.5 DSC traces of pristine and annealed Goodfellow PMMA as well as pristine AIN PMMA.

gaseous materials (volatiles like CO, CH_3OH, etc.)[15] produced upon irradiation, thus reducing swelling during X-ray exposure.

Investigations of possible differences in the PMMA sheets upon thermal annealing focused on differential scanning calorimetry of PMMA, Figure 3.5. The pristine Goodfellow PMMA exhibits a T_g of 112.2 °C, Figure 3.5A, as expected for PMMA possessing syndiotactic regions. Upon annealing to 100 °C for 1 h, the T_g value shifts to a slightly lower (statistically significant—reproduciblities on T_g values are ±0.7 °C) value of 110.3 °C, Figure 3.5B. This could be due to the cracks and fissures formed in the polymer matrix due to crazing. The cracks and fissures allow for the expulsion of small molecules from the matrix of the polymer, thus changing the thermal properties of the polymer. Alternatively, the fissures formed in the PMMA sheets due to crazing may

allow for the slight rearrangement of the pendant groups in the PMMA, thus changing the T_g of the PMMA after thermal annealing. In such a scenario, the pendant groups would have to "rearrange" such that the regions of syndiotacticity are decreased as compared to the pristine PMMA.

In Figure 3.5C is shown the data for a pristine AIN sample. This material has a much lower T_g (94.6 °C) —this observation is characteristic of PMMA with decreased regions of syndiotacticity in it. That is, because of its lower T_g, the AIN PMMA most likely exhibits polymer chains with fewer regions of syndiotacticity as compared to the pristine Goodfellow PMMA sample.[16] This difference in glass transition temperature may be due to the difference in PMMA manufacturing methods. The interesting observation is *the pristine AIN material swells the least when compared to the pristine Goodfellow PMMA*. Thus, it is believed that the changes observed in the Goodfellow PMMA upon thermal annealing for short periods of time tend to increase either the number of cracks and fissures (new sites) or the size of the existing cracks and fissures, resulting in the expulsion of gaseous materials or "rearrangement" of PMMA pendant groups. Such changes in the structure of the polymer could result in exposure/creation of nanoscopic pores leading to nanoscopic channels within the matrix of the polymer. More DSC experiments are needed to note changes in tacticity as a function of annealing time and then a correlation relating these changes to swelling should be possible. These preliminary results presented here point to a relationship between swelling and crazing.

The reason for the time-variant swelling of the samples (after irradiation) that were annealed at T>60 °C is not understood. As stated above, it is possible that there

are trapped volatiles left over from the irradiation that do not exist during the irradiation. For the amount of swelling that occurs (~60-100 μm), this does not seem plausible. Another possibility is that trapped radicals within the PMMA sheet continue to react (chain propagation mechanism) and form gaseous materials. Previous electron spin resonance has indicated the presence of trapped radicals in irradiated polymers. What is curious from the results of this study is that there is no post-irradiation swelling with the samples annealed at T<60 °C. At this point, the exact cause of the post-irradiation swelling in the thermally annealed samples is not understood.

3.7 Conclusions

By judicious treatment of PMMA sheets and metal surfaces, we have been able to decrease radiation-induced swelling in the PMMA resist and increase the adhesion of the PMMA to the metal surface by thermally treating the PMMA sheets prior to X-ray exposure. It has been found, using SPME, that a variety of gaseous products, including MMA and oligomeric MMA, are formed upon X-ray irradiation. In addition, the molecular mass of the sheet PMMA decreases nearly 45-fold upon X-ray irradiation as noted by GPC analyses. A proposed mechanism for the decreased swelling observed after thermal treatment involves the formation of channels in the PMMA that are present at grain boundaries of crystals formed during the annealing process. These channels allow for the rapid release of gaseous products during the irradiation process, and thus prevent swelling.

3.8 References

1) Vladimirsky, Y.; Vladimirshy, O.; Morris, K.J; Klopf, J.M.; Calderon, G.M.;Saile, V. *Microelectronic Engineering* **1996**, *30*, 543-546.

2) Ichikawa, T.; Yoshida, H. *J. Polym. Sci. A: Polym. Chem.* **1990**, *28*, 1185-1196.

3) Yates, B.W.; Shinozaki, D.M. *J. Polym. Sci. B: Polymer Physics* **1993**, *31*, 1779-1784.

4) Sotobayashi, H.; Asmussen, F.; Thimm, K.; Schnabel, W.; Betz, H.; Einfeld, D. *Polym. Bull.* **1982**, *7*, 95-100.

5) El-Kholi, A.; Mohr, J.; Nazmov, V. *Nucl. Inst. Met. Phys. Res. A* **2000**, *448*, 497-500.

6) Campana, J.E.; Sheng, L.-S.; Shew, S.L.; Winger, B.E. *Trends in Anal. Chem.* **1994**, *13*, 239-247.

7) Beavis, R.C. *Organ. Mass Spectrom.* **1992**, *27*, 653-659.

8) Belu, A.M.; DeSimone, J.M; Linton, R.W.; Lange, G.W.; Friedman, R.M. *J. Am. Soc. Mass Spectrom.* **1996**, *7*, 11-24.

9) Pasch, H.; Gores, F. *Polymer* **1995**, *36*, 1999-2005.

10) Dogruel, D.; Nelson, R.W.; Williams, P. *Rapid Comm. Mass Spectrom.* **1996**, *10*, 801-804.

11) Larsen, B.S.; Simonseck, Jr., W.J.; McEwen, C.N. *J. Am. Soc. Mass Spectrom.* **1996**, *7*, 287-292.

12) Zhang, Z.; Yang, M.J.; Pawliszyn, J. *Anal. Chem.* **1994**, *66*, 844A-853A.

13) Zhang, Z.; Pawliszyn, J. *Anal. Chem.* 1993, *65*, 1843-1852.

14) Kawagoe, M. *Polymeric Materials Encyclopedia*, J.C.Salsone, Editor, p. 2807-2812, CRC Press, Boca Raton, 1996.

15) Moore, J.A.; Choi, J.O. *Radiation Effects on Polymers*, R.L. Clough, S.W. Shaleb, Editors, p. 156, ACS Symposium Series 475, American Chemical Society: Washington, DC, 1991.

16) Hatada, K.; Kitayama, T. *Polymeric Materials Encyclopedia*, J.C.Salsone, Editor, p. 7965-7973, CRC Press, Boca Raton, 1996.

Chapter 4

Surface Characteristics of Commercial PMMA Sheets

4.1 Introduction

Described here is the characterization of various commercial brands of PMMA sheets used in the LIGA process. Previous experiments have indicated that the adhesive strength of a given PMMA sheet to an electroplating substrate is a function of the source of the PMMA, thermal treatment of the PMMA, and the face of the PMMA sheet. We have used contact mode scanning force microscopy (SFM) to inspect the topography of the faces of PMMA routinely used in the LIGA process. Depending on the thickness of the PMMA or what face of a given PMMA sheet is inspected, the surface topography is found to vary from almost completely smooth to that where pits populate the surface. The dimensions and number of the pits depend on the thermal treatment of the PMMA sheets (annealing at an elevated temperature). Gas chromatography-mass spectrometry (GC-MS) analyses indicate that residual methyl methacrylate (MMA) monomer content in the PMMA decreases upon annealing. Sampling of the local atmosphere during annealing through use of solid phase microextraction (SPME) confirms that residual MMA is released. The variation in pit number and size—the result of different amounts of expelled MMA—leads to the noted differences in adhesive strength of the various PMMA sheets to the substrate.

4.2 Surface Topography of PMMA Sheets

Shown in Figure 4.1 are representative 10 μm x 10 μm scanning force micrographs, as well as diagonal cross-sections, of the two faces of a pristine (as-

received) Goodfellow 1.6 mm PMMA sheet. As is clearly seen in Figure 4.1A, the surface is relatively smooth and free of surface defects. The few high spots are due to debris remaining from the cleaning process. The large defect in the upper portion of Figure 4.1A is approximately 650 nm in diameter and 220 nm in depth and is assumed to be due to handling of the sheet after manufacture. The opposite face of the sheet, Figure 4.1B, shows a strikingly different morphology as is evidenced by the presence of ~2-nm-deep, 70 to 90-nm-diameter pits on the surface. At this time, it is not prudent to comment on the origin of the pits in Figure 4.1B. Regardless of pit origin, the smooth and rough faces of a given PMMA sheet were labeled as such in order to differentiate surface defects possibly induced by heating versus those defects initially present. Other as-received Goodfellow samples (other thicknesses) in some cases exhibited pits on both faces of the PMMA sheet rather than only one face (*vide infra*). We are unable to speculate at this time why the Goodfellow 1.6 mm PMMA sheets contained pits on only one face rather than both. After heating the Goodfellow 1.6 mm sample shown in Figure 4.1A at 80 °C for 4 h, pits that are 270–330 nm in diameter and 5–7 nm in depth were found on the surface, Figure 4.1C. Also, it was noted that the face shown in Figure 4.1B exhibited increases in the depth of the initial pits (8–10 nm in depth) and new pits (as judged by the increase in number, ~60%), were found as well, Figure 4.1D. Statistically speaking, the *diameter* of the pits exhibited in Figures 4.1B and 4.1D is approximately equal (~80 nm for the pristine PMMA surface compared to roughly 77 nm for the annealed PMMA surface). We have studied other thicknesses of Goodfellow PMMA and have obtained results that suggest that the depth and/or the diameter of the

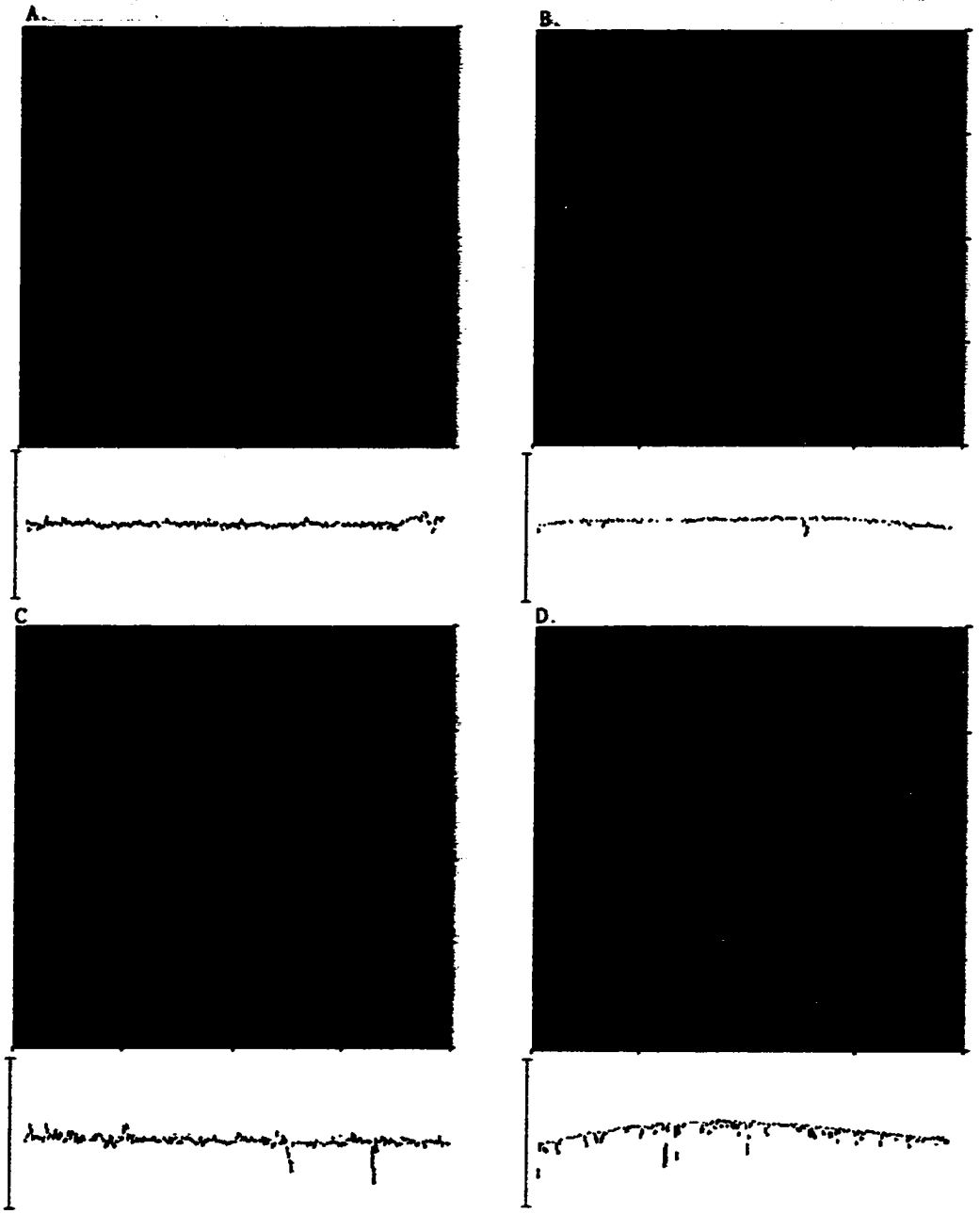

Figure 4.1 **Representative 10 μm X 10 μm SFM micrographs and diagonal cross-sections of Goodfellow 1.6 mm PMMA: A. face A of pristine sample, B. face B of pristine sample, C. face A of annealed sample, D. face B of annealed sample. The Z-range is 25 nm for A and C and 50 nm for B and D. The bar in the cross sections is 50 nm for A and C and 100 nm for B and D.**

present pits increase (Table 4.1). The most striking observation during evaluation of the different types of Goodfellow PMMA is that only the 1.0 mm sheets exhibited defects on *both* faces. Displayed in Figure 4.2A is a representative 10 μm x 10 μm micrograph of one face of an as-received Goodfellow 1.0 mm PMMA sheet with its diagonal cross-section. It is evident that the surface of the as-received material is riddled with pits; these pits are approximately 200–340 nm in diameter and 10–20 nm deep. The opposite face of this same sheet of pristine PMMA was similar in appearance to the face shown with respect to size and number of pits. SFM images of the sheet in Figure 4.2A after being heated at 80 °C for 4 hours indicate a change in the morphology. In Figure 4.2B is displayed a representative 10 μm x 10 μm micrograph and diagonal cross-section of the same face as in Figure 4.2A after such an annealing cycle. The holes that are present on the annealed Goodfellow 1.0 mm PMMA sheet are deeper (~170% increase) and more plentiful (~10% more) than those exhibited on the pristine sample. This is clearly evident in the diagonal cross-section of Figure 4.2B. From the data in Table 4.1, it is apparent that pit diameter increased to 260-410 nm and pit depth increased to 30-50 nm after controlled annealing.

Upon inspection of Table 4.1, it is readily noted that the deepest pit measured is 56(±9) nm. One may question, because this pit is quite deep, whether or not the SFM probe tip actually contacted the bottom of the pits without coming into contact with the other side of the pit. Based on the observed pit diameters (65–160 nm) and the tip dimensions, we can easily calculate the maximum pit depth that can be properly imaged by the tip; these values are in excess (~2-fold) of those measured in all cases.

Table 4.1 **Defect characteristics as a function of PMMA vendor, thickness, face and heat treatment.**

Vendor	Thickness (mm)	Face	Diameter (nm)	Depth (nm)	Number of pits/ 2.5 μm^2
Goodfellow	1.0	A	279(±60)	15(±5)	38(±2)
		B	252(±70)	15(±3)	36(±2)
		A (annealed)	392(±66)	23(±3)	44(±3)
		B (annealed)	281(±38)	56(±9)	40(±3)
Goodfellow	1.6	A	N/A	N/A	N/A
		B	80(±11)	2(±0.4)	5(±2)
		A (annealed)	301(±30)	6(±1)	2(±2)
		B (annealed)	77(±12)	9(±1)	8(±3)
Goodfellow	2.0	A	N/A	N/A	N/A
		B	N/A	N/A	N/A
		A (annealed)	305(±77)	8(±2)	3(±1)
		B (annealed)	279(±60)	15(±5)	2(±2)
AIN Plastics	0.225	A	373(±52)	14(±3)	26(±3)
		A (annealed)	461(±55)	22(±5)	34(±3)

[a]Although there was the occasional observation of pits, the surface density was often less than 2 pits per 25 μm^2.

[b]No distinguishable pits, such as those in Figure 4.2B, could be observed. Only localized depressions ~500 nm in diameter were found on the pristine samples.

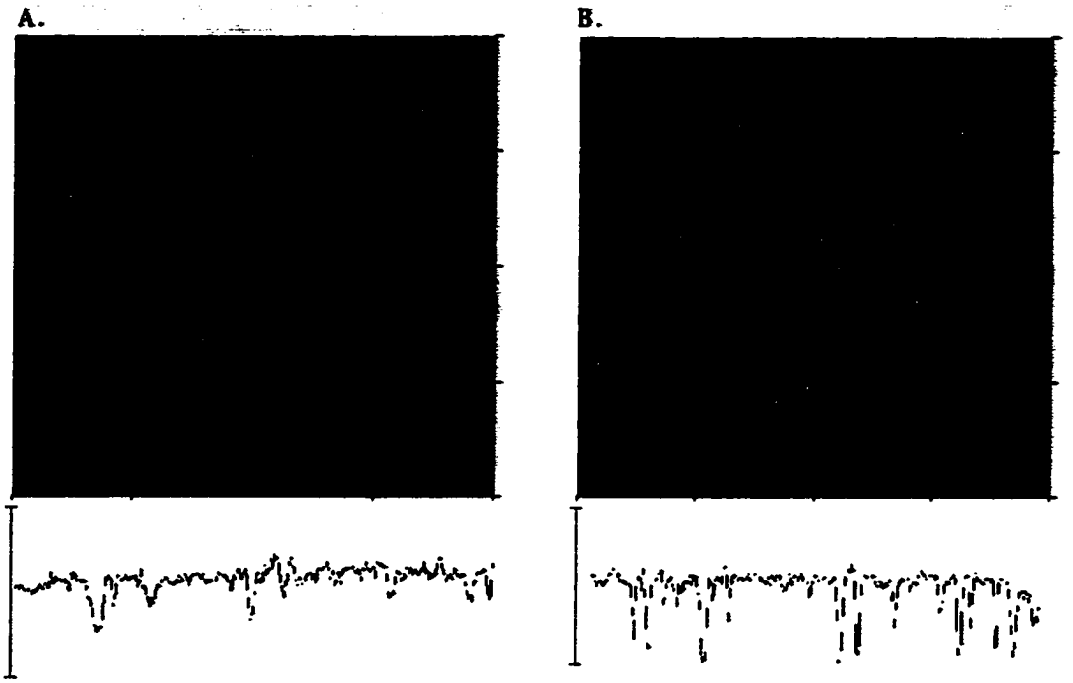

Figure 4.2 **Representative 10 μm X 10 μm SFM micrographs and diagonal cross sections of Goodfellow 1.0 mm PMMA: A. face A of pristine sample, Z-range 50 nm; B. face A of annealed sample, Z-range is 50 nm, bar in the cross sections is 100 nm.**

A very interesting aspect of the above discussion is that each thickness of Goodfellow PMMA discussed above exhibits a different *pristine* surface topography. As was stated above, Goodfellow is a re-seller of PMMA; however, the brand that is re-sold is ICI, which happens to be the manufacturer of all the Goodfellow PMMAs discussed here. One would assume that the surface topography of the same brand of PMMA would be quite similar, providing that the sheets were manufactured using the same process and undergo similar post-manufacture treatment. We have seen that this is indeed not the case; that is, three different sheet thicknesses of the same brand of

PMMA exhibit three different surface topographies. Thus, we speculate that the process is different for the PMMA sheets investigated in this study. However, once each of these sheets are annealed, the surfaces in all cases increase in roughness.

We were interested in whether or not the above-noted trends in surface topography, both for as-received and annealed samples, could be observed for PMMA sheets from another vendor. The vendor we chose was AIN Plastics due to the wide-spread use of AIN PMMA in the LIGA process at our micromachining facility. Displayed in Figures 4.3A and 4.3B are 10 μm x 10 μm micrographs, as well as diagonal cross-sections, of pristine and annealed samples of a particular 225-μm-thick AIN PMMA sheet. The surface of the pristine AIN PMMA is extremely rough, as we have seen before with samples of Goodfellow PMMA, but instead of holes distributed on the surface, there are what appear to be bumps. Once the sample was annealed (Figure 4.3B), these bumps appear to have ruptured into holes.

The SFM images, as well as the diagonal cross-sections, displayed in Figures 4.3A and 4.3B are perhaps our best evidence for what is postulated to occur during the annealing process of PMMA sheets. It is assumed that there is some volatile compound trapped in the matrix of the polymer that, when heated, expands due to the increase in vapor pressure. Under certain conditions, this volatile compound is violently expelled out of the polymer matrix giving rise to the pits that are found on the surface of the annealed samples. In Figure 4.3A, we have presumably imaged a piece of PMMA that has been annealed (before our receiving the material) almost to the point where some volatile compound is expelled into the atmosphere from the polymer matrix. It is

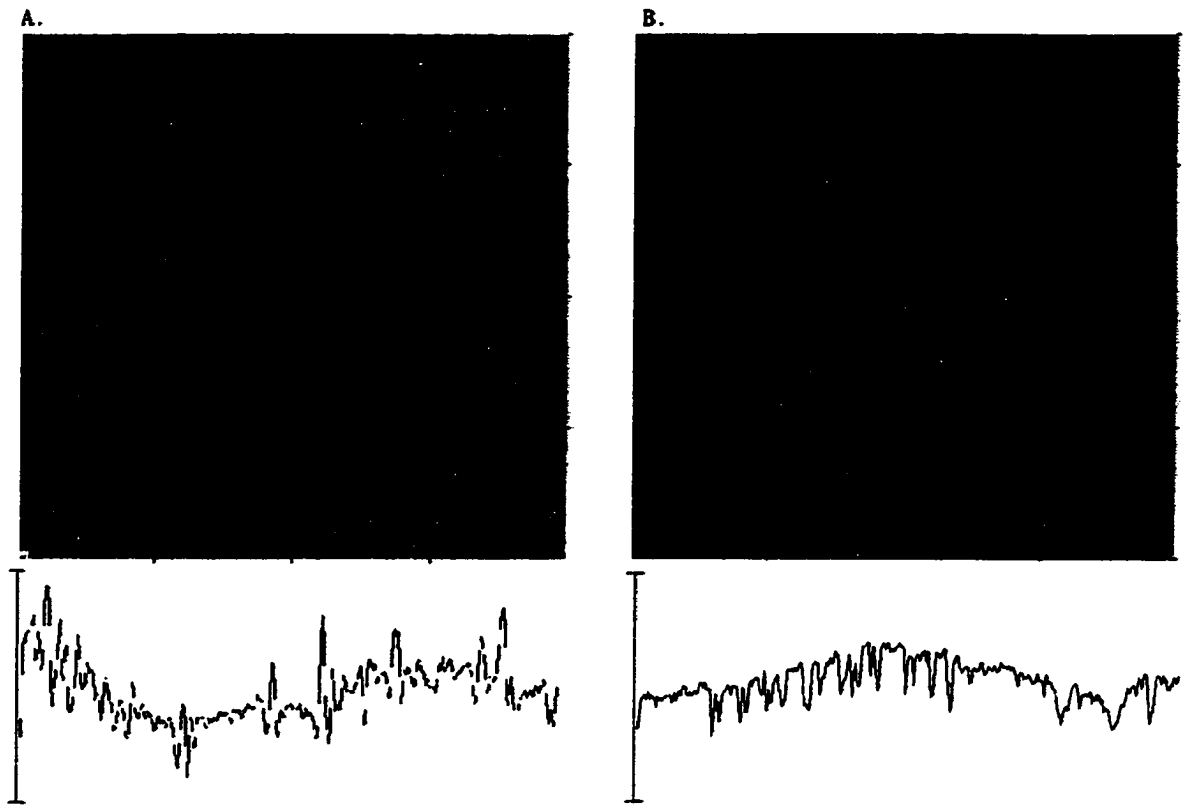

Figure 4.3 **Representative 10 μm X 10 μm SFM micrographs and diagonal cross sections of AIN 225 μm PMMA: A. face A of pristine sample and B. face A of annealed sample. The Z-range is 50 nm in both images and the bar in the cross sections is 100 nm.**

important to state here that the *as-received* sample of AIN PMMA discussed above is one of only a few samples of the AIN PMMA which exhibited bumps; the large majority of the pristine AIN samples imaged by SFM were found to exhibit pits rather than the bumps seen in Figure 4.3A. In all cases, once the PMMA was annealed, pits were evident; the depth of the pits after annealing was always greater than that found for pristine samples.

From the SFM data presented thus far, a picture for the formation of pits in PMMA can be proposed. It is assumed that a freshly manufactured piece of PMMA exhibits a smooth surface. Upon initial heating (either purposeful or accidental) of the PMMA, bumps form, as a result of the expansion of a volatile compound due to its increase in vapor pressure. Once the PMMA is heated for longer periods of time or at much elevated temperatures, the local pressure becomes greater than that which can be accommodated by the PMMA, and a rapid expulsion of the volatile materials occurs, resulting in the formation of defect structures. We have seen on both brands of PMMA studied here statistically significant changes in depth and diameter of existing holes and also the appearance of new holes. Thus, we assume that the holes found on as-received sample surfaces are due to some sort of heat exposure of the sheet after manufacture, such as during delivery to our laboratory.

4.3 Analysis of Volatiles Present in PMMA Samples as Determined by Gas Chromatography-Mass Spectrometry (GC-MS)

We were interested in determining both the identity and the concentration of any volatiles present in the polymer sheets before and after annealing. During polymerization of MMA to form PMMA, the only compounds used for the reaction are MMA monomer and a free-radical initiator. We focused our efforts on determining whether or not any volatiles present in the polymer matrix could be MMA, because it is well known that many polymerizations do not completely deplete the monomer used in the reaction. Pristine and annealed PMMA samples of known mass were dissolved in a given volume of chloroform. The three types of Goodfellow PMMA, and the AIN

Table 4.2 MMA content in various PMMA sheet samples.

Vendor	g MMA/ g PMMA
Goodfellow 1.0 mm	
Pristine	0.0440(±0.0042)
Annealed	0.0351(±0.0002)
Goodfellow 1.6 mm	
Pristine	0.0466(±0.0059)
Annealed	0.0398(±0.0053)
Goodfellow 2.0 mm	
Pristine	0.0590(±0.0047)
Annealed	0.0311(±0.0033)
AIN 225 μm	
Pristine	0.0207(±0.0024)
Annealed	0.00758(±0.00123)

PMMA, were annealed at 80 °C for 24 hours. Butyl methacrylate (BMA) was added to the solutions as an internal standard. The solutions that resulted was colorless, clear, and gel-like in nature. A portion of each of the solutions was injected into the GC-MS, and the intensity of the MMA peak was compared to that of the BMA peak. A standard calibration curve was used to calculate the concentration of MMA in each PMMA sample. In all cases, it was found that the annealed samples contained less MMA than those that had not experienced any thermal treatment in our laboratory. The results of these experiments are displayed in Table 4.2. The amount of MMA lost as a result of heating ranged from ~15–60% and did not seem to follow any trend.

Although it might be tempting to try and correlate the amount of MMA lost during heating with the volume of the resulting pits for a given type of PMMA, such an

attempt would have as one of its assumptions the fact that the volume of the pits translates into the volume of liquid MMA initially present. This assumption is not correct, due to the fact that the amount of MMA initially present could be less than the volume of the newly formed pits and heating of the PMMA would causes *gaseous* MMA to be expelled from the polymer matrix. Gaseous MMA occupies more volume than liquid MMA; hence, the volume of the pits on the surface depends on the expansion of MMA and its subsequent expulsion from the polymer matrix to the atmosphere. In addition, there might also be voids below the surface which form during the heating and cannot be detected by SFM, unless a cross-sectioned image of the PMMA sheet could be imaged using SFM (*vide infra*).

We believe that the volatile MMA is actually trapped deeper in the matrix of the PMMA than the maximum pit depth that we found for each of the samples. That is, we believe that the MMA is being expelled into the atmosphere during annealing but some of the deep-set MMA remains within the polymer matrix, as evidenced by the GC-MS data.

4.4 Confirmation of Volatiles Identity as MMA—Solid Phase Microextraction (SPME) Studies of MMA in PMMA Samples

Our data has shown that there is a lower amount of MMA in annealed samples of PMMA versus pristine samples of PMMA; these data were obtained after the annealing process occurred. However, we were interested in a more direct proof of the emission of MMA from PMMA samples. That is, we wanted to actually sample the atmosphere, or headspace, into which we believe the volatile MMA is expelled from the

matrix of the PMMA polymer. We turned to the technique of solid phase microextraction (SPME)[1] coupled to GC-MS.

SPME is a relatively new method for the extraction of organic materials from various sample matrices.[1-2] There are two processes that occur in SPME/GC-MS—the partitioning of the analyte between the sample (or its local atmosphere/environment) and the coating on the SPME sampling fiber and subsequent desorption of the absorbed analytes into the injector of the GC-MS. In the case at hand, we were interested in sampling possibly trapped volatiles in PMMA sheets. It is assumed that when the PMMA (in a sealed vial) is heated, the trapped volatiles are released from the polymer matrix into the headspace (the interior of the sealed vial). Thus if an SPME sampling fiber were to be exposed to the headspace of the vial containing the PMMA, the gaseous components would partition between the coating of the SPME fiber and the headspace. In order to ensure an equilibrium concentration of volatiles in the SPME fiber, the fiber was exposed to the headspace for two hours. After analysis by GC-MS, the only volatile compound that was observed was found to be MMA. At this time we are unable to quantitate the amount of released MMA per gram of PMMA, but it has been observed in preliminary studies that as the amount of PMMA in the sampling vial is increased, a corresponding increase in MMA chromatographic peak height is observed.

4.5 Surface Topography of PMMA Cross-Sections as Studied by Scanning Force Microscopy (SFM)

We have postulated above that the MMA that is expelled into the atmosphere during annealing may be originating from deep within the polymer and not merely from the outermost layer of the PMMA. To investigate this hypothesis, we used SFM to

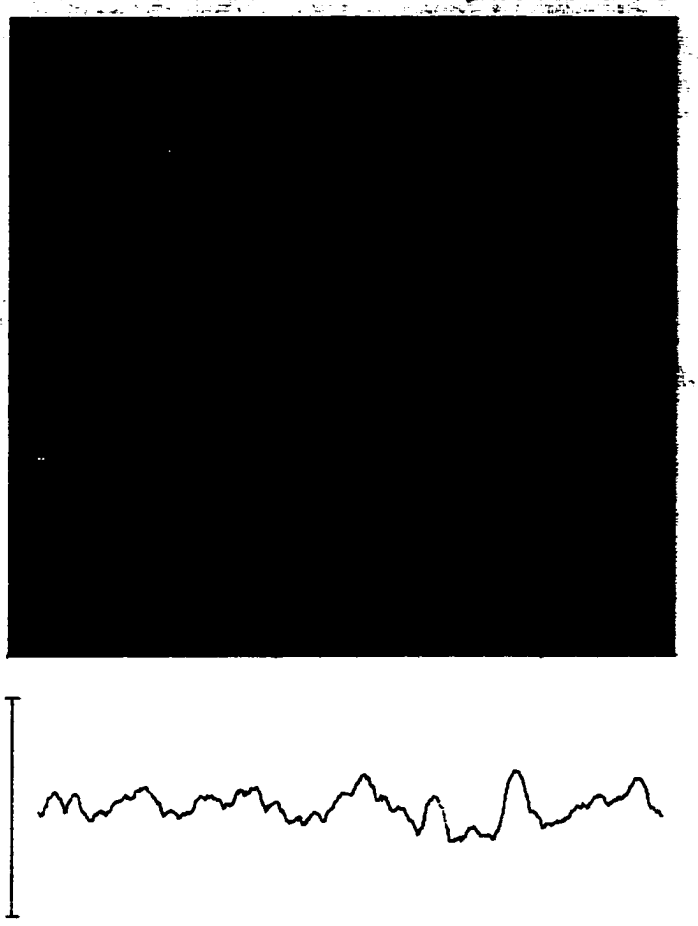

Figure 4.4 **Representative 10 μm X 10 μm SFM micrograph and diagonal cross section of Goodfellow 1.6 mm PMMA that has been microtomed. The Z-range is 50 nm and the bar in the cross section is 100 nm.**

study the surface topography of microtomed cross-sections of PMMA. Figure 4.4 is a representative 10 μm x 10 μm micrograph of a vertical cross-section of as-received Goodfellow 1.6 mm PMMA. The uniform ridges that appear on this micrograph, as well as those that appear on its cross-section, are due, presumably, to the "chatter" of the microtoming blade during cutting of the sample. All SFM images of microtomed cross-sections (both vertical and horizontal) exhibited these ridges. Upon careful inspection of the cross-sections, we were unable to observe any features that could be attributed to

voids within the PMMA due to the inherent roughness of the cross-sections. In addition, due to the presence of the ridges, it was impossible to note any changes in the PMMA cross-sections (pit formation) after such cross-sections were heated.

4.6 Conclusions

It has been shown in previous work that the microroughening of the electroplating base substrate used in the LIGA process greatly increases the adhesion of PMMA sheets to the substrate, and adhesion of PMMA sheets to a given substrate is increased if the PMMA has first been annealed prior to gluing on the substrate surface.[10] Through SFM studies, we have learned that the surface topography among various brands of as-received PMMA, as well as various thicknesses of the same brand of as-received PMMA, is different from sample to sample. Furthermore, using scanning force microscopy, we have observed that each face of the same sheet of PMMA has its own surface topography and it is changed once the sheet is annealed. This correlates with the results in Figure 1 where differences in adhesive strength were found among various brands of PMMA, as well as various thicknesses of the same brand of PMMA. Differences in adhesive strength were also noted between as-received and annealed samples in addition to the two faces of the same sheet of PMMA. The differences we have noted are the result of the presence of pits; the size and number of pits depend on the type of PMMA sheet and its thermal treatment. GC-MS studies indicate that the possible reason for pit formation is the expulsion of trapped pockets of MMA from the matrix of the PMMA sheet. Through SPME/GC-MS experiments, we have been able to

demonstrate that it is indeed MMA which is expelled from the PMMA during the annealing process.

4.7 References

1) Zhang, Z.; Yang, M.L.; Pawliszyn, J. *Analytical Chemistry*, **1994**, *66*, 844A-853A.

2) Pawliszyn, J. *Solid Phase Microextraction: Theory and Practice*; Wiley-VCH: New York, 1997.

Chapter 5

Surface Modification of PMMA Surfaces to Yield Primary Amines and Long-Chain Alkyl Functionalities

5.1 Introduction

The chemical modification of PMMA surfaces to yield amine-terminated PMMA, referred to as NH_2-terminated PMMA or AT-PMMA, allows for the presence of a reactive functional amine group on the surface of the PMMA. Such amine-terminated PMMA surfaces are produced through reaction of PMMA films or commercially available PMMA sheets used in the construction of microelectromechanical systems (MEMS). Amine-terminated PMMA surfaces are the products of the reaction of pristine PMMA sheets with the monoanion of α,ω-diaminoalkanes (aminolysis reaction). It is found that the PMMA surfaces can be modified so as to provide amine functionalities which are tethered to the PMMA backbone through an alkane bridge to amide bonds formed during the aminolysis of the surface ester functionalities. The distribution of the amine termini is quite uniform as determined by fluorescence micrographs of the fluorescently labeled primary amines. It is found that the electroosmotic flow (EOF) in aminated-PMMA microchannels is reversed when compared to that in unmodified channels. Biological molecules, such as enzymes, can be tethered to the amine-terminated PMMA surface using a dialdehyde spacer. Finally, the availability of the surface amine groups is further demonstrated by their reaction with *n*-octadecane-1-isocyanate to form PMMA surfaces terminated with well ordered and highly crystalline octadecane chains, which bodes well for their use as stationary phases in the construction of miniaturized electrochromatography devices.

5.2 Modification of Pristine Sheet PMMA to Yield Amine-Modified PMMA Surfaces

Pristine PMMA sheets and thin films were subjected to reaction with α,ω-diaminoalkanes to produce NH_2-terminated PMMA, Figure 5.1. Pristine and amine-terminated PMMA sheets and thin films were characterized by means of wetting analysis, infrared spectroscopy, X-ray photoelectron spectroscopy, confocal fluorescence microscopy, and scanning force microscopy.

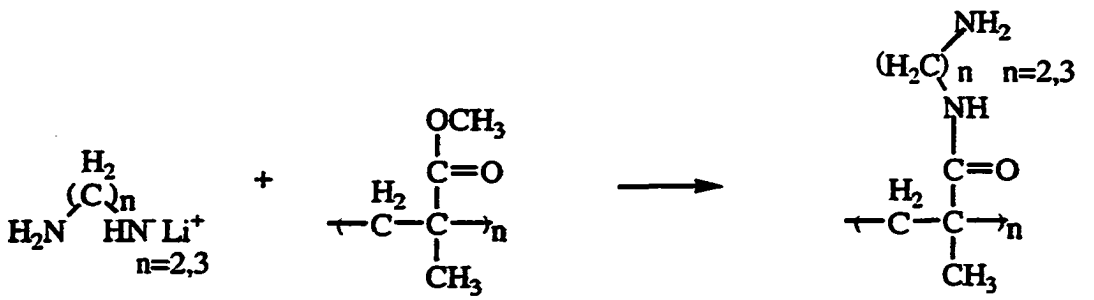

N-Lithiodiamine Pristine PMMA NH_2-Terminated PMMA

Figure 5.1 Reaction scheme producing NH_2-terminated PMMA from pristine PMMA and an *N*-lithiodiamine.

5.2.1 Sessile-Drop Water Contact Angle Measurements of Pristine versus NH_2-Modified PMMA Surfaces

A relatively quick, qualitative measure of the success of the amination reaction (Figure 5.1) can be had through the use of sessile-drop water contact angle measurements. The average water contact angle for pristine PMMA was found to be 66° ± 2°, which correlates well with the literature value of 67° for a highly ordered methyl ester-terminated monolayer.[1] Water contact angle measurements for NH_2-terminated PMMA sheets yielded an average of 33° ± 4°, a value consistent with that

obtained for self-assembled monolayers terminated with hydrophilic functional groups.[1,2] The decreased water contact angles of NH_2-modified PMMA surfaces indicate that a modification of the pristine PMMA surface did indeed occur, resulting in a more hydrophilic surface.

5.2.2 Analysis of Pristine and NH_2-Terminated PMMA Thin Films by Reflection-Absorption Infrared Spectroscopy (RAIRS)

In order to provide spectroscopic evidence that covalent linking of the diamines to the PMMA surface occurred, infrared spectroscopy was employed. Upon examination of Figure 5.1, the product of the reaction between the PMMA surface and the lithiated diamine is a primary amine linked by an alkyl chain to an amide on the PMMA surface. The presence of the primary amine, as well as the amide linkage (due to aminolysis of the surface esters), on the amine-modified PMMA makes infrared spectroscopy an excellent choice for characterization of the modified surfaces.

In Figure 5.2 is a representative RAIR spectrum of pristine PMMA on Au (Au-coated, Cr-primed glass microscope slides).[3] This spectrum correlates well with the transmission spectrum of PMMA documented in the literature.[4] Band assignments are compiled in Table 5.1. The most prominent band is the carbonyl stretch, ν(C=O), at approximately 1733 cm^{-1}. The band maximum position is characteristic of methyl esters, particularly those found for films of PMMA. The remaining vibrational bands observed are characteristic of the alkane and ester moieties present in the polymer.

Also displayed in Figure 5.2 is a representative RAIR spectrum of an NH_2-modified PMMA thin film; the band assignments are tabulated in Table 5.1. The major observations that arise upon comparison of the spectra in Figure 5.2 are the presence of

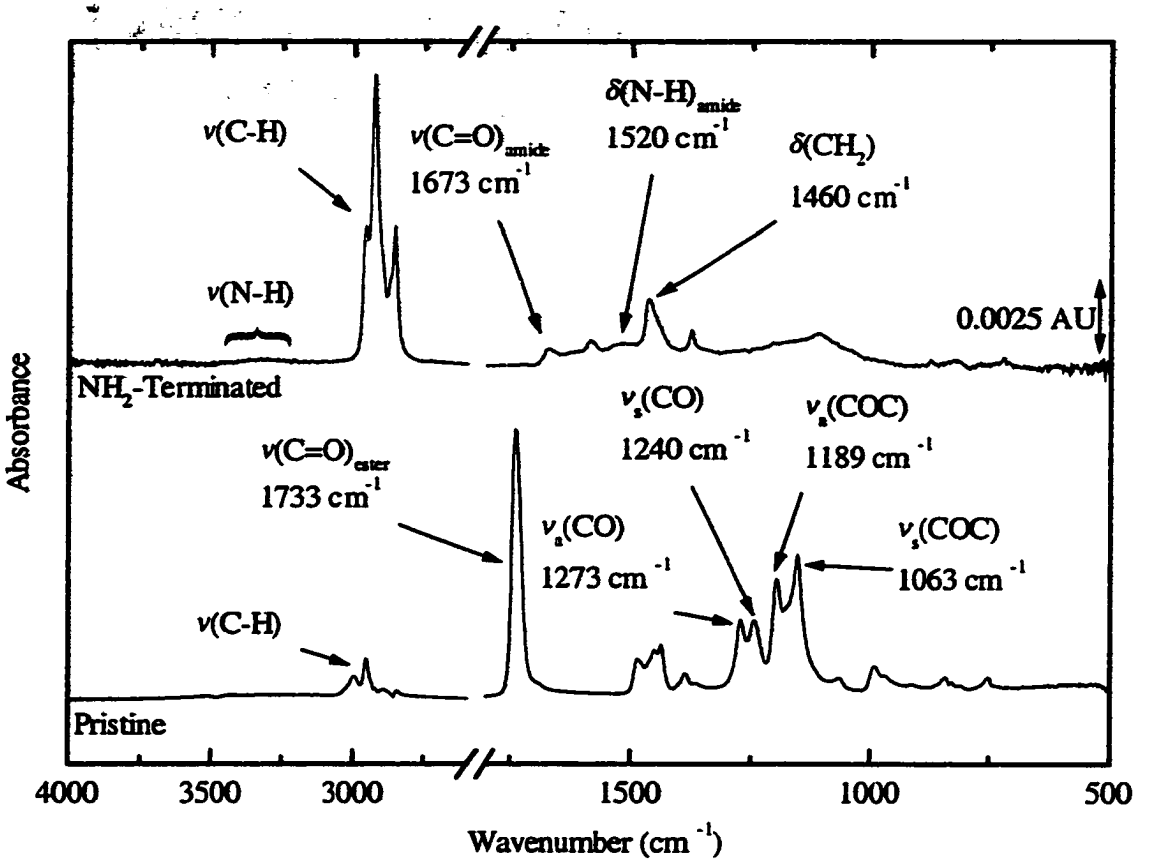

Figure 5.2 Reflection-absorption infrared spectra of pristine and NH_2-terminated PMMA spin-coated on Au.

the Amide I (ν(C=O)) and the Amide II (δ(N-H)) bands at approximately 1673 cm^{-1} and 1520 cm^{-1}, respectively, as well as substantially smaller methyl ester bands—the ν(C=O), ν(C-O), and ν(C-O-C) modes—in the spectrum of the aminated PMMA film. These data point to the fact that exposure of PMMA films to a lithiated diamine results in replacement of the ester functionalities by an amide linkage, as expected (Figure 5.1). In addition, a broad, ill-defined band centered at approximately 3314 cm^{-1} is present in the spectrum of the aminated PMMA film. We tentatively assign this band to the ν(N-H) transition associated with 1° amines on the surface of the PMMA film.

Table 5.1 Infrared band positions and assignments for pristine PMMA and NH_2-terminated PMMA

pristine PMMA		NH_2-Terminated PMMA	
Position (cm^{-1})	Assignment	position (cm^{-1})	assignment
2955	$\nu_a(CH_3)$	~3314	ν(N-H)
2920	$\nu_a(CH_2)$	2955	$\nu_a(CH_3)$
2850	$\nu_s(CH_2)$	2926	$\nu_a(CH_2)$
1733	ν(C=O)	2871	$\nu_s(CH_3)$
1487	$\delta(CH_2)$	2856	$\nu_s(CH_2)$
1454	$\delta_a(CH_3)$	1673	$\nu(C=O)_{amide}$
1436	$\delta_s(CH_3)$	1520	$\delta(N-H)_{amide}$
1389	$\delta_s(CH_3)$	1460	$\alpha(CH_3)/\delta(CH_2)$
1273			
1240			
1189			
1063			

5.2.3 Analysis of Pristine and NH_2-Modified PMMA Sheets by X-ray Photoelectron Spectroscopy (XPS)

Although the infrared spectroscopy results presented above point to the successful formation of amide linkages upon reaction of pristine PMMA with a lithiated diamine, these results were obtained for *films* of PMMA rather than as-manufactured *sheets* of PMMA typically used in the fabrication of MEMS devices. Thus, our specific aims for the XPS analysis of pristine and NH_2-modified PMMA sheets include determining the presence and identity of nitrogen entities on *sheet* PMMA.

The X-ray photoelectron survey spectrum of pristine PMMA displayed only two features –a peak at 285.0 eV and another at approximately 532.1 eV, indicative of C1s and O1s core levels, respectively. However, the survey spectrum of aminated PMMA

displayed a peak at approximately 400 eV in addition to the C1s and O1s peaks at 285.0 eV and 532.1 eV. The peak centered at approximately 400 eV is characteristic of surfaces possessing nitrogen containing functionalities (N1s core level). This peak can be deconvoluted into *two* individual peaks, one centered at 399.4–399.5 eV and the other at 400.0–400.1 eV. The peak at lower binding energy corresponds well with that found for the N1s core level of an amine[5] whereas the peak at higher energy can be assigned as that of an amide.[5]

Upon further analysis of the XPS data, it was found that the ratio of the peak area of the O1s peak to the C1s peak is approximately 12% less for NH_2-modified sheet PMMA when compared to pristine sheet PMMA. Thus, the XPS results demonstrate that not only is nitrogen present in two forms on the surface of the NH_2-modified sheet PMMA, but the amount of oxygen present on the surface of the NH_2-modified PMMA is less than what was present on the surface of the pristine PMMA.[6] This latter observation is in agreement with the infrared data (vide supra) that indicated the presence of fewer ester groups for the NH_2-terminated PMMA films. Collectively, these results indicate that the amination reaction can be successfully carried out on *sheet* PMMA, an outcome which is important for applications requiring modification of commercially available PMMA substrates.

5.2.4 Confocal Fluorescence Microscopy Studies of Pristine and NH_2-Terminated PMMA Sheets

Confocal fluorescence microscopy was employed to examine the surface of NH_2-Terminated PMMA sheets with the intention of demonstrating that the surface is terminated with uniformly distributed, accessible primary amines. After exposure of

A.

B.

Figure 5.3 **Confocal fluorescence micrographs of A. pristine and B. NH_2-terminated PMMA exposed to 1 μM FITC (pH 9).**

the surface to fluorescein isothiocyanate (FITC)—which should allow for fluorescent labeling of accessible primary amines—we examined the surface using confocal fluorescence microscopy. Displayed in Figure 5.3A is a representative confocal fluorescence microscopy image of pristine sheet PMMA (control) that had been exposed to a 1 μM solution of FITC in sodium borate buffer (pH 9.2) for 23 h. As can easily be seen, the image displays no bright areas (fluorescence) that would indicate the presence of FITC-labeled amines. Variations in laser power did not result in the observation of fluorescence from the surface of these control samples.

An entirely different image is presented in Figure 5.3B. This image represents one of many images we collected for NH_2-Terminated PMMA that had been exposed to FITC. As is clearly evident, the image in Figure 5.3B is much brighter than the image in 5.3A, indicating an abundance of accessible amine sites on the surface of the NH_2-modified PMMA surface. In addition, the homogeneity of the amine surface population, as judged by the lack of significant variations in the fluorescent signal with respect to position, is quite high.

5.2.5 Quantitative Determination of NH_2 Groups on the Surface of NH_2-Terminated PMMA Sheets.

For the reaction of sheet PMMA with *N*-lithiodiaminoethane, it has been found that a reaction time of 2 min leads to the maximum observable apparent surface coverage of amines, 6.85±0.60 nmol cm^{-2}. As for the reaction of sheet PMMA with *N*-lithiodiaminopropane, it was found that the apparent surface coverage of amines remains steady at approximately 6 nmol cm^{-2} (no statistical difference in coverage with

time at the 95% confidence level). There appears to be no clear trend of amine coverage with time; however, upon exposure of the PMMA to the *N*-lithiodiamine for extended periods of time, the surface of the plastic appears frosted. The apparent amine surface coverage values are approximately six to eight times higher than the surface coverage of thiols self-assembled on Au[1] or silanes on silica.[7] Data from side roughness studies indicate that the amine surface concentration on only the faces of the modified PMMA is roughly 5 nmol cm^{-2}. In addition, the intrinsic roughness of the *faces* of the NH_2-modified PMMA sheets may also contribute somewhat to the high amine surface coverage of the modified PMMA; we address this issue next.

5.2.6 Characterization of the Surface Topography of Pristine and NH_2-Terminated PMMA Sheets Using Scanning Force Microscopy (SFM)

By understanding the surface topography of the PMMA sheets, it may be possible to determine the impact of face surface roughness on the surface coverage of amines. Further, we are interested in employing amine-modified PMMA in the fabrication of microanalytical separation channels (chromatographic stationary phase) and for improving adhesion between PMMA and another sheet of PMMA *or* between PMMA and a conductive substrate. Therefore, it was necessary to ascertain the surface topography of the pristine PMMA surfaces, as well as the amine-modified PMMA surfaces.

Displayed in Figure 5.4A is a representative 2 μm x 2 μm contact-mode scanning force microscopy image of 3 mm Goodfellow sheet PMMA. This surface, as can be seen, is smooth and relatively free of defects; the RMS roughness (entire 10 μm x 10 μm range) is 0.39 nm and the roughness factor, *R*, which is the surface cross-

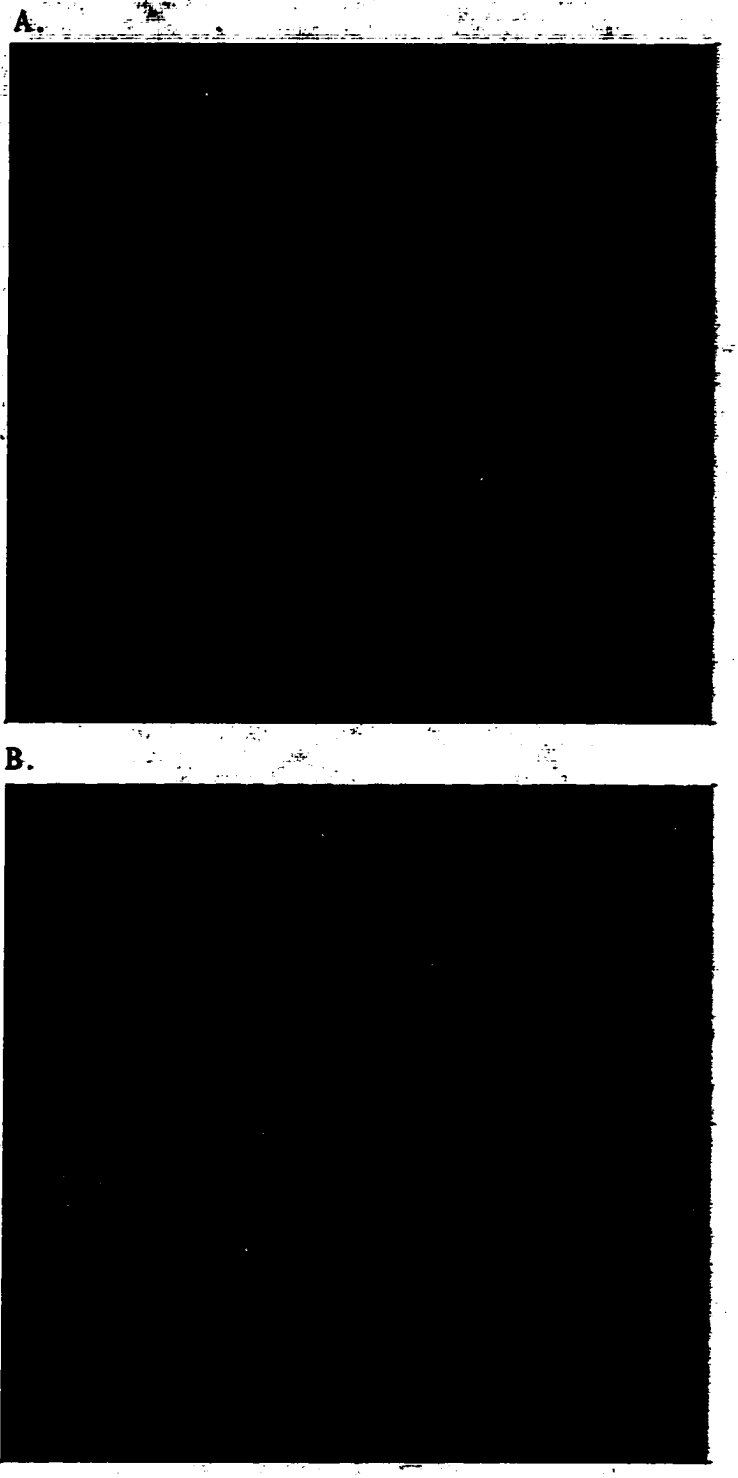

Figure 5.4 **Representative 2 μm X 2 μm SFM micrographs of A. pristine and B. NH_2-terminated PMMA. The Z-range is 10 nm.**

sectional distance divided by the horizontal distance, is 1.002. Shown in Figure 5.4B is a typical 2 μm X 2 μm scanning force microscopy image of 3 mm Goodfellow sheet PMMA that was modified with *N*-lithiodiaminopropane for 2 min. The modified surface is obviously much different than the pristine surface, for the surface roughness is approximately 3.5 times higher (1.45 nm RMS roughness, R = 1.013) than that of the pristine surface. The RMS roughness value for PMMA surfaces exposed to *N*-lithiodiaminoethane was determined to be 1.80, while the roughness factor was found to be 1.015. The observed increase in surface roughness may be due to a slight swelling/dissolution of the PMMA by the lithiated diamine because it has been found that the cyclohexane solvent used in the aminolysis reaction does not affect the surface of the PMMA in any way.

Based on the SFM studies and the preliminary investigations of edge roughness, the roughness-corrected amine surface coverage is a little less than 5 nmol cm^{-2}. This value is roughly 6 times that expected for a close-packed alkane monolayer.[1] This larger-than-expected number of surface amines is most likely the result of amination reactions that occurred below the surface of the original PMMA sheet surface. Thus, at short reaction times, it would appear that the amination reactions occur to a depth of roughly 6 repeat units or ~1.6 nm. For a solution-based polymer modification protocol, this level of penetration is actually quite low.

5.3 Manipulation of Electroosmotic Flow in PMMA Microchannels

The EOF has recently been determined in PMMA-based microdevices to be approximately 1.4 x 10^{-4} cm^2/Vs (positive value indicates EOF runs from anode to cathode) with this value found to be virtually independent of solution pH.[8] In order to

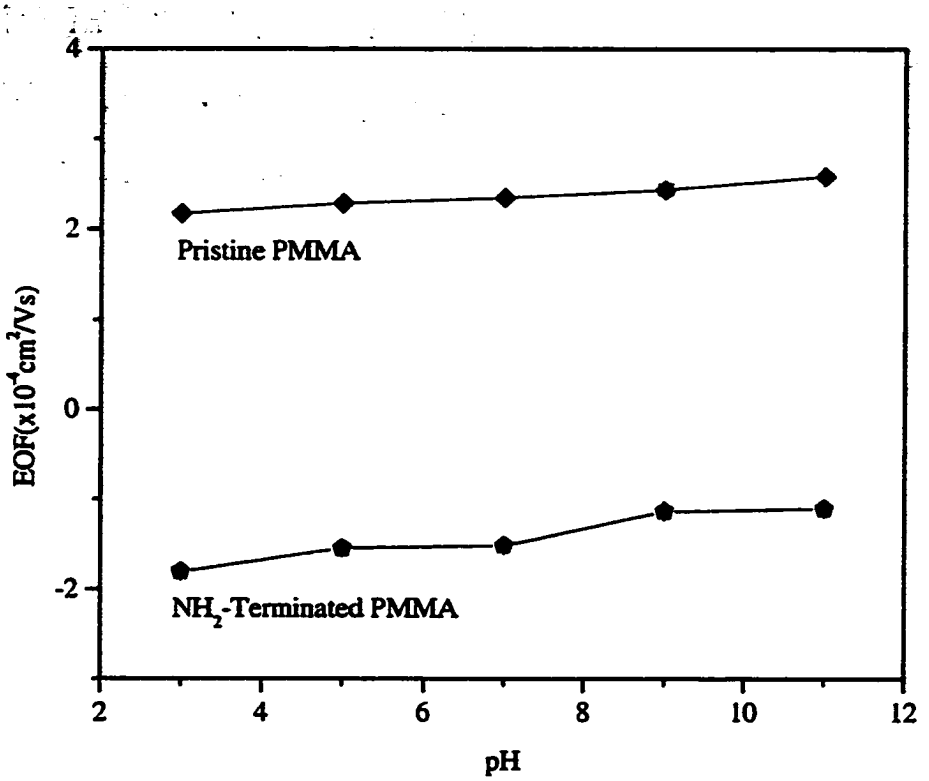

Figure 5.5 **EOF versus pH for modified and unmodified PMMA microdevices. In both cases, the EOF was measured from a pH range of 3-11 using acetate or borate buffers. The low concentration buffer was 10 mM, and the higher concentration buffer was 100 mM. The field strength used (150 V/cm) was selected to minimize Joule heating in the channel, which measured 100 μm X 100 μm X 4 cm.**

investigate the ability to manipulate the EOF through surface modification of PMMA microdevices, a microchannel was machined into PMMA and then aminolysis of both the substrate and cover plate was performed prior to thermal bonding of the cover plate to the machined PMMA sheet. The EOF values as a function of pH for both unmodified and modified PMMA microdevices are shown in Figure 5.5. As can be seen from this figure, the EOF was reversed (negative EOF value indicates solution flow from cathode to anode) in the case of AT-PMMA microchannel, consistent with a

surface having an excess positive charge on its wall. In addition, the EOF is shown to decrease as the solution pH becomes more alkaline (EOF = -1.80 x 10^{-4} cm^2/Vs at pH = 3.0; EOF = -1.05 x 10^{-4} cm^2/Vs at pH = 11.0). This decrease results from the fact that the accessible 1° amines are protonated at low pH and become deprotonated with increasing pH. In the case of the unmodified PMMA microdevice, the EOF does show a slight increase in magnitude at higher pH values, but not to the same degree as seen for the modified device (EOF = 2.17 x 10^{-4} cm^2/Vs at pH = 3.0; EOF = 2.58 x 10^{-4} cm^2/Vs at pH = 11.0).

Recently, Morris et al.[9] reported a ten-fold increase in the EOF of a polyester-based microdevice upon exposure to 0.1 N NaOH for 5 min. To probe the hydrolytic stability of the modified PMMA surfaces, we exposed our amine-modified, micromachined PMMA channels to 0.1 N NaOH for 1 hour. We found that the EOF of our amine-modified channels did not change significantly (initial EOF = -1.13 x 10^{-4} cm^2/Vs versus final EOF = -1.15 x 10^{-4} cm^2/Vs at pH = 9.0) after exposure to 0.1 N NaOH for 1 h.

5.4 Modification of Amine-Terminated PMMA Surfaces to Yield Alkyl-Terminated Surfaces

We were also interested in modifying the PMMA surface so as to create a microanalytical separation device that is lithographically patterned on a "chip" of PMMA and also possesses a hydrophobic phase for electrochromatography applications as has been demonstrated for glass-based microdevices.[10-11] We thus turned our attention toward derivatizing the PMMA such that its surface is terminated in $C_{18}H_{37}$ groups, Figure 5.6. After such a reaction sequence, it was found that the $C_{18}H_{37}$-

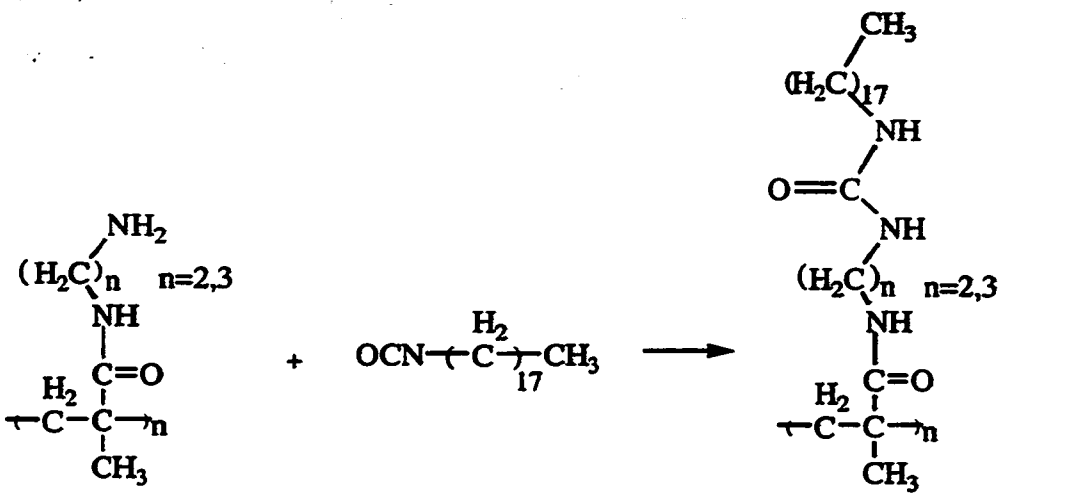

Figure 5.6 Reaction scheme producing $C_{18}H_{37}$-terminated PMMA from NH_2-terminated PMMA reaction with *n*-octadecane-1-isocyanate.

Terminated PMMA sheet was colorless and transparent, exactly like the pristine and AT-PMMA sheets.

5.4.1 Sessile Drop Water Contact Angle Measurements of $C_{18}H_{37}$-Terminated PMMA Surfaces

As mentioned above, the water contact angle of the amine-terminated PMMA surface is quite low, 33° ± 4°, as is to be expected for a relatively hydrophilic surface. The $C_{18}H_{37}$-terminated PMMA surface yielded a water contact angle of 103° ± 10°, a value that is consistent with a smooth poly(ethylene) surface (exposed methylene units).[1] For a close-packed methyl surface (ordered, long-chain *n*-alkanethiols on Au), the expected water contact angle is roughly 113°.[1] The contact angle values obtained here for the $C_{18}H_{37}$-Terminated PMMA would seem to indicate that the chains are either highly disordered or that the chains have a substantial tilt from the surface normal (> ~30° that is observed for *n*-alkanethiols on Au), such that the methylene units of the

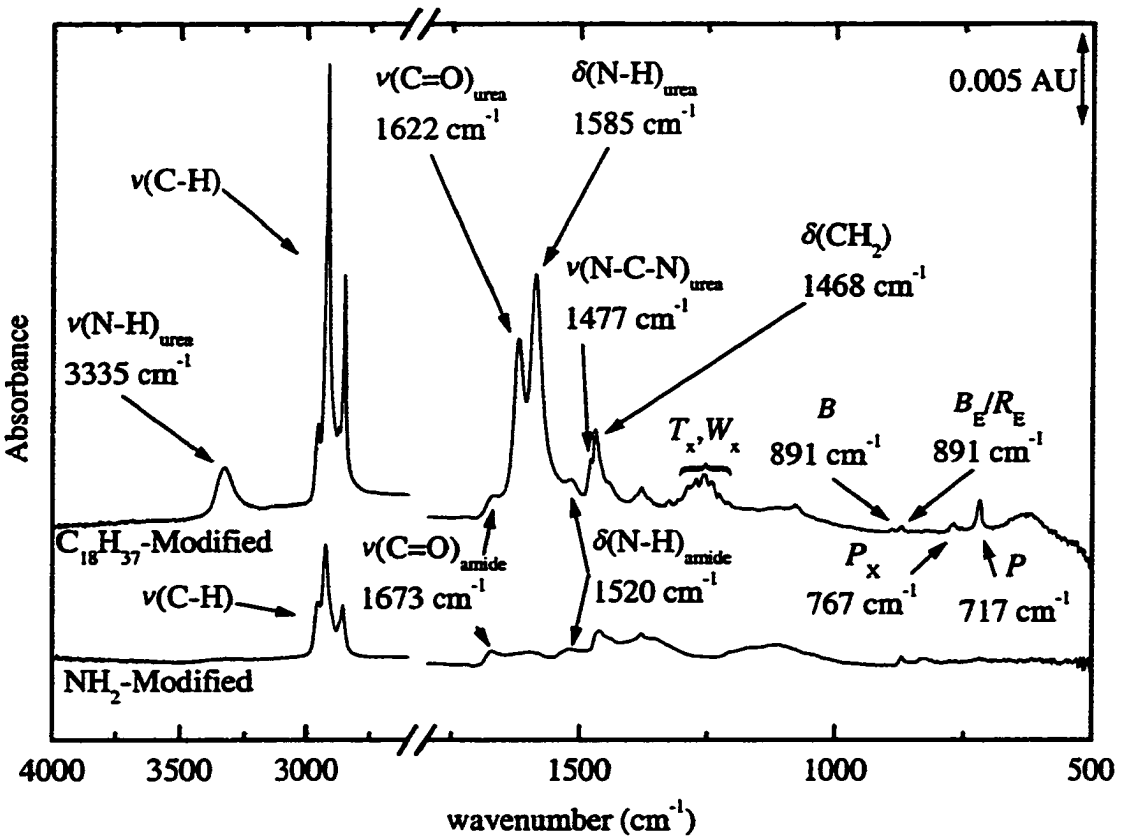

Figure 5.7 Reflection-absorption infrared spectra of NH_2-terminated PMMA and $C_{18}H_{37}$-terminated PMMA spin-coated on Au.

alkane chains are significantly exposed. Based on the infrared data (vide infra), we conclude that the chains are ordered but have a substantial tilt from the surface normal.

5.4.2 Reflection-Absorption Infrared (RAIR) Spectroscopy Studies of $C_{18}H_{37}$-Terminated PMMA Surfaces.

Displayed in Figure 5.7 are representative RAIR spectra of $C_{18}H_{37}$-terminated and NH_2-Terminated PMMA; Table 5.2 lists the band assignments. For the $C_{18}H_{37}$-terminated surface, the primary bands to note are those associated with $\nu(\text{N-C-N})_{\text{urea}}$ at

Table 5.2 Infrared band positions and assignments for NH_2-terminated PMMA and $C_{18}H_{37}$-terminated PMMA.

NH_2-Terminated PMMA		$C_{18}H_{37}$-Terminated PMMA	
Position (cm^{-1})	assignment	position (cm^{-1})	assignment
~3314	ν(N-H)	3335	$\nu(N\text{-}H)_{urea}$
2955	$\nu_a(CH_3)$	2955	$\nu_a(CH_3)$
2926	$\nu_a(CH_2)$	2920	$\nu_a(CH_2)$
2871	$\nu_s(CH_3)$	2873	$\nu_s(CH_3)$
2856	$\nu_s(CH_2)$	2849	$\nu_s(CH_2)$
1673	$\nu(C{=}O)_{amide}$	1673	$\nu(C{=}O)_{amide}$
1520	$\delta(N\text{-}H)_{amide}$	1622	$\nu(C{=}O)_{urea}$
1460	$\alpha(CH_3)/\delta(CH_2)$	1585	$\delta(N\text{-}H)_{urea}$
		1520	$\delta(N\text{-}H)_{amide}$
		1477	$\nu(N\text{-}C\text{-}N)_{urea}$
		1468	$\delta(CH_2)$
		1460	$\alpha(CH_3)$
		1441	$\delta_D(CH_2)$
		1376	U
		1288-1233	Tx;Wx
		891	B
		871	B_E/R_E
		767	Px
		717	P

1477 cm^{-1}, the $\nu(C{=}O)_{urea}$ band at 1622 cm^{-1}, the $\delta(N\text{-}H)_{urea}$ band at 1585 cm^{-1}, and the $\nu(N\text{-}H)_{urea}$ band at 3335 cm^{-1}. In addition, a large increase in the intensity of the ν(C-H) bands in the 2800-3000 cm^{-1} region is observed. Overall, these data indicate that the amine-modified PMMA surface has undergone a chemical reaction with the *n*-octadecane-1-isocyanate to form a urea linkage. Finally, because there is no band at 2200 cm^{-1} corresponding to ν(C≡N), there is no physisorbed *n*-octadecane-1-isocyanate

present on the surface of the PMMA. The order (crystallinity) of the $C_{18}H_{37}$ chains bound to the PMMA surface is very high, as judged by the presence and position of certain infrared bands in Figure 5.8. The band positions of the $\nu_a(CH_2)$ and $\nu_s(CH_2)$ modes, 2920 cm^{-1} and 2847 cm^{-1}, indicate that the alkane chains are highly ordered.[12-16] This is further supported by the presence of a series of bands known as the progression bands in the 1300-1200 cm^{-1} region, which are associated with the twisting/rocking and wagging of the methylene C-H groups (T_x and W_x modes). The position and morphology of the progression bands are characteristic of a highly crystalline alkane environment.

5.4.3 Scanning Force Microscopy Studies of $C_{18}H_{37}$-Terminated PMMA Surfaces

The alkane-terminated PMMA sheet surfaces exhibits a surface morphology that is slightly different from the amine-modified surface, Figure 5.8. The $C_{18}H_{37}$-modified PMMA surface is reminiscent of alkylsilane-coated silicon surfaces,[17] in that the $C_{18}H_{37}$-modified PMMA surface appears as if it possesses fluid-like characteristics, thus making it difficult to obtain well-resolved SFM images. A RMS roughness of 2.8 nm and a roughness factor of 1.034 were obtained from SFM images of $C_{18}H_{32}$-modified PMMA surfaces. This is approximately 1.6–2 times greater than that of the amine-modified PMMA surfaces.

5.5 DNA Digestion with Restriction Enzymes Immobilized on AT-PMMA

In order to demonstrate the application of functionalized PMMA for enzyme immobilization and reactions, an *Hae III* restriction endonuclease enzyme was covalently attached through a glutaric dialdehyde linkage to AT-PMMA. The *Hae III* restriction enzyme recognizes a four base sequence in dsDNA and cuts between the G

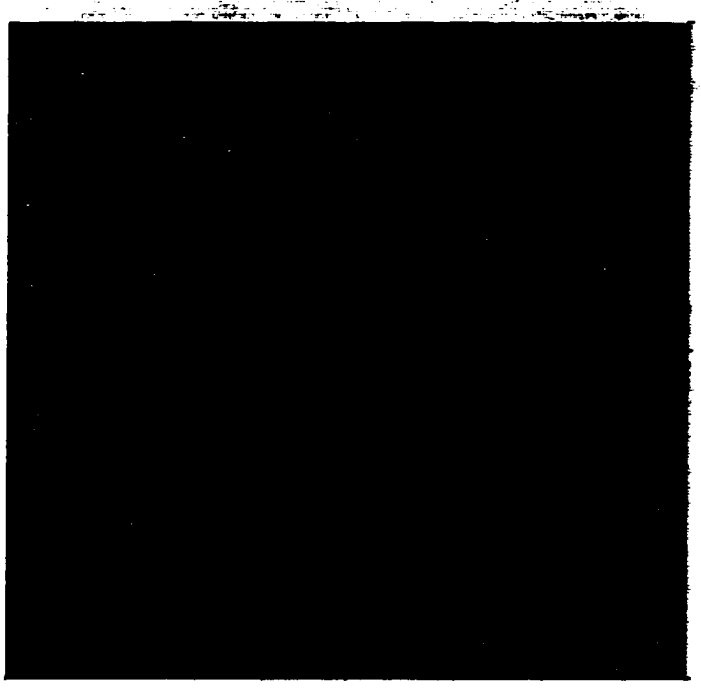

Figure 5.8 Representative 2 μm X 2 μm scanning force micrograph of $C_{18}H_{37}$-Terminated PMMA. The Z-range is 10 nm.

(guanidine) and C (cytosine) residues within this sequence. Digestion of the dsDNA phage, ΦX174-RF (5386 bp), with *Hae III* produces 11 fragments and is commonly used as a standard for size determinations of linear, dsDNA from 72 to 1353 bp in length. In order to verify coupling of the restriction endonuclease to the functionalized PMMA and to determine if the enzyme would retain its activity when attached to the PMMA surface, the digestion fragments produced were identified by their sizes using conventional CE. Shown in Figure 5.9 are the electropherograms for the digests of ΦX174-RF phage resulting from exposure to *Hae III* in free solution and immobilized on PMMA. From Figure 5.9, there is no detectable difference in the DNA digestion patterns, which indicates that the recognition sequence for the enzyme was unaffected by its immobilization on PMMA. The migration time for the free-solution digest

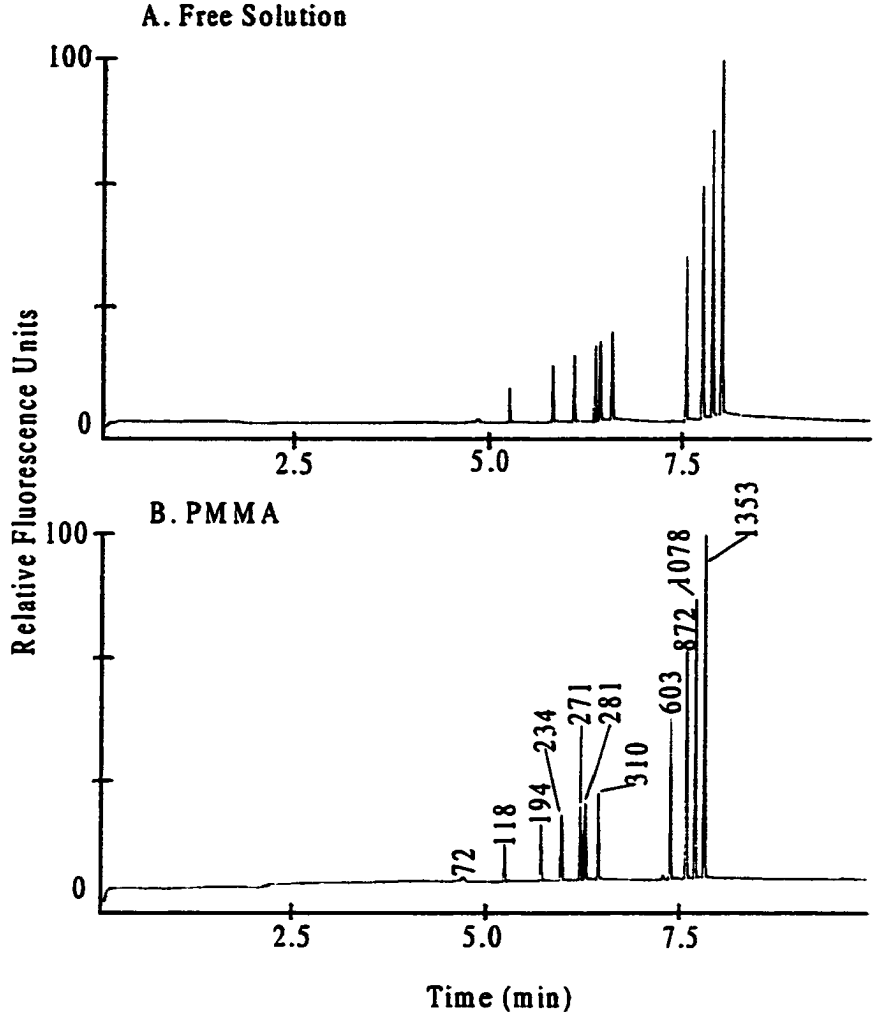

Figure 5.9 Capillary electropherograms of A. a free solution and B. a PMMA-immobilized enzyme digest of ΦX174-RF DNA.

(Figure 5.9A) was consistently slower than that of the immobilized case and can be explained by the fact that the free-solution digest buffer is much more viscous than the CE running buffer.

5.6 Conclusions

In this study, we have demonstrated the successful modification of PMMA sheets used in the manufacture of miniaturized analytical instrumentation. Specifically,

we have shown that PMMA can be modified so as to have accessible amine sites on its surface which can be used to change the flow properties of microelectrophoresis devices or can be used as a platform for further functionalization. Finally, the synthesis of hydrophobic surfaces appropriate for future electrochromatography applications is demonstrated.

5.7 References

1) Ulman, A. *An Introduction to Ultrathin Organic Films: From Langmuir-Blodgett to Self-Assembly*, Academic Press, Inc.: San Diego, CA, 1991.

2) Bain, C.D.; Whitesides, G.M. *J. Am. Chem. Soc.* **1988**, *111*, 7155.

3) Peanasky, J.S.; McCarley, R.L. *Langmuir* **1998**, *14*, 113-123.

4) Omastova, M.; Pavlinec, J.; Pionteck, J.; Simon, F.; Kosina, S. *Polymer* **1998**, *39*, 6559-6566.

5) Briggs, D.; Seah, M.P. *Practical Surface Analysis by Auger and X-Ray Photoelectron Spectroscopy*, John Wiley, New York, New York, 1983.

6) Karandikar, B.; Puschett, J.; Matyjaszewzki, K. *Polymer Prep.* **1989**, *30*, 250-251.

7) Proctor, K.G.; Ramirez, S.K.; McWilliams, K.L.; Huerta, J.L.; Kirkland, J.J. in *Chemically Modified Surfaces: Recent Developments*, pp. 45-60; Pesek, J.J.; Matyska, M.T.; Abuelafiya, R.R.; Eds., **1996**, The Royal Society of Chemistry: Cambridge.

8) Ford, S.M.; Davies, J.; Kar, B.; Qi, S.; McWhorter, C.S.; Soper, S.A.; Malek, C.K. *J. Biomech. Eng.* **1999**, *121*, 13-21.

9) Wang, S.-C.; Perso, C.E.; Morris, M.D. *Anal. Chem.* **2000**, *72*, 1704-1706.

10) He, B.; Tait, N.; Reigner, F. *Anal. Chem.* **1998**, *70*, 3790-3797.

11) Kulter, J.P.; Jacobson, S.C.; Matsubara, N.; Ramsey, J.M. *Anal. Chem.* **1998**, *70*, 3291-3297.

12) Hostetler, M.J.; Stokes, J.J.; Murray, R.W. *Langmuir* **1996**, *12*, 3604-3612.

13) Schachtschneider, J.H. *Spectrocim. Acta* **1963**, *19*, 85-116.

14) Schachtschneider, J.H.; Snyder, R.G. *Spectrochim. Acta* **1963**, *19*, 117-178.

15) Snyder, R.G. *J. Chem. Phys.* **1967**, *47*, 1316-1325.

16) Maroncelli, M.; Qi, S.P.; Strauss,H.L.; Snyder, R.G. *J. Am. Chem. Soc.* **1982**, 7-22.

17) Dunaway, D.J.; McCarley, R.L. *Langmuir*, **1994**, *10*, 3598-3606.

Chapter 6

Modification of PMMA Sheets to Yield Anionic Terminal Functionalities—Manipulation of the Electoosmotic Flow through PMMA-Based Microdevices

6.1 Introduction

Described here is the synthesis and characterization of carboxylic acid-terminated (CT) and sulfonic acid-terminated (ST) PMMA sheets used to construct microelectrophoretic devices. These anionic moieties were chosen in order to manipulate the electroosmotic flow (EOF) in chemically modified PMMA microchannels. Recent reports have focused on the manipulation of EOF in plastic[1-5] and glass[6-8] microdevices using noncovalent methods.[1-8] By modifying the surface charge in microchannels, it is possible to control the flow rate and direction in microanalytical separation devices. Described in this work is the manipulation of the EOF in microchannels that have been chemically modified to yield *covalent* linkages. Protocols for the surface modification of amine-terminated (AT) PMMA to yield CT-PMMA and ST-PMMA surfaces using standard carbodiimide coupling procedures[9] are presented. Characterization of CT-PMMA and ST-PMMA thin films was accomplished using reflection-absorption infrared (RAIR) spectroscopy. CT- and ST-terminated Au films were also characterized by RAIR spectroscopy and compared to CT- and ST-PMMA. CT-PMMA and ST-PMMA microchannels were assembled and their EOF profiles were obtained. It was found that the EOF in CT-PMMA microchannels is pH dependent and runs from anode to cathode at pH values above the pK_a of the carboxylic acid. In ST-PMMA microchannels, the EOF is slightly pH dependent and runs from anode to cathode; at pH values above the pK_a of the sulfonic acid, the EOF is positive as compared to the cathode-to-anode direction of the EOF in AT-PMMA microchannels.

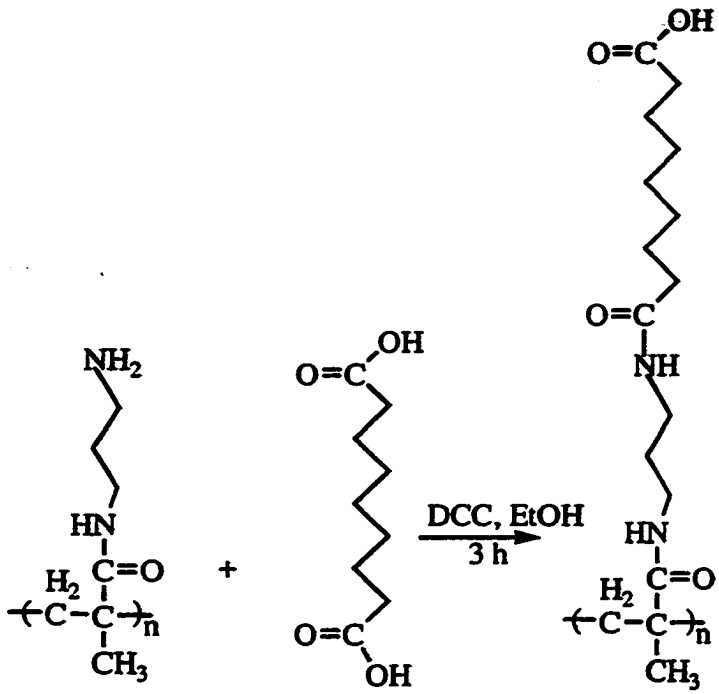

Figure 6.1 **Reaction scheme of AT-PMMA with 1,9-nonanedioic acid to yield CT-PMMA.**

6.2 Characterization of CT-PMMA and CT-Au by Reflection-Absorption Infrared (RAIR) Spectroscopy

In a previous report,[10] we extensively characterized the molecular nature of pristine PMMA and AT-PMMA by the use of RAIR spectroscopy, as well as a variety of surface analysis methods, including XPS, confocal fluorescence microscopy, and SFM.. In that work, the infrared spectra of pristine and AT-PMMA were compared. The main differences in the two spectra are in the 1750-1500 cm^{-1} region due to the presence of a methyl ester on the pristine PMMA surfaces and the conversion of that ester to an amide on the AT-PMMA. That is, in the case of pristine PMMA, the $\nu(C=O)_{ester}$ band is present at approximately 1720 cm^{-1}; but AT-PMMA displays bands

at approximately 1670 cm^{-1} and 1520 cm^{-1} corresponding to the $\nu(C=O)_{amide}$ and $\delta(N-H)_{amide}$ vibrations, respectively.[10]

Reaction of AT-PMMA with 1,9-nonanedioic acid in the presence of DCC yields an amide linkage like that produced to yield AT-PMMA, Figure 6.1. Displayed in Figure 6.2 are representative RAIR spectra of AT-PMMA and CT-PMMA. A band at 1720 cm^{-1} is evident in both spectra; in the case of AT-PMMA, this band corresponds to $\nu(C=O)_{ester}$ of the unreacted methyl ester. The more intense band at 1720 cm^{-1} on the CT-PMMA corresponds not only to $\nu(C=O)_{ester}$ but also the C=O stretch of the terminal carboxylic acid, $\nu(C=O)$. The bands at 1672 cm^{-1} and 1526 cm^{-1} are associated with the $\nu(C=O)_{amide}$ and $\delta(N-H)_{amide}$ modes, respectively.[11] It is important to note that the intensities of the amide bands in the CT-PMMA spectrum are greater than those present in the AT-PMMA spectrum, indicating that more amide functionalities are present on the CT-PMMA surface. Although the increase in the intensities of the Amide I and II bands could be due to orientational differences, from a qualitative standpoint there appears to be more amide functionalities in the CT-PMMA spectrum than in the AT-PMMA spectrum. The ratio of the Amide I and II bands are similar to those calculated for isotropic systems; thus, it is postulated that the increase in intensity of the Amide I and II bands are due, in fact, to the higher amount of amide linkages on the CT-PMMA surface.

The band at 1260 cm^{-1} present in both spectra in Figure 1 corresponds to $\nu(C-N)_{amide}$. In the CT-PMMA spectrum, this band is much more intense; the increased intensity could be due to $\nu(C-O)_{carboxylic\ acid}$ present in addition to the $\nu(C-N)_{amide}$. The presence of this more intense band also indicates that more amide linkages are on the

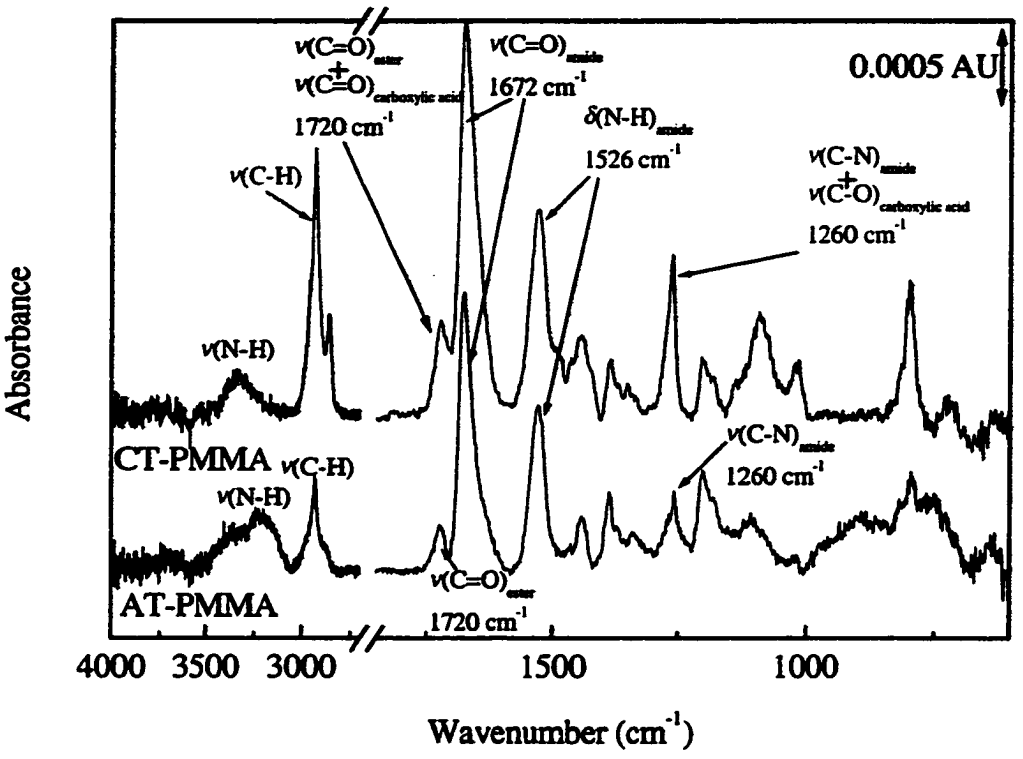

Figure 6.2 Representative RAIR spectra of AT-PMMA and CT-PMMA spin-coated on Au.

CT-PMMA surface compared to those present on the AT-PMMA surface. Finally, the band at 1093 cm^{-1} on the CT-PMMA spectrum is indicative of $\nu(CO_2)_{carboxylic\ acid}$, pointing to the fact a carboxylic acid can be found on the surface.[11] Control experiments consisting of exposing AT-PMMA to 1,9-nonanedioic acid in the absence of DCC resulted in no change of the intensisties of the Amide I and II bands.

The spectra shown in Figure 6.2 indicate that a chemical reaction has most likely occurred, yielding a carboxylic acid-terminated surface. However, because the molecular nature of the AT-PMMA and the CT-PMMA are so similar, it is necessary to determine that the reaction took place using a model system. To verify this chemistry, we prepared an AT-Au surface using 2-aminoethanethiol self-assembled on Au.[12] We

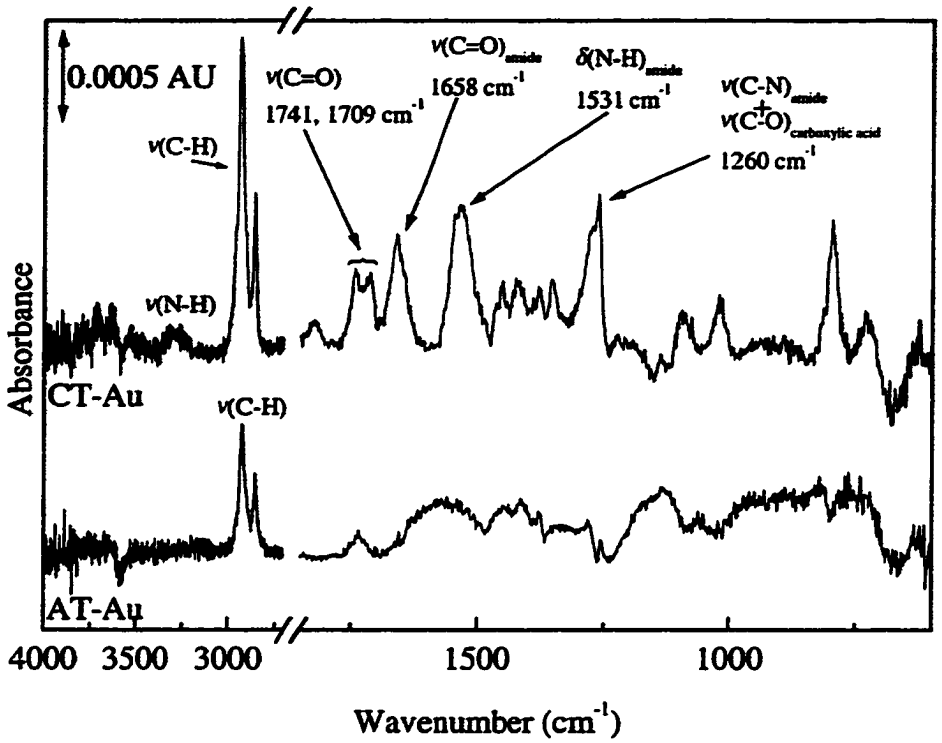

Figure 6.3 Representative RAIR spectra of AT-AU and CT-Au.

then reacted the surface-bound amines with 1,9-nonanedioic acid to produce CT-Au; this reaction was performed in the same manner as the reaction involving AT-PMMA and 1,9-nonanedioic acid. Displayed in Figure 6.3 are representative RAIR spectra of AT-Au and CT-Au surfaces. In the CT-Au spectrum, bands at 1741 cm^{-1} and 1709 cm^{-1} corresponding to $\nu(C=O)_{carboxylic\ acid}$ are present; in addition, bands at 1658 cm^{-1} and 1531 cm^{-1} corresponding to $\nu(C=O)_{amide}$ and $\delta(N-H)_{amide}$ exist. A band at 1260 cm^{-1} corresponding to $\nu(C-N)_{amide}$ and $\nu(C-O)_{carboxylic\ acid}$, as well as a band at 1093 cm^{-1} corresponding to $\nu(CO_2)_{carboxylic\ acid}$, are present, indicating the presence of an amide linkage and a carboxylic acid.[11] The data presented demonstrate that surface-bound primary amines on Au surfaces react with 1,9-nonanedioic acid to yield amide linkages and the surface is terminated in carboxylic acids. Many of the same bands present on

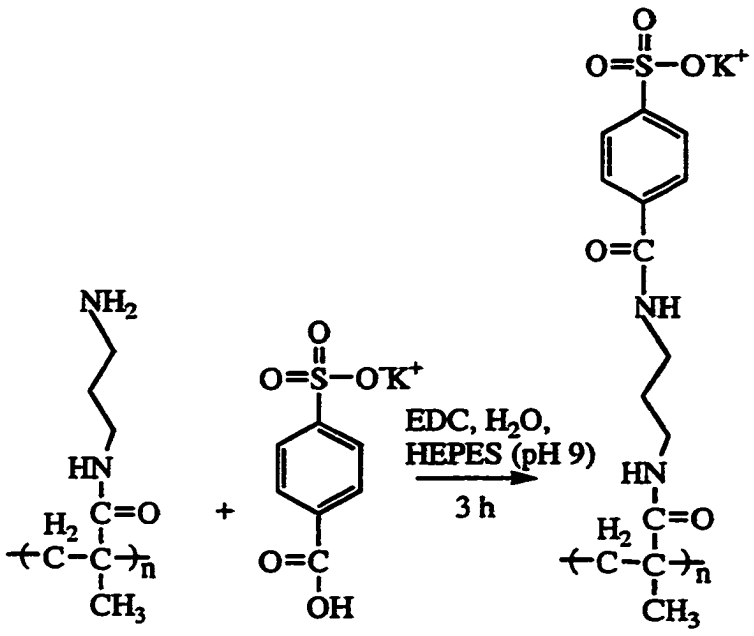

Figure 6.4 **Reaction scheme of AT-PMMA with 4-sulfobenzoic acid to yield ST-PMMA.**

the CT-Au spectrum are also present on the CT-PMMA spectrum; thus, surface-bound amines on PMMA react with nonanedioic acid to produce CT-PMMA.

6.3 Characterization of ST-PMMA and ST-Au by RAIR Spectroscopy

Displayed in Figure 6.4 is the coupling reaction used here for AT-PMMA or AT-Au with 4-sulfobenzoic acid in the presence of EDC in HEPES buffer (pH 9). The coupling of the carboxylic acid with the surface-bound amines should yield amide linkages; the surface should be terminated in sulfonate groups.

Shown in Figure 6.5 are representative RAIR spectra of AT-PMMA and ST-PMMA. The bands at 1672 cm^{-1} and 1526 cm^{-1} present on both spectra are due to the $\nu(C{=}O)_{amide}$ and $\delta(N\text{-}H)_{amide}$ transitions, respectively. Displayed on the ST-PMMA PMMA surface due to the higher number of amide linkages on this surface as compared

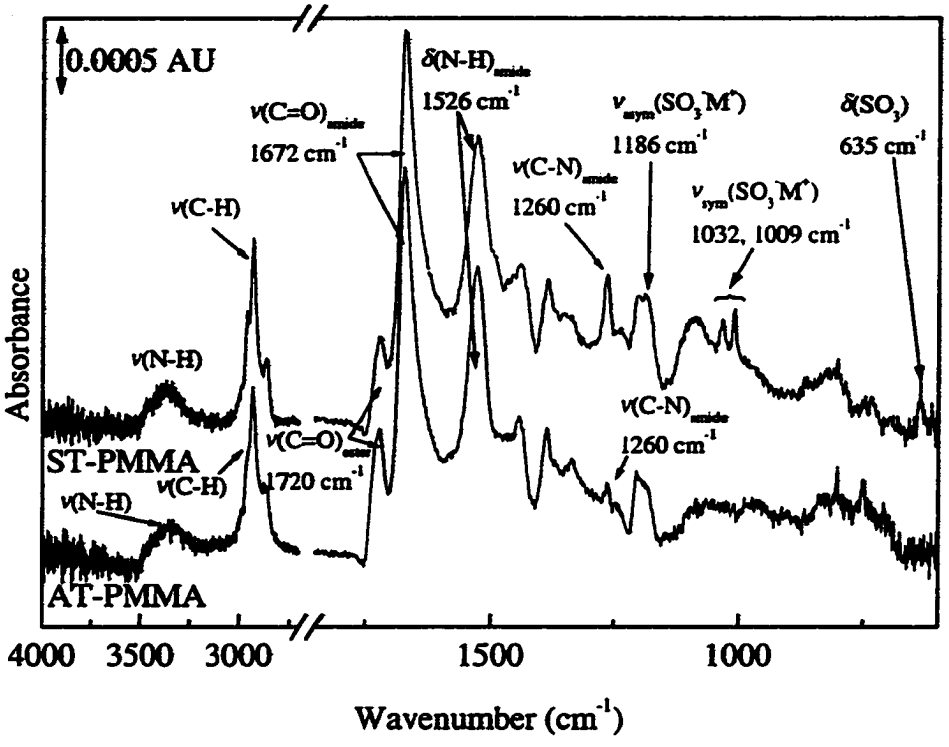

Figure 6.5 **Representative RAIR spectra of AT-PMMA and ST-PMMA spin-coated on Au.**

to the AT-PMMA surface. The band at 1186 cm^{-1} is because of $\nu_{asym}(SO_3^-M^+)$ of the sulfonate on the PMMA surface. Also indicative of the sulfonate groups are bands at 1032 cm^{-1} and 1009 cm^{-1}, corresponding to $\nu_{sym}(SO_3^-M^+)$, and at 635 cm^{-1}, corresponding to $\delta(SO_3^-)$.[11]

The data displayed in Figure 6.5 indicate that a metal coordinated sulfonate species is present on the surface. In addition, bands can be seen which most likely indicates that an amide linkage is produced upon reaction of the surface-bound amines with 3-sulfobenzoic acid in the presence of EDC in HEPES buffer. Control experiments involving the exposure of AT-PMMA to 4-sulfobenzoic acid in the absence of EDC were performed; the results indicate that no reaction occurred.

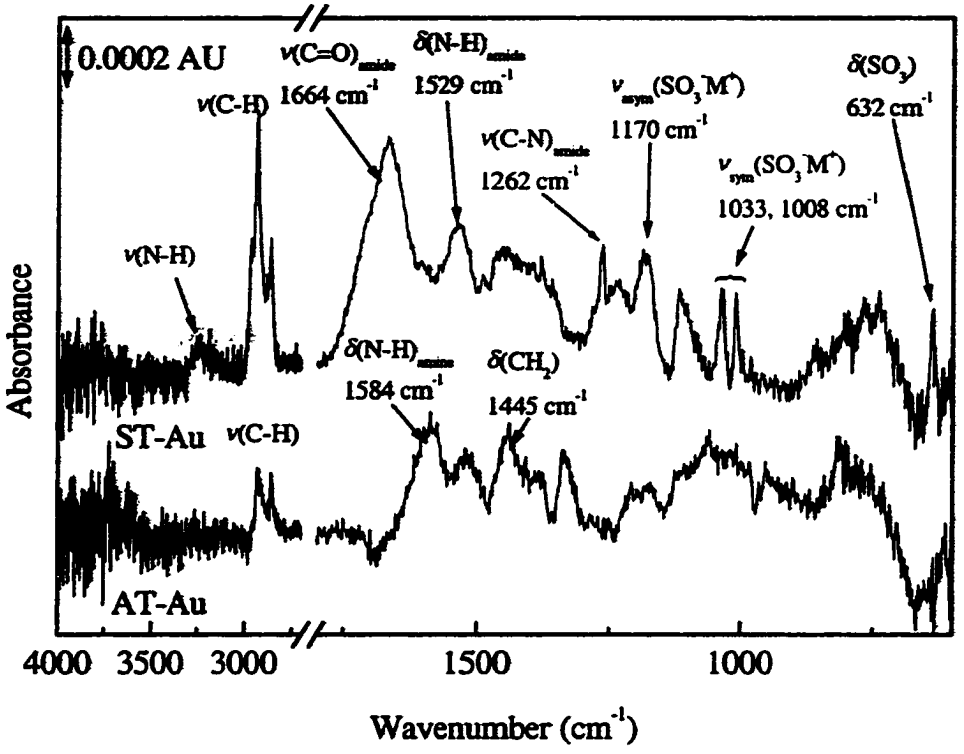

Figure 6.6 Representative RAIR spectra of AT-Au and ST-Au.

As with the CT-PMMA system, because amide linkages are present in the AT-PMMA spectrum, it is necessary to employ a model amine-terminated surface that does not contain amide functionalities in this reaction. We thus prepared AT-Au surfaces; the surface-bound primary amines were utilized in a reaction with 4-sulfobenzoic acid in the presence of EDC in HEPES buffer (identical conditions as for AT-PMMA). Displayed in Figure 6.6 are representative RAIR spectra of AT-Au and ST-Au surfaces. Evident on the AT-Au spectrum are bands at 1584 cm^{-1} and 1445 cm^{-1}, corresponding to $\delta(N\text{-}H)_{amine}$ and $\delta(CH_2)$, respectively. However, present in the ST-Au spectrum are bands at 1664 cm^{-1} and 1529 cm^{-1} corresponding to $\nu(C{=}O)_{amide}$ and $\delta(N\text{-}H)_{amide}$, respectively. The presence of these amide bands as well as a band at 1260 cm^{-1}

corresponding to $\nu(C\text{-}N)_{amide}$ indicates that an amide functionality has been produced and is present on the surface. Thus, the reaction involving surface-bound amines and 4-sulfobenzoic acid has produced an amide functionality. In addition, a band at 1170 corresponding to $\nu_{asym}(SO_3^-M^+)$, bands at 1033 cm^{-1} and 1008 cm^{-1} corresponding to $\nu_{sym}(SO_3^-M^+)$, and a band at 632 cm^{-1} corresponding to $\delta(SO_3^-)$ are present on the ST-Au spectrum, indicating that sulfonate species are present on the surface.[11]

It has been shown that reactions involving surface-bound primary amines on Au surfaces with 4-sulfobenzoic acid result in amide linkages and terminal sulfonate groups. Many of the same bands present on the ST-Au spectrum are also present on the ST-PMMA spectrum, indicating that the reaction involving surface-bound primary amines on PMMA with 4-sulfobenzoic acid produced a ST-PMMA surface.

6.4 Manipulation of EOF in PMMA Microchannels by Chemical Modification of the PMMA Surface

The goal of this work is to change the EOF in PMMA microchannels by chemical modification of the PMMA surface. Previously, it was reported that the EOF profiles of acetate and borate buffers in pristine PMMA and AT-PMMA microchannels.[10] It was found that the EOF changes direction upon amination of the PMMA microchannel due to the presence of positive charges on the AT-PMMA microchannel. Thus, the EOF runs from cathode to anode through AT-PMMA microchannels, whereas the EOF runs from anode to cathode in pristine PMMA microchannels. In addition, while the EOF is almost pH independent in pristine PMMA microchannels, the EOF decreases in magnitude at high pH values in AT-PMMA microchannels due to the deprotonation of amine moieties on the AT-PMMA surface.

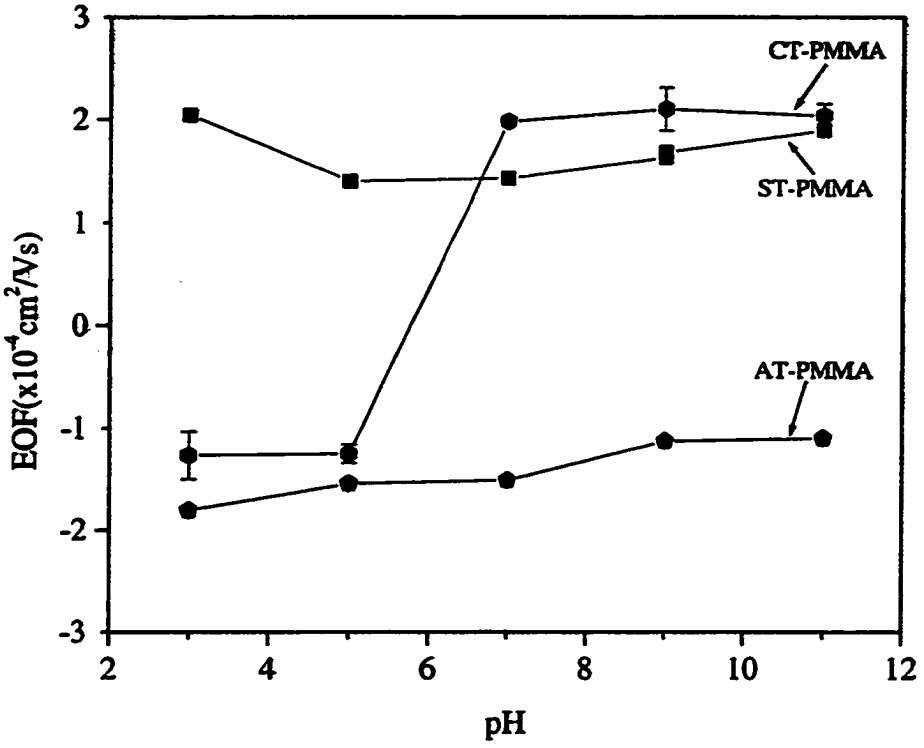

Figure 6.7 **EOF profiles of AT-PMMA, CT-PMMA, and ST-PMMA. In all cases, the EOF was measured from a pH range of 3-11 using acetate or borate buffers. The low concentration buffer was 10 mM, and the higher concentration buffer was 100 mM. The field strength used (150 V/cm) was selected to minimize Joule heating in the channel, which measured 100 μm X 100 μm X 4 cm.**

AT-PMMA was chemically modified to yield carboxylate and sulfonate species on the surface of the PMMA microchannels. To achieve this, all chemical modifications were performed on the machined microchannel and top plate prior to thermal bonding of the top plate to the microchannel substrate. EOF profiles of CT-PMMA and ST-PMMA are displayed in Figure 5. In the case of CT-PMMA at pH 3–5, the EOF is negative, indicating that the EOF runs from cathode to anode. This is not surprising because the AT-PMMA displayed negative EOF values at this pH;[10] there are

evidently some free amine sites that did not react with 1,9-nonanedioic acid, possibly due to inaccessibility of the amine group during the coupling reaction or hindrance of the carboxylic acid by the alkane chain. The carboxylic acid species that are present on the surface are protonated at pH ~3–5,[12] which explains the decrease in magnitude of the EOF in this region as compared to AT-PMMA. At pH 7, the EOF = -1.50 x 10^{-4} $cm^2V^{-1}sec^{-1}$ in AT-PMMA microchannels, whereas the EOF = 1.05 x 10^{-4} $cm^2V^{-1}sec^{-1}$ in CT-PMMA microchannels. Thus, at pH 7, the EOF in CT-PMMA runs from anode to cathode, or opposite in direction as compared to the EOF in AT-PMMA microchannels. This is due to the deprotonation of the carboxylic acid species present on the CT-PMMA surface, yielding a negative surface charge. These data indicate that, although there are some amine species present on the CT-PMMA surfaces, the vast majority of the surface is negatively charged. Thus, there are more carboxylic acid groups present on the CT-PMMA surface than there are amine groups. The EOF remains relatively constant at pH 9–11 in the CT-PMMA microchannel due to the deprotonated carboxylic acid moieties and the lack of more carboxylate moieties being formed.

Also displayed in Figure 5 is the EOF profile of ST-PMMA. At pH=3, the EOF = 2.10 x 10^{-4} $cm^2V^{-1}sec^{-1}$ in the ST-PMMA microchannel, compared to -1.80 x 10^{-4} $cm^2V^{-1}sec^{-1}$ in the AT-PMMA microchannel. These data indicate that there is an excess of negative charge of the ST-PMMA surface, thus driving the EOF from anode to cathode. While there may be some unreacted amine moieties on the surface of the ST-PMMA, the overall direction of the EOF indicates that sulfonate moieties are more prevalent on this surface at the pH values noted. The magnitude of the EOF in ST-PMMA microchannels decreases to 1.40 x 10^{-4} $cm^2V^{-1}sec^{-1}$ at pH 5, remains relatively

close to this value at pH 7, and increases at pH 9–11. The variation of EOF with pH are as yet unexplained.

In order to determine whether the modified microchannels are hydrolytically stable, the CT-PMMA and ST-PMMA microchannels were exposed to 0.1 M NaOH for 1 h. It was found that the EOF values obtained did not differ significantly from those obtained before exposure to 0.1 M NaOH. These data are consistent with hydrolytic stability tests previously performed on AT-PMMA surfaces,[10] and point to the fact that the use of amide bonds for tethering chemical modifiers is prudent.

6.5 Conclusions

This work demonstrates the successful chemical modification of amine-terminated PMMA surfaces to yield carboxylate-terminated PMMA and sulfonate-terminated PMMA surfaces. The chemical modification of surface-bound amines present on Au surfaces to yield carboxylate-terminated and sufonate-terminated Au as investigated by infrared spectroscopy was also discussed and compared to results obtained for carboxylate-terminated and sulfonate-terminated PMMA. EOF profiles of carboxylate-terminated PMMA and sulfonate-terminated PMMA microchannels were determined, and it was found that the magnitude and direction of the EOF can be changed by covalent modification of PMMA microchannels. The outcomes of this research will be of great importance to future applications of plastic-based analytical microdevices.

6.6 References

1) Roberts, M.A.; Rossier, J.S.; Bercier, P.; Girault, H. *Anal. Chem.* **1997**, *69*, 2035-2042.

2) Locascio L.E.; Perso, C.; Lee, C.S. *J. Chromatogr. A* **1999**, *857*, 257-284.

3) Wang, S.-C.; Perso, C.E.; Morris, M.D. *Anal. Chem.* **2000**, *72*, 1704-1706

4) Barker, S.L.R.; Tarlov, M.J.; Canavan, H.; Hickman, J.J.; Locascio, L.E. *Anal. Chem.* **2000**, *72*, 4899-4903.

5) Liu, Y.; Fanguy, J.C.; Bledsoe, J.M.; Henry, C.S. *Anal. Chem.* **2000**, *72*, 5939-5944.

6) Pinto, D.M.; Ning, Y.; Figeys, D. *Electrophoresis* **2000**, *21*, 181-190.

7) Chiem, N.; Harrison, D.J. *Anal. Chem.* **1997**, *69*, 373-378.

8) Culbertson,C.T.; Ramsey, R.S.; Ramsey, J.M. *Anal. Chem.* **2000**, *72*, 2285-2291.

9) Atherton, E. *Solid-Phase Peptide Synthesis: A Practical Approach*, IRL Press: New York, 1989.

10) Henry, A.C.; Tutt, T.J.; Galloway, M.; Davidson, Y.Y.; McWhorter, C.S.; Soper, S.A.; McCarley, R.L. *Anal. Chem.* **2000**, *72*, 5331-5337.

11) Socrates, G. *Infrared Characteristic Group Frequencies*, Wiley: New York, 1994.

12) Ulman, A. *An Introduction to Ultrathin Organic Films: From Langmuir-Blodgett to Self-Assembly*, Academic Press, Inc.: San Diego, CA, 1991.

13) Harris, D.C. *Quantitative Chemical Analysis*, W.H. Freeman and Co.: New York, 1991.

Chapter 7

Photo-Directed Deposition of Metal Features on PMMA Surfaces

7.1 Introduction

Described here is the use of AT-PMMA surfaces as a substrates for the electroless deposition of Au nanoparticle films (Au-EDNPFs), the adsorptive deposition of Au colloids, the laterally patterned formation of Au-EDNPFs, and the use of the patterned Au-EDNPFs to form electrolessly deposited Ag films with micrometer features. Au-EDNPFs were formed by chemical reduction of $AuCl_4^-$ films coordinated to AT-PMMA sheets. The Au-EDNPFs act as autocatalytic seed layered substrates for the conventional electroless deposition of Ag. Such Ag films can be used in the construction of functional Ag/AgCl reference electrodes, as demonstrated by electrochemistry experiments. In addition, sequentially deposited, multilayer Au colloid films formed on the AT-PMMA surfaces are shown, using electrochemistry, to be effective electrochemical working electrodes in aqueous media. In the final portion of the work, laterally patterned (selective) deposition of Ag films was accomplished by photoremoval of photolabile protecting groups attached to the amine functionalities of AT-PMMA. Fluorescence micrographs of patterned PMMA indicate the presence of patterned amines. These patterned amines were used in the Au-EDNPF formation process, followed by the subsequent electroless deposition of Ag onto the Au-EDNPF surface. The selectivity of the Au-EDNPF pattern formation process (deposition on only the deprotected amine sites and not the protected sites) is shown to be dictated by the pH of the $AuCl_4^-$ solution in contact with the photo-deprotected surfaces.

7.2 Electroless Deposition of Au Seed Layers on AT-PMMA Surfaces

Au was electrolessly deposited on AT-PMMA surfaces by adaptation of a novel electroless deposition protocol that has been described previously.[1] Briefly, exposure of amine-terminated silane monolayers on glass or quartz to aqueous solutions of $AuCl_4^-$ followed by exposure to either aqueous $NaBH_4$ or NaH_2PO_2 results in formation of Au nanoparticle films. These electrolessly deposited Au nanoparticle films (Au-EDNPFs) are catalytically active for the electroless deposition of a variety of metals (Au, Cu, Ag, Ni) and remain active after exposure to laboratory ambient for time periods of up to one year. AT-PMMA was manufactured as previously described by reacting pristine, commercially available PMMA sheets with *N*-lithiodiaminopropane dissolved in cyclohexane.[2] This procedure gives rise to primary amines on the PMMA sheet surface with a surface concentration of roughly 5×10^{-9} mole cm^{-2}.[2] After immersion of AT-PMMA in 0.1 mM $HAuCl_4$ for various lengths of time, the pieces were rinsed with 18 $M\Omega$ •cm water, dried with a stream of N_2, and then exposed to 1 M $NaBH_4$ for 1 min. Following reduction, the formerly transparent AT-PMMA sheets exhibited a uniform raspberry-colored surface film that could not be removed by the standard tape test.[3-4]

Displayed in Figure 7.1 are optical absorption spectra of electrolessly deposited Au on AT-PMMA sheets. The feature at ~520 nm is evident in the spectra corresponding to immersion times (in the $HAuCl_4$) of 15 min and greater. In addition, the intensity of the band at 520 nm increases with increased time of immersion in the $HAuCl_4$ solution. These data indicate that ionic Au species are being coordinated by the surface amines and then are subsequently reduced to form nanoparticle structures on associated with nanometer-sized Au particles, as previously observed for similarly

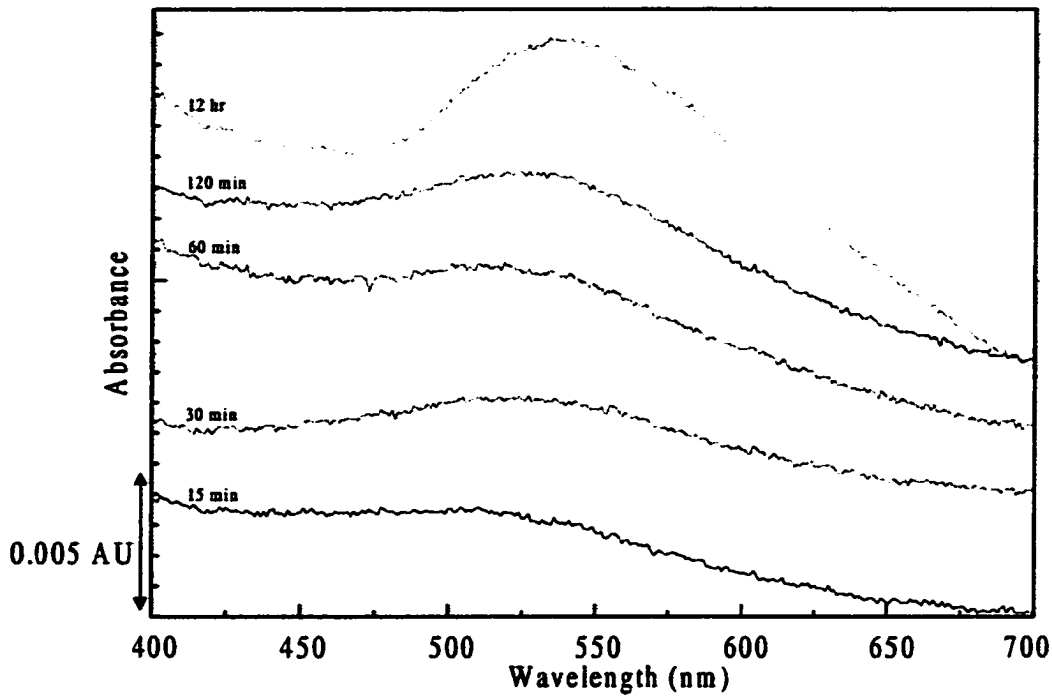

Figure 7.1 **Ultraviolet-visible absorption spectra AT-PMMA pieces exposed to 0.1 mM $HAuCl_4$ for given lengths of time and then reduced in 1 M $NaBH_4$.**

prepared Au nanoparticles on amine-terminated glass and quartz surfaces.[6] Due to the roughness of AT-PMMA,[2] it was impossible to determine the size of the Au nanoparticles using scanning probe microscopy methods. Based on our previous results for Au-EDNPFs on amine-terminated silane layers on silicon oxide,[1] we estimate the size of the Au particles to be in the 50-100 nm range.[7]

The observed increase in intensity of the Au plasmon band with respect to time of exposure of the AT-PMMA to the $HAuCl_4$ solution is due to the formation of oligomeric chloro-hydroxy Au(III) species, Figure 7.2. This phenomenon is not unique

$$AuCl_4^- + H_2O \rightleftharpoons Cl^- + Cl_3Au(H_2O)$$

$$Cl_3Au(H_2O) \rightleftharpoons H^+ + Cl_3Au(OH)^-$$

$$Cl_3Au(H_2O) + H_2O \rightleftharpoons Cl^- + Cl_3Au(H_2O)_2^+$$

$$Cl_3Au(H_2O)_2^+ \rightleftharpoons H^+ + Cl_2Au(H_2O)(OH)$$

$$Cl_3Au(H_2O) + Cl_3Au(H_2O)(OH) \longrightarrow Cl_4Au_2(H_2O)(OH)^+ + Cl^- + H_2O$$

$$Cl_4Au_2(H_2O)(OH)^+ + H_2O \longrightarrow \longrightarrow$$

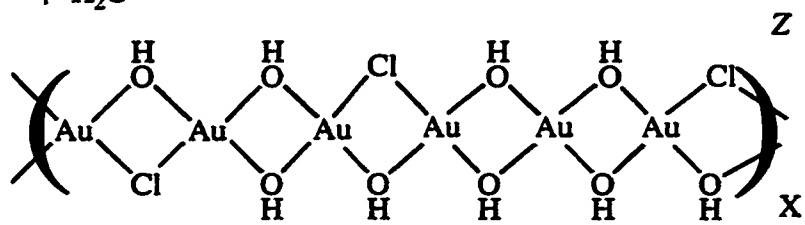

Figure 7.2 **Reaction scheme of $AuCl_4^-$ hydrolysis to produce gold-hydroxy oligomers.**

to AT-PMMA, for a similar observation has been observed for amine-terminated silane monolayers exposed to $HAuCl_4$ solutions.[6] This has been explained previously due to the formation of oligomeric, bridged Au(III) chloro-hydroxy materials on the amine layers.[1] It is well known that $PdCl_4^{2-}$ undergoes hydrolysis to form chloro-hydroxy oligomers, and formation of these Pd(II) oligomers is a key step in the deposition of Pd colloids on surfaces that are used in fabrication of electroless deposits on insulator surfaces.[8] These metal chloro-hydroxy species have a strong propensity to adsorb on surfaces. Relatively few studies have been carried out on the hydrolysis of $AuCl_4^-$, but it has been found that the key intermediates for forming oligomeric chloro-hydroxy Au(III) species, namely $AuCl_2(H_2O)(OH)$ and $AuCl_3(H_2O)$, are formed if the pH and chloride concentration are not controlled.[9-10] Indeed, we have found that, within minutes, aqueous solutions of $HAuCl_4$ exhibit optical spectra characteristic of

hydrolyzed $HAuCl_4$ (loss of band at ~315 nm), but such a transformation can be prevented if excess chloride or acid is added.[6] In the latter scenarios, we have seen little to no deposition of Au upon reduction of amine surfaces exposed to such stabilized $AuCl_4^-$ solutions. We conclude that formation of oligomeric Au(III) chloro-hydroxy materials occurs in solution, and these species adsorb onto the amine sites of the AT-PMMA through a ligand-metal (amine-Au bonding) interaction. Further exposure of the AT-PMMA to the hydrolyzed $AuCl_4^-$ solution results in increased numbers of Au(III) sites deposited, leading to more Au(0) species (increased number of nanoparticles) upon reduction, and thus a larger plasmon band intensity.

7.3 Conventional Electroless Deposition of Ag on Au-EDNPF/AT-PMMA Sheets and the Use of Ag/PMMA Surfaces in the Construction of Reference Electrodes

Due to the need for miniature reference electrodes useful in controlling the potential of working electrodes in microanalytical devices, we investigated the electroless deposition of Ag on the Au-EDNPFs supported on AT-PMMA for possible construction of a macroscopic Ag/AgCl reference electrode.

Immediately upon addition of Au-EDNPF/AT-PMMA sheets to the Ag electroless bath, a yellow-gray film was evident on the PMMA surface. Within two minutes of exposure to the Ag bath, a highly reflective silver coating had formed that completely covered the entire PMMA sheet surface. Ag films were not formed on pristine PMMA or AT-PMMA sheets in any instance; a layer of Au nanoparticles was required to catalyze the electroless deposition of Ag onto the plastic surface. Displayed in Figure 7.3A is a photograph of AT-PMMA immersed in the electroless Ag bath. As is clearly evident, there is minimal plating of Ag on the surface. In Figure 7.3B is a

Figure 7.3 Photographs of A. AT-PMMA and B. Au-EDNPF/AT-PMMA immersed in an electroless Ag bath for 2 min.

photograph of Au-EDNPF/AT-PMMA that has been exposed to the electroless Ag bath. Ag is uniformly distributed over the surface or the PMMA. Attempts to remove the Ag films from the Au-EDNPF/AT-PMMA substrate using adhesive tape failed in all instances,[3-4] indicating that the Ag films are firmly bound to the Au/AT-PMMA surface. We have obtained comparable results for the conventional electroless deposition of Cu on Au-EDNPF/AT-PMMA; highly reflective and conductive Cu films result upon exposure of Au-EDNPF/AT-PMMA to a standard Cu electroless bath,[1] a result similar to that found for Au-EDNPFs on glass.[6]

In order to evaluate the feasibility of using electrolessly deposited Ag films on PMMA in the construction of reference electrodes, Ag/Au-EDNPF/AT-PMMA substrates, along with an Au working and Pt reference electrodes, were placed in an aqueous solution containing 1 M KCl and 5 mM $K_3Fe(CN)_6$, and then appropriate electrical connections were made to the potentiostat. Upon cycling the potential of the Au working electrode between –0.1 and +0.5 V vs the Ag/Au-EDNPF/AT-PMMA substrate, a steady voltammetric response was obtained at the working electrode that was virtually indistinguishable from that when a SSCE reference was used, except the positions of the peak potentials were shifted negative in comparison to those observed with a SSCE reference, Figure 7.4. In addition, the color of the Ag/Au-EDNPF/AT-

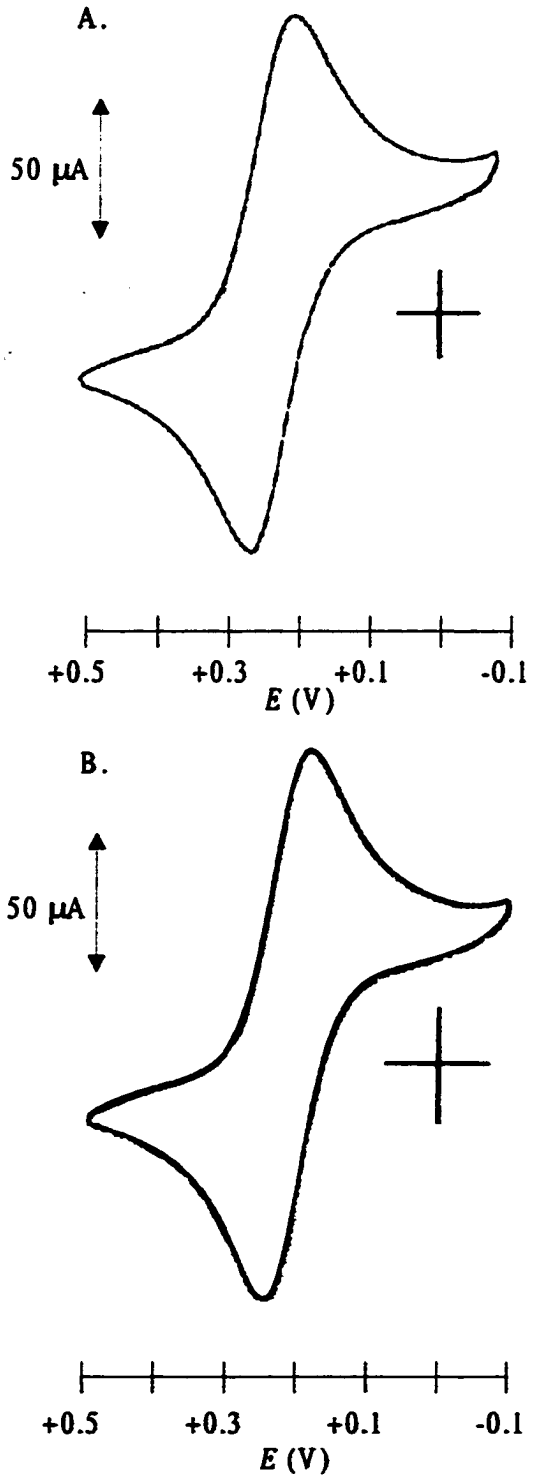

Figure 7.4 **Cyclic voltammograms of 5 mM $K_3Fe(CN)_6$ in 1 M KCl employing a Pt working electrode, Pt counter electrode and A. an SSCE and B. an Ag/Au-EDNPF/AT-PMMA reference electrode.**

PMMA changed to a whitish tone, and the surface was less reflective, indicating the successful formation of a AgCl film. The observed potential difference between the Ag/Au-EDNPF/AT-PMMA substrate (denoted as AgCl/Ag/PMMA) and the SSCE reference was 0.018±0.002 V, in agreement with the expected 0.019 V difference at 20°C.[11] This potential difference did not vary with time of exposure to the electrolyte solution. The stability of the AgCl/Ag/PMMA electrodes with respect to delamination was found to be outstanding in aqueous electrolyte, as noted by the strong adhesion between the Ag film and the plastic surface after prolonged (~12 h) exposure to the KCl/ $K_3Fe(CN)_6$ solution. Thus, these macroscopic AgCl/Ag/PMMA reference electrodes show much promise in the fabrication of miniaturized reference electrodes based on Ag films with small lateral dimensions, vide infra.

7.4 Deposition of Au Colloid Multilayers on AT-PMMA–Working Electrodes Fabricated Directly on PMMA Surfaces

To demonstrate the diversity in the type of metal films that can be attached to AT-PMMA surfaces, multilayer films of Au colloids were formed on AT-PMMA. It has previously been shown that Au colloids made by traditional solution methods[12-13] can be immobilized onto amine-terminated silane layers on glass and quartz to yield ~monolayer or multilayers of the colloidal material.[14-16] The latter route is attractive for the straightforward construction of metal films that can be utilized as working electrodes in electrochemical experiments.

Exposure of AT-PMMA surfaces to an aqueous solution of citrate-capped colloidal Au[12-16] leads to the rapid formation of a raspberry film on the entire surface of the PMMA sheet. Displayed in Figure 7.5 are optical absorption spectra of AT-PMMA pieces that have been immersed in a solution of citrate-stabilized Au colloid (diameter =

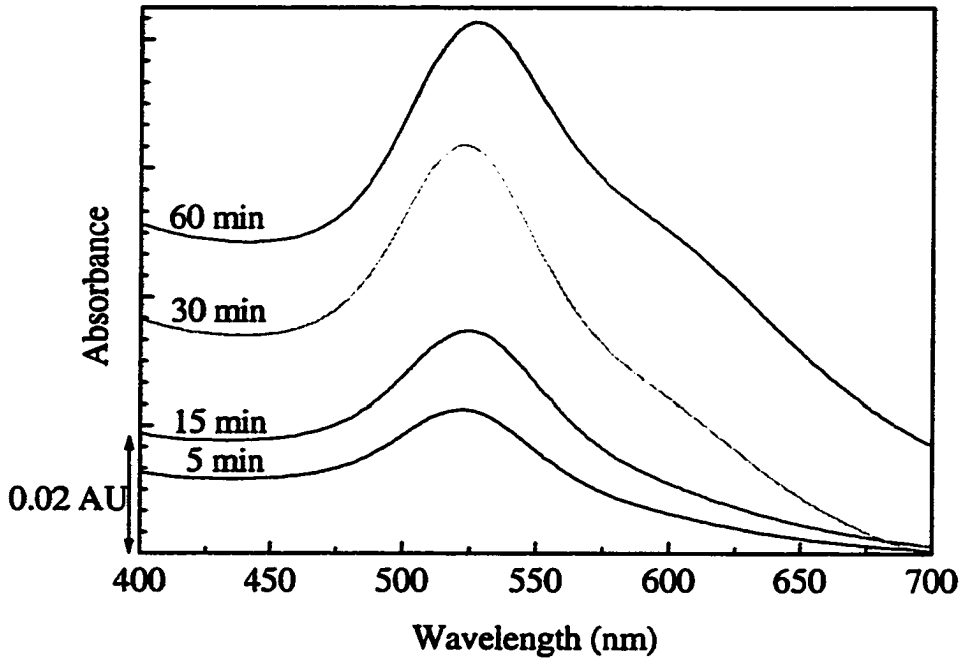

Figure 7.5 Ultraviolet-visible absorbance spectra of AT-PMMA exposed to an Au colloid solution for given lengths of time.

~13 nm) for various amounts of time. The characteristic surface plasmon band of Au colloids at approximately 525 nm is clearly evident in each of the four spectra shown, and the intensity of the plasmon band of the Au colloids increases with adsorption time as previously observed for amine-terminated silane layers on glass.[14] Long immersion times lead to a lower energy band in the spectrum in addition to that at 525 nm indicating the initial stages of Au colloid-Au colloid aggregation on the AT-PMMA surface.[14]

Similar to the Au-EDNPFs on AT-PMMA discussed above, the adhesion of the colloidal Au layer on the AT-PMMA surface is outstanding. Upon repeated application and removal of adhesive tape,[3-4] no loss of Au colloids was observed. The nature of the adhesive interaction is most likely due to anion-cation charge interactions between the

colloidal Au and the AT-PMMA surface. A good number of the amine sites of the AT-PMMA are protonated at the Au colloid solution pH (~5) used, and the surface of the colloids is negatively charged as a result of the citrate stabilizer. Thus, the charge-charge interactions result in a strongly adherent Au colloid film on the AT-PMMA surface. However, amine-Au binding resulting from interactions between the lone pair of the amine groups (there are some present due to acid-base equilibrium) and the Au surface cannot be ruled out.

It has been determined, in previous work, that the surface coverage of amines on PMMA surfaces is approximately 5 nmole cm^{-2}, which corresponds to 30 amine sites nm^{-2}.[2] This larger-than-expected surface coverage (closest-packed configuration corresponds to ~1 nmole cm^{-2}) is due to the formation of a swelled amine-PMMA layer on the PMMA substrate during the aminolysis reaction. This slightly swelled surface that results during the aminolysis leads to amination of the methyl ester groups to a depth that is ~6 monomer repeats.[2] If we assume that a 15 nm Au colloid particle is cubic,[14] there are approximately 6000 amine sites available for interaction with the face of a Au particle. This assumes an electrostatic mode of interaction that would operate over fairly long distances. If the binding of the Au to the AT-PMMA is actually due to interactions between the lone pair on the amines and the Au surface, then fewer amine sites can participate in the binding process due to their being sub-surface. Regardless, the Au colloids are very strongly bound to the AT-PMMA surface.

The immobilized Au colloid particles can be used as a platform for the formation of functional Au working electrodes on the PMMA surfaces. Multilayers of Au colloids were fabricated on the AT-PMMA surface by immersing a Au colloid/AT-

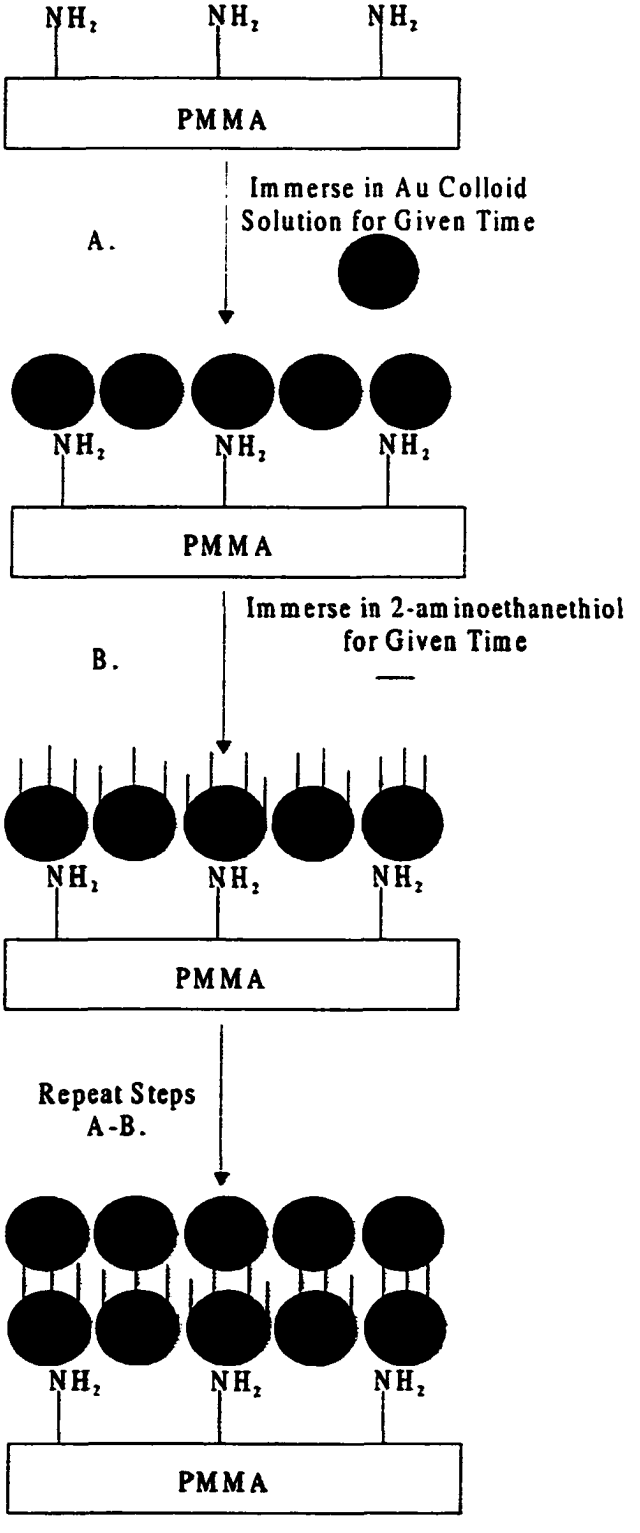

Figure 7.6 Pictorial depiction of multilayer colloid growth on AT-PMMA surfaces.

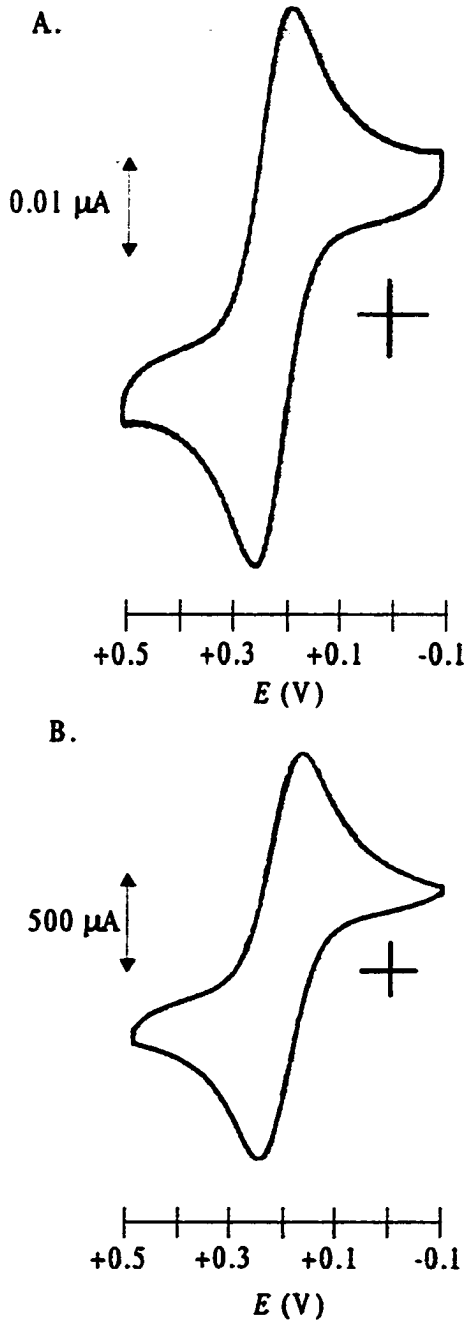

Figure 7.7 **Cyclic voltammograms of 5 mM $K_3Fe(CN)_6$ in 1 M KCl utilizing a SSCE reference electrode, Pt counter electrode and A. Au disk electrode or B. Au colloid multilayer/AT-PMMA working electrode.**

PMMA surface, prepared as described above, in 2-aminoethane-1-thiol for one hour followed by ethanol and water rinses, and then immersion in the Au colloid solution for 1 h; these steps were repeated a given number of times (minimum of 12), Figure 7.6. The resulting Au colloid multilayers on AT-PMMA were gold in color and highly reflective, and the films were not removed using the standard tape test.[3-4]

The resultant Au colloid multilayer/AT-PMMA sheets were used as working electrodes in aqueous electrochemistry studies of $K_3Fe(CN)_6$. Displayed in Figure 7.7 are representative cyclic voltammograms of $K_3Fe(CN)_6$ at an Au disk electrode (Figure 7.7A) and an Au colloid multilayer/AT-PMMA electrode (12 layers of colloid, Figure 7.7B). The peak potential difference ($\Delta E_p = E_{p,anodic} - E_{p,cathodic}$) for $K_3Fe(CN)_6$ using the Au colloid multilayer/AT-PMMA electrode was found to be 0.065±0.001 V and that at the Au wire electrode is 0.055±0.002 V (both at 20°C). Uncompensated resistance correction was not made during these measurements. The relatively small ΔE_p for the colloid multilayer electrode demonstrates that the Au film has a fairly high conductivity. Thus, such multilayer Au colloid electrodes should be viable in the construction of electrochemical detection systems for analytical microdevices based on PMMA.

7.5 Photo-Directed Patterning of Ag on PMMA Surfaces

In order to develop metal microelectrodes useful in electrochemical or conductivity applications and metal circuitry designs useful in the construction of polymer-based microanalytical devices, methodologies for the patterned (selective) formation of metal film features are needed. In addition, the method should be relatively inexpensive, involve simple chemistry, and lead to strongly adherent films.

The approach we chose for the patterned deposition of metal features on PMMA has as its key element the protection of metal-binding groups followed by laterally selective photo-deprotection of the metal-binding moieties. Once the surface has patterned on it a design consisting of a functionality capable of binding metal, the electroless method described above for forming metal films can be used to decorate the patterned area with metal and no where else. In the case at hand, protection of the surface amine groups of AT-PMMA is achieved by reaction of AT-PMMA with the photolabile protecting group 4,5-dimethoxy-2-nitrobenzylcarbonyl, also known as nitroveratryloxycarbonyl or NVOC.[17-21] The NVOC protecting group was chosen due to the fact that its removal is achieved by irradiation of the NVOC-amine with ~350 nm light, a wavelength that will not cause structural damage to the underlying PMMA backbone (possible scission reactions).[22] To our knowledge, this is the only photo-protecting group for amines that absorbs light in the visible region of the electromagnetic spectrum. However, the NVOC protecting group is only available in the form of the chloroformate, a material which can only be used in solvents that would be deleterious to the PMMA (dissolution of the polymer). Thus, a carboxylic acid derivative of NVOC, namely glycine, NVOC-Gly, was synthesized.[21] NVOC-Gly is amenable to carbodiimide-aided peptide coupling reactions due to the presence of the carboxylic acid on the NVOC-Gly. The solvent used was ethanol because it does not destroy the PMMA surface. Once the NVOC-Gly is attached to the amines of the AT-PMMA through amide bonds, amine groups can be selectively removed by irradiation of the NVOC-Gly-protected surface using a mask and visible radiation. The entire process is outlined in Figure 7.8.

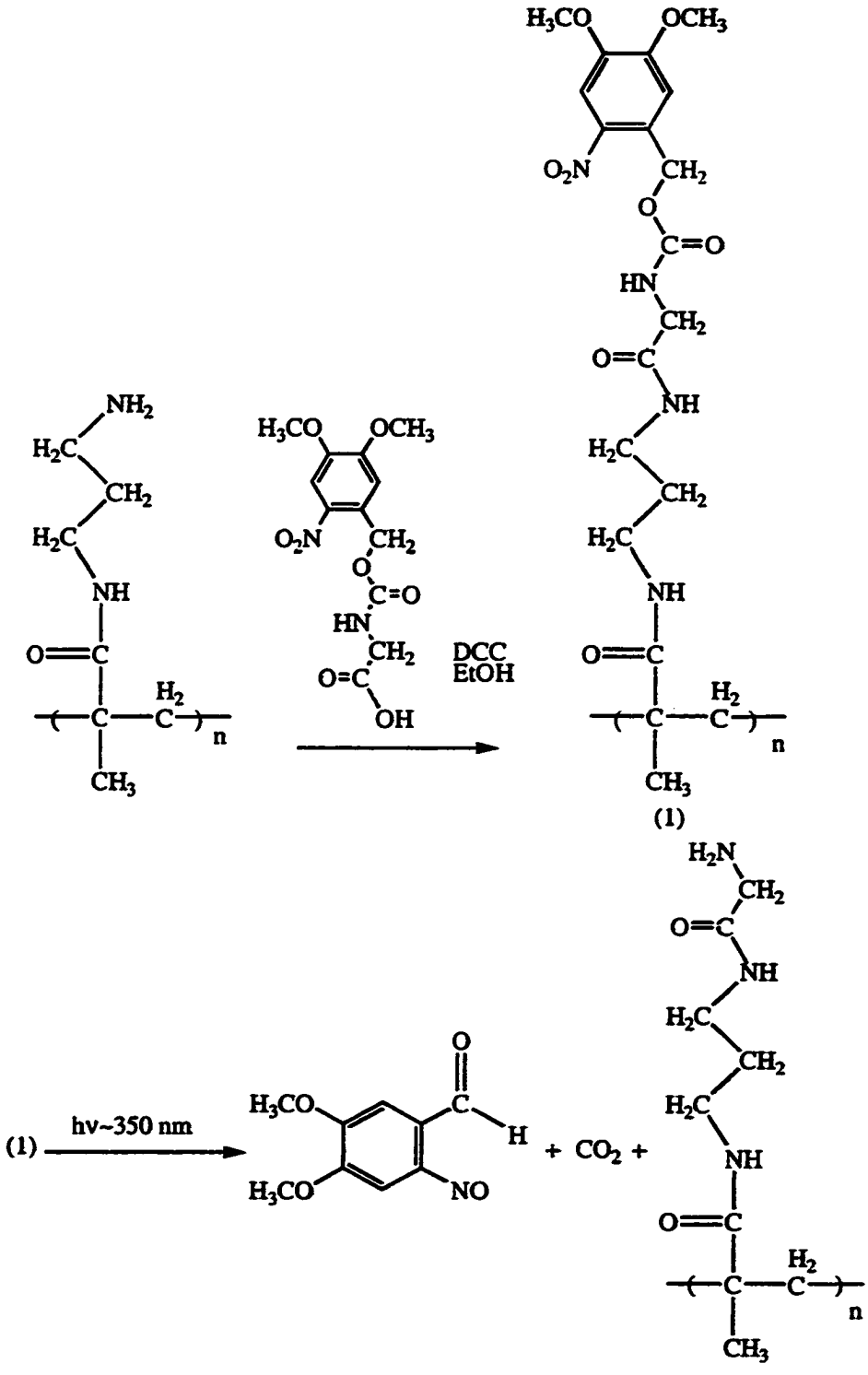

Figure 7.8 **Reaction scheme of AT-PMMA protected with NVOC-Gly and then deprotected with 350 nm radiation.**

To demonstrate the ability to effectively protect the amine groups of the AT-PMMA with NVOC-Gly and subsequently remove the NVOC functionality selectively to yield well-defined patterns of amine sites, AT-PMMA substrates treated as outlined in Figure 7.8 were examined with fluorescence microscopy. The patterned substrate was placed in a solution containing a near-infrared dye selective for labeling amines and then imaged using a scanning fluorescence microscope described elsewhere.[23] Shown in Figure 7.9 is a typical fluorescence microscope image obtained for an NVOC-Gly-protected AT-PMMA surface that was irradiated using a mask having 300 μm-wide features. The bright areas in Figure 7.9 corresponding to dye-labeled amines are found to be 300 μm in width and very straight. At this scale, there is no evidence to suggest that the regions that were not exposed to the 350 nm light during the de-protection step contain any free amine sites. Fluorescence microscopy images of unexposed NVOC-Gly-protected AT-PMMA surfaces show a similar dark background.

We subjected patterned AT-PMMA sheets to the Au electroless deposition procedure outlined above to form Au-EDNPFs. The patterns of the AuEDNPFs were readily observable as raspberry-colored features surrounded by colorless regions (no exposure to the 350 nm light occurred). Upon placing the patterned Au-EDNPFs supported on the AT-PMMA surface substrate in the conventional Ag electroless bath for two minutes, reflective Ag film patterns were formed on the PMMA, as noted by optical micrographs, Figure 7.10A. However, the formation of Ag deposits on the protected PMMA surface (unexposed areas) was evident on several of the PMMA surfaces patterned, as seen in the regions outside of the "piano key" region that was

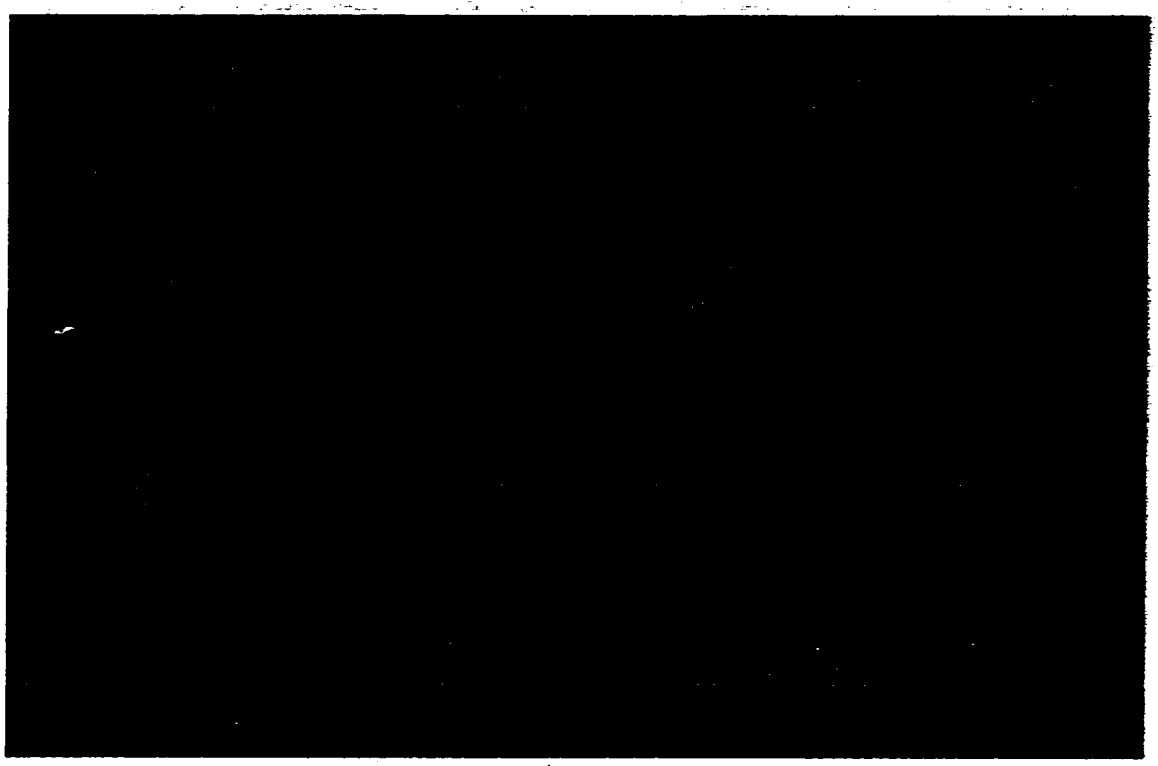

Figure 7.9 Fluorescence microscope image of NVOC-Gly-protected PMMA surface that has been masked, irradiated and labeled with a near infrared fluorescent dye. The bright areas are 300 μm wide.

irradiated in Figure 7.10A. Neither the desired Ag features nor the "non-specifically" formed Ag features were removed by adhesive tape.

As discussed previously, the presence of Au-EDNPFs on the AT-PMMA surface is required for Ag electroless plating to occur, so there must be Au-EDNPFs present on the NVOC-Gly-protected regions. In order for the Au-EDNPFs to be present, it is possible that binding of Au(III) species to either the NVOC-Gly groups or free amine sites due to in complete NVOC-Gly protection occurred. Also, it is possible that stray light or light in the laboratory ambient caused removal of some fraction of the NVOC groups to yield a surface with amine groups speckled throughout. Because the

A.

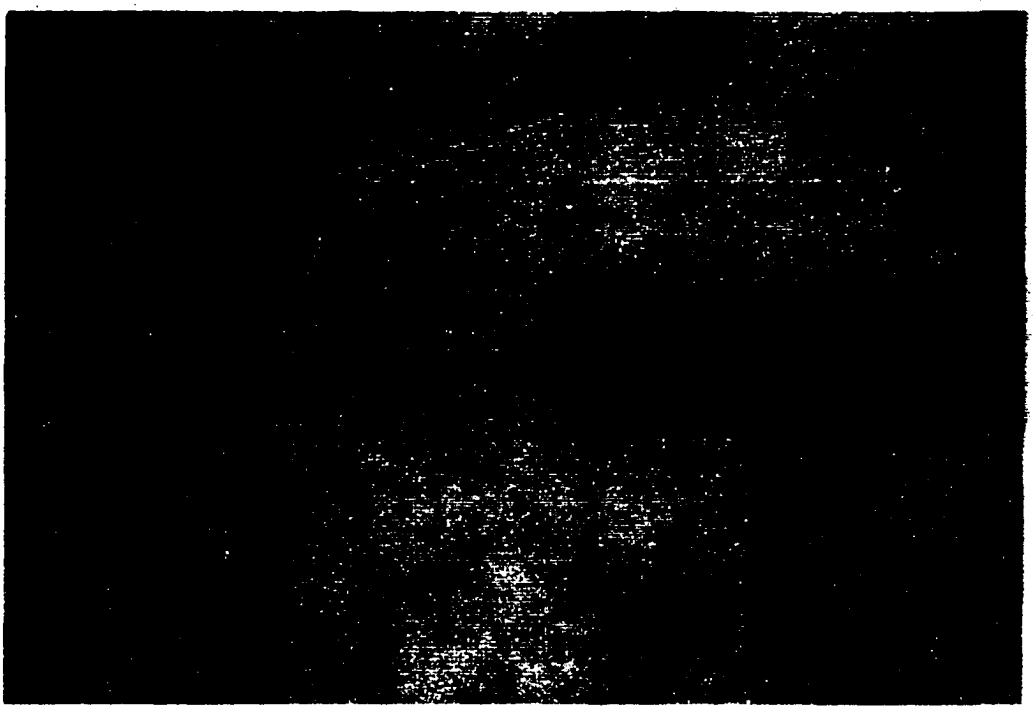

B.

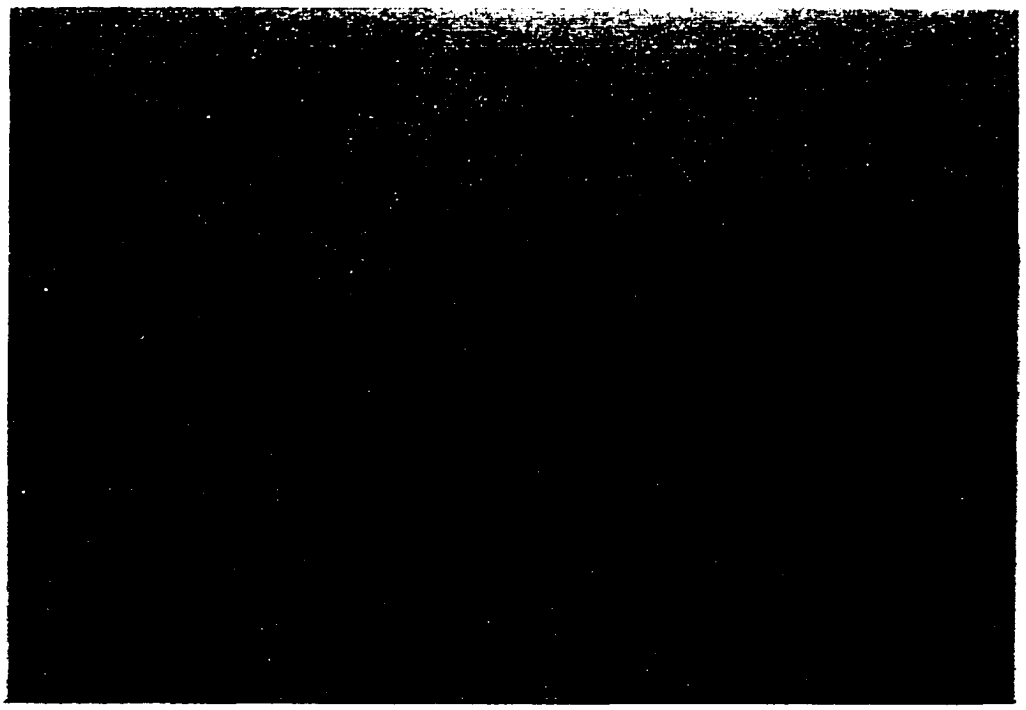

Figure 7.10 Micrographs of Ag photopatterned on PMMA A. before and B. after seed layer optimization. The smallest feature in the micrograph is 10 μm.

NVOC-Gly-AT-PMMA was always handled in the dark, we were certain that a light-mediated deprotection of the NVOC-protected surfaces did not occur.

We hypothesized that the AT-PMMA surfaces were indeed fully protected by the NVOC-Gly, but the protecting groups were removed as a result of acid hydrolysis of the urethane linkage (Figure 7.8) during the first step of the Au-EDNPF formation process. The pH of the $HAuCl_4$ solution used is 3.2, a value sufficient to result in urethane hydrolysis. This hydrolysis would leave behind amine groups to which the Au(III) species could bind. In order to test this hypothesis regarding hydrolysis of the urethane linkage, the pH of the $HAuCl_4$ solution was raised to 7, and it was then used in the patterned Au-EDNPF formation procedure. Once again, we observed the raspberry-colored pattern of the Au-EDNPF. Upon placing the patterned Au nanoparticle surface in the Ag electroless bath for 2 min, followed by observation with an optical microscope, images like that in Figure 7.10B were routinely observed. As is evident in Figure 7.10B, there are no Ag features outside of the desired "piano key" design. Thus, metal film features with sizes as small as 10 μm (the width of the smallest feature in Figure 7.10B) and lengths up to several cm can be selectively formed on chemically modified PMMA surfaces.

7.6 Conclusions

Procedures for the deposition of metals and metal colloids on PMMA surfaces were developed. A novel electroless deposition method was used to form Au seed layers (Au nanoparticles) on AT-PMMA surfaces; the seed layer was used in the conventional electroless deposition of Ag films. These Ag films were used to construct robust AgCl/Ag reference electrodes. In addition, Au working electrodes were fabricated by

depositing Au colloid multilayers on AT-PMMA surfaces. It was found that voltammetry at the Au colloid/AT-PMMA electrodes compared favorably to that at a traditional Au disk electrode. Finally, a method for the selective deposition of metal films was developed using a photolabile protecting group. Micron-scale patterned Ag metal films on PMMA surfaces could be achieved with the photo-directed protocol outlined here. This work has direct relevance to the development of auxiliary detection schemes, as well as on-chip microcircuitry, for microanalytical devices fabricated using polymer substrates.

7.7 References

1) Moberg, P.; McCarley, R.L. *J. Electrochem. Soc.* **1997**, *144*, 151-153.

2) Henry, A.C.; Tutt, T.J.; Galloway, M.; Davidson, Y.Y.; McWhorter, C.S.; Soper, S.A.; McCarley, R.L. *Anal. Chem.*, **2000**, *72*, 5331-5337.

3) Willicut, R.J.; Mcarley, R.L. *Langmuir* **1995**, *11*, 296-301.

4) Simon, R.A.; Ricco, A.J.; Wrighton, M.S. *J. Am. Chem. Soc.* **1982**, *104*, 2031-2034.

5) Hulst, H.C. *Light Scattering by Small Particles*; Wiley: New York, 1957.

6) Moberg, P.; McCarley, R.L. Unpublished results.

7) Kriebig, U.; Gartz, M.; Hilger, A. *Berichte Der Bunsen-Gesellschaft-Phys Chem. Chem Phys.* **1997**, *101*, 1593-1604.

8) Dressick, W.J.; Dulcey, C.S.; Georger, J.J.; Calabrese, G.S.; Calvert, J.M. *J. Electrochem. Soc.* **1994**, *141*, 210-220.

9) Bekker, P. v. Z.; Robb, W. *Inorg. Nucl. Chem. Lett.* **1972**, *8*, 849-854.

10) Peck, J.A.; Tait, C.D.; Swanson, B.I; Brown, G.E *Geochim. Cosmochim. Acta* **1991**, *55*, 671-676.

11) Bard, A.J.; Failkner, L.R. *Electrochemical Methods: Fundamentals and Applications*; Wiley: New York, 1980.

12) Frens, G. *Nature Phys. Sci.* **1973**, *241*, 20-22.

13) Sutherland, W.S.; Winefordner, J.D. *J. Colloid Interface Sci.* **1992**, *48*, 129-141.

14) Grabar, K.C.; Freeman, R.G.; Hommer, M.B.; Natan, M.J. *Anal. Chem.* **1995**, *67*, 735-743.

15) Grabar, K.C.; Allison, K.A.; Baker, B.E.; Bright, R.M.; Brown, K.R.; Dolan, C.M.; Freeman, R.G.; Fox, A.P.; Musick, M.D.; Natan, MJ. *Langmuir* **1996**, *12*, 2353-2361.

16) Musick, M.D.; Pena, D.J.; Sotsko, S.L.; McEvoy, T.M.; Richardson, J.N.; Natan, M.J. *Langmuir* **1999**, *15*, 844-850.

17) Fodor, S.P.A.; Read, J.L.; Pirrung, M.C.; Stryer, L.; Lu, A.T.; Solas, D. *Science* **1991**, *251*, 767-769.

18) Cho, C.Y.; Moran, E.J.; Cherry, S.R.; Stephans, J.C.; Fodor, S.P.A.; Adams, A.; Sundaram, A.; Jacobs, J.W.; Schultz, P.G. *Science* **1993**, *261*, 1303-1305.

19) Patchornik, A.; Amit, B.; Woodward, R.B. *J. Am. Chem. Soc.* **1970**, *92*, 6333-6334.

20) Jennane, J.; Boutros, T.; Giasson, R. *Can. J. Chem.* **1996**, *74*, 2509-2517.

21) Vossmeyer, T.; DeIonno, E.; Heath, J.R. *Angew. Chem. Int. Ed. Engl.* **1997**, *36*, 1080-1083.

22) Henry, A.C.; McCarley, R.L.; Das, S.S.; Khan Malek, C.G.; Poche, D.S. *Microsystem Technologies* **1998**, *4*, 104-109.

23) Waddell, E.; Wang, Y.; Stryjewski, W.; McWhorter, S.; Henry, A.C.; Evans, D.; McCarley, R.L; Soper, S.A. *Anal. Chem.* **2000**, *72*, 5907-5917.

Chapter 8

Conclusions and Future Directions

8.1 Summary of Conclusions

In this work, the bulk and surface properties of commercial PMMA sheets have been characterized. It has been determined that PMMA sheets supplied by different vendors exhibit different thermal properties. The molecular masses of the commercial PMMA sheets average 1— 3 Mamu and decrease substantially after X-ray irradiation. In addition to the bulk properties of commercial PMMA sheets, their surface properties were probed as well. It was determined that the surface topography of the PMMA sheets varied with vendor, sheet thickness, and thermal treatment. In addition, it was found that variations in surface topography after heat treatment were due to the expulsion of MMA monomer from the matrix of the polymer.

The surface chemical modification of commercial PMMA sheets was also described. It has been shown that pristine PMMA can be reacted, in an aminolysis reaction, to yield AT-PMMA. The amines on the surface of AT-PMMA can be used as a reactive scaffold onto which other organic moieties can be *covalently* attached. It has been shown that AT-PMMA can be reacted with neat *n*-octadecane-1-isocyanate to yield $C_{18}H_{37}$-terminated PMMA surfaces; this reaction is useful for the development of stationary phases bonded to PMMA microchannels for microCEC devices. AT-PMMA can be reacted with carboxylic acids in the presence of a carbodiimide; PMMA surfaces terminated in ω-substituted carboxylic acids and sulfonic acids were produced in this manner. An enzymes was immobilized on AT-PMMA surfaces through the use of a

dialdehyde immobilization agent and the immobilized enzyme was used in a DNA digestion protocol. The amines on AT-PMMA were also used in the deposition of metal colloid multilayers. In addition, AT-PMMA substrates were used in the electroless deposition of Au nanoparticles on the AT-PMMA surface. These Au nanoparticles were used in the conventional electroless deposition of Ag using a commercial electroless Ag bath.

Finally, a method for the *selective deposition* of metals and organic species on PMMA surfaces was developed. AT-PMMA was reacted with a carboxylic acid derivative of a photolabile protecting group in the presence of a carbodiimide. After the spatially defined deprotection of the amines using 350 nm radiation, the patterned surfaces were subjected to sequential electroless deposition steps to yield patterns of electroless Ag with features as small as 10 μm on the exposed amine patterns.

This research is pertinent to the continued use of commercial sheet PMMA as a photoresist in the microstructure and microdevice industry. In addition, this research has described the surface chemical modification of a common substrate used for the fabrication of microanalytical separation devices. These chemical modifications can be used to incorporate stationary phases into microCEC devices as well as change the EOF in PMMA microchannels. The procedures outlined for the deposition of metals and metal colloids can be used to fabricate analytical detection schemes, such as those based on surface-enhanced Raman spectroscopy, electrochemistry, and conductivity. Finally, the selective deposition procedure that has been described can be used for the fabrication selectively-deposited organic moieties and metal films used for microarrays and microcircuitry on microanalytical separation device surfaces.

8.2 Summary of Observations Supporting Conclusions

The thermal properties of PMMA sheets from various vendors were determined using DSC. The T_g of the sheets was different with respect to vendor and was in the range of 95 — 115 °C. The molecular masses of the PMMA sheets were also determined to be 1 — 3 M amu and decreased nearly 45-fold after irradiation with X-rays. The molecular masses of PMMA standards were determined by MALDI-MS; the molecular mass of the PMMA standards as determined by MALDI-MS agreed with those determined by the vendor using GPC.

The surface topography of commercial PMMA sheets was determined using SFM. It was found that the surface topographies of the PMMA sheets varied with vendor, thickness, and thermal treatment. The topographical differences present on the PMMA sheets were in the form of pits; that is, depending on sheet vendor, thickness and thermal treatment, defect pits were present in varied numbers and sizes. It was found, in all cases, that the size and number of the pits on the PMMA surface increased after thermal treatment. Thus, it was postulated that thermally treating the polymer allowed for the expulsion of volatiles trapped within the matrix of the polymer. In order to test this assumption, GC-MS analyses were performed on pristine and thermally treated PMMA pieces dissolved in chloroform. It was determined that the concentration of MMA in thermally treated PMMA pieces is significantly less than that in pristine PMMA pieces. In order to monitor the expulsion of the MMA from the matrix of the PMMA, SPME coupled to GC-MS was employed. It was found that MMA is expelled from the matrix of the polymer during thermal treatment, and it is the sole organic volatile species that expelled from the matrix of the PMMA.

The surface chemical modification of commercial PMMA sheets was described. This work has pertinence in the field of microanalytical separation device development. Commercial sheet PMMA was subjected to an aminolysis reaction with either *N*-lithiodiaminoethane or *N*-lithiodiaminopropane. The resulting product, AT-PMMA, was characterized using a variety of analytical techniques, including contact angle goniometry, RAIR spectroscopy, fluorescence microscopy, XPS, and SFM. The results from these experiments indicate that primary amines are present on the surface and they are linked to the surface by means of an amide bond. The surface roughness of the AT-PMMA is roughly 3.5 times higher than the pristine PMMA, and the amines are accessible for reaction with other organic moieties. The amines are present on the surface of the PMMA at a concentration of ~5 nmol cm^{-2} as determined by a variation of the ninhydrin method. EOF profiles of pristine and AT-PMMA indicated an anode-to-cathode flow of solvents in pristine PMMA as compared to a cathode-to-anode flow direction in AT-PMMA microchannels.

This is due to the differences in surface ionizable groups of the pristine and AT-PMMA. AT-PMMA surfaces were subjected to reaction with neat *n*-octadecyl-1isocyanate and characterized using water contact angle goniometry, RAIR spectroscopy, and SFM. Results from these experiments indicate that a urea linkage is formed upon reaction of the primary amines with the isocyanate. The surface is terminated in highly ordered alkane chains, as evidenced by the progression bands present in the RAIR spectrum. The chains are tilted somewhat from the surface normal, as evidenced by the water contact angles obtained for the $C_{18}H_{37}$-terminated PMMA

surface. The surface roughness of $C_{18}H_{37}$-terminated PMMA is roughly 1.6 — 2 times higher than the AT-PMMA surface.

AT-PMMA beads were used for restriction endonuclease enzyme immobilization. The enzyme was covalently attached to the PMMA surface by means of a glutaric dialdehyde linkage. Digestion of a dsDNA phage resulted in 11 fragments; these fragments were separated and detected using conventional CE and compared to results obtained in free solution; there was no detectable difference in the DNA digestion patterns.

AT-PMMA was subjected to peptide coupling reactions with ω-substituted carboxylic acids, 1,9-nonanedioic acid and 4-sulfobenzoic acid, using a carbodiimide in ethanol or water. The products from these reactions, CT-PMMA and ST-PMMA, respectively, were characterized using RAIR spectroscopy. RAIRs data indicates that an amide linkage is formed upon reaction with the primary amine on the AT-PMMA and the carboxylic acid in solution. For comparison purposes, AT-Au surfaces were prepared and subjected to the same reaction conditions as with AT-PMMA. RAIR spectroscopy from these experiments indicates the formation of an amide linkage between the amine on the surface of the Au and the carboxylic acid in solution. EOF profiles were obtained in CT- and ST-PMMA microchannels. In the CT-PMMA microchannel, the EOF profile is strongly pH dependent. At pH values less than ~5, the EOF runs from cathode to anode, indicating that there are accessible amines on the surface in addition to the neutral, protonated carboxylic acid groups on the surface of the microchannel at all pH values studied. At pH values greater than ~5, the EOF runs from anode to cathode, indicating that the carboxylic acid groups are deprotonated and

negatively charged. In the case of ST-PMMA microchannels, the EOF runs from anode to cathode at all pH values probed. This is due to the deprotonation of the sulfonic acid groups on the surface of the ST-PMMA microchannel. By chemically modifying the surface of the PMMA microchannel, it is possibly to change the magnitude and direction of the EOF.

Due to the high metal-coordinating affinity of primary amines, AT-PMMA was investigated for its use as a substrate for metal colloid and film deposition. Au colloids were synthesized and AT-PMMA was immersed in the Au colloid solution for given amounts of time. The colloids deposited on the AT-PMMA surface were characterized by UV-vis spectroscopy; the spectra displayed the characteristic Mie Au plasmon band. The Au colloid/AT-PMMA surface was exposed to a solution of the bifunctional cross-linker 2-aminoethanethiol and then immersed in the Au colloid solution repeatedly in order to form a thick colloidal film on the AT-PMMA surface. The multilayer Au colloid/AT-PMMA was used as a working electrode in electrochemistry experiments involving $K_3Fe(CN)_6$ in KCl. Results from these experiments indicate that the Au colloid/AT-PMMA electrode is similar to a conventional Au electrode.

AT-PMMA surfaces were used for the electroless deposition of Au. AT-PMMA was immersed in 0.1 mM $HAuCl_4$ for given amounts of time, rinsed, and placed in 1 M $NaBH_4$ for 1 min. Electrolessly deposited Au nanoparticle films prepared in this manner were characterized by UV/vis spectroscopy; the spectra displayed the characteristic Au Mie plasmon band. The Au nanoparticles were used as autocatalytic sites for the electroless deposition of Ag using a conventional electroless deposition bath. Ag/AT-PMMA was used as a reference electrode in electrochemistry experiments

involving $K_3Fe(CN)_6$ in KCl. It was found that Ag/AT-PMMA electrodes in KCl operate in the same manner as a standard Ag/AgCl reference electrode. Thus, this protocol can be used for the fabrication of on-column reference electrodes in electrochemical detection schemes.

The selective deposition of organic moieties and metals using photo-directed procedures was described. A glycine derivative of a photolabile protecting group, nitroveratryloxycarbonyl-glycine, NVOC-Gly, was synthesized. NVOC-Gly was coupled, using carbodiimide coupling procedures, to the AT-PMMA surface. The protected surface was masked and exposed to visible radiation. After the deprotection, the free amines were subjected to an electroless deposition protocol or to reaction with an isothiocyanate-based dye. It was found, through optical microscopy and fluorescence microscopy, that patterned features as small as 10 μm were evident on the PMMA surface. Thus, by this photoprotection/deprotection scheme, patterns of metals or organic moieties can be created on a PMMA surface. This has direct application in the fabrication of array technology or microcircuitry on PMMA surfaces.

8.3 Future Studies

In this work, the bulk characterization of commercial PMMA sheets, as well as the surface modification and characterization of commercial PMMA sheets, was described. The chemical modification of PMMA surfaces to yield various organic moieties for different purposes can be realized using procedures similar to those presented here. For example, thermoresponsive polymers, such as poly(*N*-isopropylacrylamide), PNIPAAm, covalently bonded to PMMA microchannels could be used as extraction matrices prior to analyte introduction into the separating

microchannel. PNIPAAms are characterized by their ability to extend their polymer chains. At low temperatures, when the chains are extended, the polymer is hydrophilic. However, at high temperatures, when the chains are retracted, the polymer is hydrophobic.[1-4] These polymers have been used as stationary phase materials in high-performance liquid chromatography (HPLC).[5-6] A temperature-mediated extraction matrix, gel-permeation chromatography packing material, or HPLC stationary phase can be envisioned for PMMA microchannels onto which have been bonded PNIPAAm polymers.

The PNIPAAm polymers can be covalently coupled to the surface of the PMMA using carbodiimide coupling procedures or, alternatively, they can be polymerized from the surface of the PMMA. Analysis of the PNIPAAm-PMMA surface would involve a temperature-controlled stage for water contact angle goniometry, as well as a temperature-controlled device for heating the substrate in RAIR spectroscopy. Due to the presence of sulfur atoms in the PNIPAAm, XPS analyses are possible for the determination of the presence of the polymers on the PMMA surface.

Because of its susceptibility to organic solvents, a method for increasing the insolubility of PMMA microdevices in organic materials will become necessary. One method for increasing the robustness of PMMA microchannels is to grow a monolayer or multilayers of a material resistant to organic solvents on the PMMA surface. This could be accomplished using sol-gel chemistry coupled to PMMA modification. Such sol-gel surface modification protocols have been performed on poly(carbonate) surfaces.[7] Sol-gel glasses are formed by the hydrolysis and polycondensation of organometallic materials, such as silicates.[8] Thus, in order to covalently link a sol-gel

glass to PMMA, the PMMA must possess alcohol moieties on its surface.[8] This can be realized by coupling AT-PMMA with a carboxylic acid-containing alcohol. The alcohol-terminated PMMA can then be reacted with silanol species. The result of this reaction is a thin film (several multilayers) of sol-gel glass on the surface of the PMMA. The reaction can be characterized using RAIR spectroscopy as well as XPS. In addition, exposure of the sol-gel-coated PMMA to organic solvents should result in no dissolution. Modification of the sol-gel surface can be accomplished using standard silane chemistry.

The selective deposition protocols described could be employed for the fabrication of in-channel electrochemical detection schemes as well as for in-channel surface-enhanced Raman spectroscopy detection schemes. In addition, patterned areas can be formed on the PMMA surface, resulting in the formation of inexpensive DNA microarrays. These microarrays can be used in DNA sequencing methodologies as well as in DNA oligomer characterization.

8.4 References

1) Ding, Z.; Chen, G.; Hoffman, A.S. *Biocunjugate Chem.* **1996**, *7*, 121-125.

2) Chen, G.; Hoffman, A.S. *Polymer Prepr.* **1992**, *33*, 468-469.

3) Chen, J.P.; Yang, H.J.; Hoffman, A.S. *Biomaterials*, **1990**, *11*, 625-630.

4) Chen, J.P.; Hoffman, A.S. *Biomaterials*, **1990**, *11*, 631-637.

5) Hosoya, K.; Kimata, K.; Araki, T.; Tanaka, N.; Frechet, J.M.J. *Anal. Chem.* **1995**, *67*, 1907-1911.

6) Kanazawa, M.; Kashiwase, Y.; Yamamoto, K.; Matsushima, Y.; Kikuchi, A.; Sakurai, Y.; Okano, T. *Anal. Chem.* **1997**, *69*, 823-830.

7) Chenghong, L.; Wilkes, G. *J. Inorganic Organic Polym.* **1997**, *7*, 203-216.

8) Brinker, C.J.; Scherer, G.W. *Sol-Gel Science*, Academic Press, Inc., San Diego, 1990.

Vita

Alyssa Catharyn Henry was born on March 30, 1973, in Ft. Walton Beach, Florida. Her formative years were spent as a child of the United States Air Force; she attended several different schools in such states as Illinois, Alaska, North Dakota, and Pennsylvania. She was awarded bachelor degrees in chemistry and biology in December 1994 from Indiana University of Pennsylvania. In 1996, she joined the research group of Professor Robin L. McCarley at Louisiana State University and is currently completing the requirements for the degree of Doctor of Philosophy in chemistry. Alyssa was awarded a National Research Council Post-Doctoral Fellowship at the National Institute for Standards and Technology (NIST). She will begin her tenure at NIST in June 2001.

DOCTORAL EXAMINATION AND DISSERTATION REPORT

Candidate: Alyssa Catharyn Henry

Major Field: Chemistry

Title of Dissertation: Surface Modification and Characterization of PMMA Used in the Construction of Microelectromechanical Systems

Approved:

Major Professor and Chairman

Dean of the Graduate School

EXAMINING COMMITTEE:

Date of Examination:

April 30, 2001